Surface Self-Assembled Colloidal Crystals

for the use in Pattern Replication by Hot Embossing

R.M. van Dommelen

Technische Universiteit Delft

TU Delft Delft University of Technology

Challenge the future

Department of Precision and Microsystems Engineering

Surface self-assembled colloidal crystals for the use in Pattern Replication by Hot Embossing

R.M. van Dommelen

Report no : 2017.041
Coaches : Dr. L. Sasso & Dr. P. Fanzio
Professor : Dr. Ir. M. Tichem
Specialisation : Micro and Nano Engineering
Type of report : Master Thesis
Date : September 11, 2017

Surface Self-Assembled Colloidal Crystals

for the use in Pattern Replication by Hot Embossing

by

R.M. van Dommelen

in partial fulfillment of the requirements for the degree of

Master of Science
in Mechanical Engineering

at the Delft University of Technology,
to be defended publicly on Friday October 6, 2017

Supervisors:	Dr. L. Sasso & Dr. P. Fanzio	TU Delft, 3ME-PME
Thesis committee:	Dr. Ir. M. Tichem,	TU Delft 3ME-PME
	Dr. H.B. Eral,	TU Delft 3ME-P&E

An electronic version of this thesis is available at http://repository.tudelft.nl/.

TU Delft Delft University of Technology

Preface

> You could find out most things, if you knew the right questions to ask. Even if you didn't, you could still find out a lot.
>
> Iain M. Banks, The Player of Games

When I started roughly a year ago on this project I had no idea about anything related to colloidal particles and self-assembly. Yet I can't believe it is almost a year later, and only when I look back I see how far I have travelled. But this was not possible without the help of some amazing people, whom I'd all like to thank for their help. In terms of scientific expertise, advice, moral support and the occasional much needed distraction.

First and foremost I'd like to thank my supervisors Luigi Sasso and Paola Fanzio. Thanks to your support and advice I have been able to make this project a success, especially at the times when I didn't know how to continue you were able to push me to look at it from a different perspective. You guys were always being able to provide feedback or help on a moments notice. Secondly, I'd like to thank Urs Staufer, who was always willing to enter a discussion and share some much needed wisdom.

Secondly I'd like to thank my friends within the department, Alkisti Gkouzou, Eleonoor Verlinden, Cristina Verone and Kai Wu for extending their companionship and employee benefits to a lowly master student such as myself. As well as all the other junior and senior staff who showed interest or have assisted me in one way or another during my project.

Lest I forget I want to thank Rob Luttjeboer, Spiridon van Veldhoven, Patrick van Holst and Harry Jansen for lending me their ear and their essential technical expertise.

I have to admit that I was very lucky to be placed in the most extravagantly and luxurious offices in the entirety of the department, as well as the people who were willing to entertain me with coffee breaks, discussions and the occasional picnic. I'd like to thank Michael Mengolini, Elena De Lazzari, Heleen Payens, Pieter Kapel, Jelmer de Zeeuw, Lili Maxime Hauzer, Leroy Boerefijn, Bart Overes, Rens van der Nolle, Rahul Harit, Adrián Estrada, Floris van Elteren, Bart Holtzer, Jimmy van Schoubroeck and Thijs Smit for making it one of the best environments to work on my master thesis.

Lastly, I'd like to thank my friends and family for supporting me throughout all of these years of my studies.

Ryan van Dommelen
Delft, September 2017

Abstract

The structuring of polymers on the micro and nanoscale is performed largely by lithographic techniques, which require complex steps and suffer from geometrical and scaling limits. Techniques such as Nanoimprint Lithography and Hot Embossing are attractive alternatives as they can produce high quality nanoscale structures with a high throughput. Colloidal building blocks offer a way to self-assemble the masters required for these replication steps. However, the difficulty with self-assembly lies in the creation of stable structures with little defect that are well controlled. This work sets out to provide a comprehensive overview of the aspects of the fabrication of colloidal crystals, the most influential parameters and how they can be qualified. Offering a basis for future research on microscale replication by colloidal crystals and resulting in development of a method for the fabrication of colloidal crystal, which can be used as a master to replicate microscale patterns through Hot Embossing.

Contents

1

Project

1.1. Introduction

In order to pattern polymers at small scales the most frequently used techniques are those where a prefabricated pattern (master) is replicated into a polymeric material (target). In these processes a viscous pre-polymer is usually compressed into the geometrical features of a master. After which it is cured by means of an energy activation, such as a temperature change or exposure to light, resulting in a cured polymeric copy of the master[1]. In order to fabricate the master a top-down method is usually applied, where material is removed from the bulk, such that the desired structure remains[2]. Photolithography is one such method commonly used to produce these masters, as it is well established. Mainly due to intensive application in the high-tech industry which, due to the existence of a continuous desire to scale down feature sizes, has led to significant advances over the last 20 years in terms of minimally achievable resolutions[3].

Photolithography can also be directly used to pattern polymers, but this is not without some significant caveats. First of all, the number of steps to produce polymeric structures this way is often tenfold or more, which are performed in a strictly linear fashion. Secondly, due to the nature of many polymeric materials, defects can be introduced by thermal deformation as a result of the exposure steps. In response to these problems, fabrication by replication of a master has become more popular and a large number of micro and nanoscale patterning strategies have been developed. These methods are especially of interest as they are often low-cost, while still allowing for complex geometrical structuring of polymers[4]

Most masters are fabricated by a top-down approach, but fabrication of the master by a bottom-up process is also possible, wherein material is added in steps until the desired structure is formed[5, 6]. One bottom-up method of especial interest is self-assembly. Where small prefabricated building blocks, such as nanoparticles, are allowed to construct themselves into final, reversible, structures. Herein inspiration is often drawn from nature, where these processes occur on an ubiquitous scale[7]. Small particles suspended in a solution, so called colloidal particles or colloids, can be used as building blocks within the self assembly process. By setting the conditions such that they form into predetermined colloidal structures[8].

Using a colloidal structure to replicate features is an area that has until thus far not seen much research, but has high potential within replication techniques. Therefore, this thesis serves as an investigation into the feasibility of using such colloidal structures as a master for a hot embossing replication technique.

1.2. Research Goal

Effective research is performed by clearly stating the desired end result. Therefore, the following goal is proposed:

"To determine the feasibility of a using self-assembled colloidal crystals in a hot embossing pattern replication technique, in order to fabricate microstructures into target polymers"

1.2.1. Research Checkpoints

To evaluate the effectiveness of the goal a number of checkpoints need to be established. These serve as a guidelines within the research and allow for reflection. These are asked in the form of questions that this thesis sets out to answer.

- What are the requirements for a colloidal stamp in a hot embossing replication technique?
- How can colloidal crystals be manufactured such that they are suitable for the stamp requirements?
- How can the quality of the colloidal crystals be determined in a qualitative manner?
- Is it possible to use these colloidal crystals in a pattern replication technique, such as hot embossing?

1.3. Thesis Outline

To achieve these checkpoints the thesis is divided into the following sections. Starting with a literature study aimed at documenting the physics, available self-assembly methods and current research on replication by colloidal structures. In order to give an overview of the current state of technology. Then follows a chapter on the experimental approach towards fabrication, quality control and replication of the colloidal structures, which aim to answer the last three questions. Finally this thesis is ended with a reflection, where the approach to the experiments is discussed and a look back is provided onto the presented work. All material not directly relevant to the main body of the thesis is located in the appendix.

2

Self-Assembly and Colloidal Particles

Self-assembly is the process wherein a structure is assembled without the influence of external forces. Excluding manipulation by robots and direct interaction with the building blocks, making the process spontaneous[7]. Due to this inherent autonomy it is seen as a promising step in fabrication of nanostructures and further miniaturization[9, 10]. Structures would be able to be assembled with a high degree of precision, due to the minimization of energy leading to the final state of assembly. Which could lead to fewer defects and higher stability[11]. An important distinction is that between direct and indirect self-assembly. In the former a global minimum energy is reached in a purely self-governing fashion. While in the latter the system is designed in such a way that the building blocks end up in a local minima. Therefore, directed self-assembly requires a high level of control. However, it does allow for a larger variety of structures[12].

One of the building blocks for self-assembly which have been intensively studied are the colloidal particles. Ranging in size from a few nanometres up to a single microns, they are of such a size that they are subject to Brownian motion, which are naturally occurring thermal fluctuations[13]. However, this also makes them suitable to be suspended in a variety of liquids, forming so called colloidal suspensions[14]. Their most attractive feature is their tendency to form organized structures. Which allows them to be used as intermediate building blocks[12].

Synthesis of colloidal particles can be difficult, although it is often performed accompanying the research on self-assembly[15]. One key challenge is the creation of monodisperse colloidal suspensions, which is an indication of the uniformity of the particles in size in a solution[16]. Fortunately, a large number of micro-size particles, especially silica (SiO2) and polystyrene (PS), are readily available commercially[17].

Next some basic aspects of colloidal particles and their physical interactions are discussed.

2.1. Colloidal Crystals

Crystallization is usually described as the process of organization of small groups of molecules into larger, well ordered structures, called phases. The process of crystal formation is largely driven by the nucleation of these groups of molecules. Different crystalline structures can exist within the final compound also know as polymorphism[18]. As colloidal particles can be seen as an analogue to simple atomic liquids and solids, they too can form crystalline structures, called colloidal crystals[19]. Spherical colloids have been used predominately in the past, as they have only a single degree of ordering[20]. The most common crystal forms for such particles are hexagonally close packed (*hcp*) and cubic close packed crystal (*ccp*) structures[6]. The formation of these can be described by looking at the thermodynamic minima or entropic differences between the two crystal lattices. In terms of minimum Gibbs energy, it was determined that the *ccp* structure was slightly more stable than the *hcp* one. However, both share a similar two-dimensional close packed structure. The difference between the two is the stacking within the third dimension[21, 22]. To express the total amount of space occupied by particles versus available space the packing density is used. For close packed structures the packing density is around 90.7%, while for a square packed lattice it is 79%[23]. To illustrate the previous points, a sketch of all possible crystal structures in two dimensions, and the structures of both

the *hcp* and *ccp* structures are shown in figure 2.1.

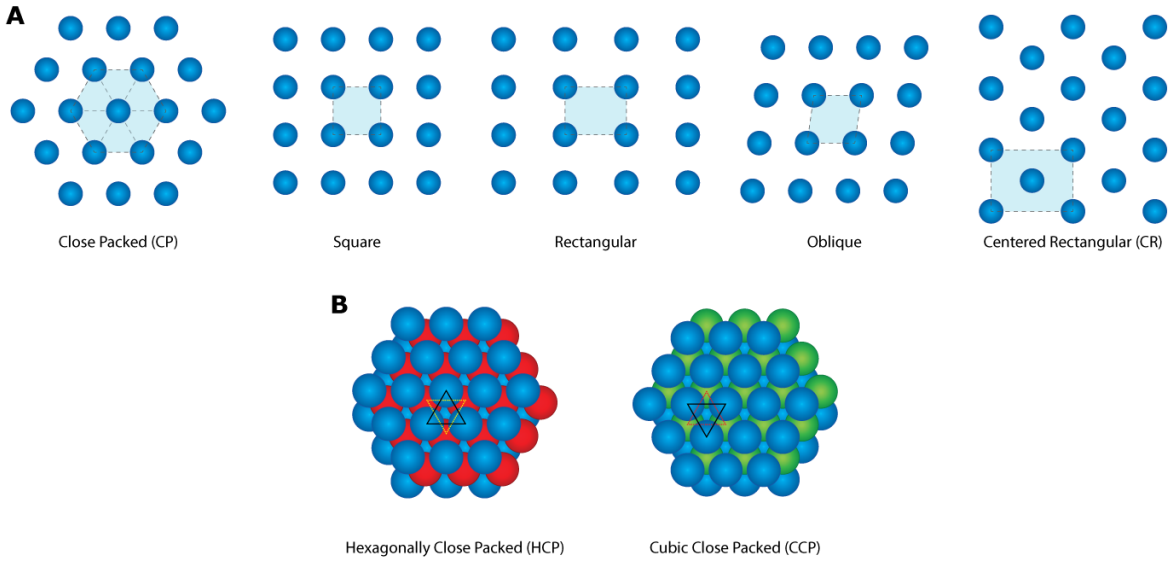

Figure 2.1: **A**) An overview of the five 2D crystal structures possible. **B**) The subtle difference between *hcp* and *ccp* crystals.

2.2. Colloidal Interaction

Understanding the interactions between colloidal particles is important to get insight into the formation of colloidal crystals. A large number of interactions exist between particles, and as such only the most important ones in the context of this project will be briefly discussed. The most important distinction to be made is between the scales of the interactions. Because colloidal particles are in fact aggregations of atoms they are subject to nanoscopic forces, but self-assembly generally deals with long range ordering and interactions. Therefore, modelling choices for such systems have to be carefully weighed dependent on the particle size[22, 24]. Because the particle range for this project ranges from 300 nm up to 5 µm, the nanoscopic forces will only briefly be treated. For a comprehensive review the reader is referred to [24].

2.2.1. van der Waals Interaction

The van der Waals (vdW) interaction is, an usually, attractive electrostatic force resulting from the electromagnetic effects of atomic interaction which is present between any two material bodies. The effect of which is significant as the energy of the vdW interaction is a hundred times higher than the thermal fluctuations causing Brownian motion, which makes it possible to exploit this energy to drive self-assembly as well. However this works most effectively for small, nanosized, particles, as the vdW interaction is short ranged. Becoming dominated by other forces when surface separations exceeds 10 nm, after which its influence falls off rapidly. The most exact continuum based estimation of the vdW forces is the Dzyaloshinskii, Lifshitz, and Pitaevskii (DLP) method, also known as the Lifshitz theory[24, 25]. Where the interaction energy between opposing continuous planes is determined. The Lifshitz interaction energy for flat parallel infinite planes, without the influence of temperature, is given by

$$U^{\mathrm{A}}_{\mathrm{vdW}}(h) = -\frac{A_{\mathrm{H}}}{12\pi h^2} \quad \text{with}$$
$$A_{\mathrm{H}} = \frac{3\hbar}{4\pi}\int_0^{\infty}\left(\frac{\epsilon\,(i\omega)-1}{\epsilon\,(i\omega)+1}\right)^2 \mathrm{d}\omega \tag{2.1}$$

Where h is the distance between the planes, A_{H} is the Hamaker constant which prescribes the magnitude of the vdW forces and $\hbar$ is the reduced Planck's constant. Lastly, $\epsilon\,(i\omega)$ is the macroscopic dielectric function, which describes the effect a time-varying field has on a charged particle. Less exact

results can be achieved by using the Hamaker integral or Derjaguins approximations[26, 27], which are slightly simpler in terms of use, and are permissible on the larger scale.

2.2.2. Electrostatic Interaction and the Electrostatic Double Layer

Electrostatic interaction prescribes the either attractive or repulsive interaction between charged particles. When particles have the same charge, that is both either are negatively or positively charged, they repel due to the effect of each others respective electric field. However, when the charges are not opposing, where one is positively and the other negatively charged, they attract. Secondly the forces can be directive and, when considering continuous bodies, surface charges can be asymmetrically distributed[24, 25].

When particles are suspended in a liquid, the electric double layer effect comes into play. Which is a phenomenon that is most prevalent in strong electrolytes. A layer of ions both positively charged (cation) and negatively charged (anion) gathers at the surface of a solid, such that a charge equalized electrostatic layer forms. As this layer creates an electric field, two or more particles will be slightly repulsive. The decay of its influence which is usually expressed in terms of the Debye screening length or screening effect. Several formulations exist to express the electrostatic potential. In terms of surface charge it can be expressed by

$$U^{\mathrm{A}}_{\mathrm{EDL}}(h) = \frac{\epsilon\kappa}{2}\left(\psi^2_{\mathrm{p},1} + \psi^2_{\mathrm{p},2}\right)\left[1 - \coth\left(\kappa h\right) + \frac{2\psi_{\mathrm{p},1}\psi_{\mathrm{p},2}}{\left(\psi^2_{\mathrm{p},1} + \psi^2_{\mathrm{p},2}\right)\sinh\left(\kappa h\right)}\right] \tag{2.2}$$

Where ϵ is the dielectric permittivity, $\psi_{\mathrm{p},1}$ and $\psi_{\mathrm{p},2}$ describe the surface potentials for two independent surfaces. Lastly, κ represents the inverse Debye screening length. Although the electric double layer provides a good estimation of the electrostatic repulsion, it does have some shortcomings. Namely, the assumption is made that the potential is constant over the entire layer and that the ionic density is constant over the entire surface. Or more simply said, a layer of ions that is considered continuous is formed. This continuum assumption results in an under or overestimation at very small scales. Treating the electrolyte as a molecular liquid instead of a continuum solves the inherent errors[22, 28].

2.2.3. Interactions in Media and at the Interface

Colloidal particles in highly concentrated media are subject to steric effects. Where the presence of other particles in the liquid physically blocks further ordering or material deformation. One key steric effect is the depletion interaction. When particles suspended in a solution approach each other, and a solute molecule no longer fits in between them. The particles are then pushed together, as the surrounding molecules of the liquid exert an osmotic pressure. This effect is especially prevalent in macromolecular solutions, such as liquid crystals and polymers[24, 30].

Attractive capillary forces originate due to the formation of liquid bridges, also known as the meniscus, which forms between particles due to surface tension. Their behaviour can be modelled with the Laplace Pressure[31].

2.3. Colloidal Self Assembly Techniques

Colloidal particle self-assembly has been intensively studied over the years[7]. And as such a wide variety of methods exist which allow the creation of either monolayer or multilayer colloidal crystals. Mostly in *ccp* or *hcp* crystalline form, due to their thermodynamically preferable states[32]. For the transfer of a micro-pattern into a polymer, it is important to have a negative with a precisely controlled morphology. As the replication of patterns into polymers can be a very sensitive process[33].

Potentially, precisely controlled structures could be achieved by directing the self-assembly of the colloids not into global minima, but into different local and stable states, such that novel structures can be developed. Where spherical colloids are of special interest as they are produced on an industrial scale[34].

A short overview of widely used self-assembly methods is given which is divided into four main

categories: Physical, Fluidic, External Fields and Chemical. These categories are chosen such as to indicate what the origin of the dominant forces within the self-assembly process is. A graphical overview of the evaluated methods is given in figure 2.2, and an overview of all relevant parameters is presented in appendix C.1.

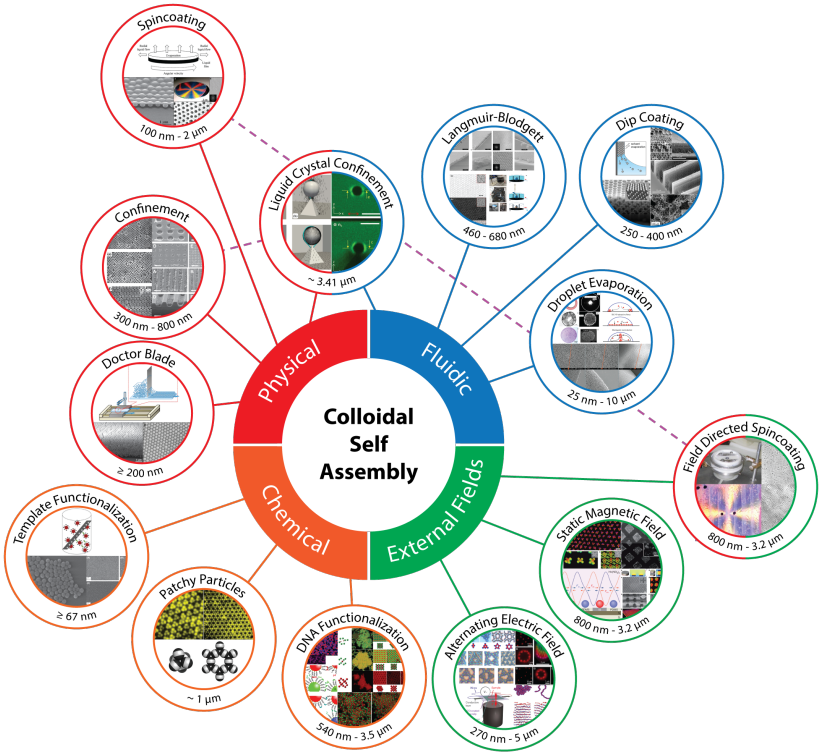

Figure 2.2: The web of colloidal self-assembly. In which each of the four domains indicate the major influence on the self-assembly process. Specific properties of the Self-Assembly methods are presented in appendix C.1.

2.3.1. Fluidic

For fluidic methods the governing forces are resultant from the interactions of the medium. That is, the crystals are a product resulting from surface tension, evaporation, capillary forces or a combination. These methods are already quite well developed because of their simplicity and compatibility with different materials. Still, they come with some unique challenges that have to be addressed in future research.

Deposition Techniques

The formation of monolayers has long been well understood as these can be simply synthesized through a device called the Langmuir-Blodgett through[35]. The working principle is simple and is commonly used with surfactants, such as oil. However, it can be applied to colloidal particles as well, as long as they allow the formation of a monolayer at an interface. When a colloidal suspension is dispersed on the surface, the colloids spread as far as possible, forming a spaced monolayer on the surface. When the film is compressed, through a barrier which reduces the available surface area, the surface tension of the film increases. When a substrate is then 'scooped' through this compressed film, the lower surface tension provided by the substrate will cause the colloids to transfer from the interface. In figure 2.3 a schematic drawing of the previously described process is shown.

A Langmuir-Blodgett type method to fabricate multilayered colloidal crystals was conceived by Reculusa and co-workers[14]. Diluted suspensions of ethanol and silica particles, were created. These were dispersed until they covered approximately 25% of the surface area of a standard, water filled, Langmuir through. All crystals were prepared on hydrophilic glass as tests with hydrophobic glass had no particle retention. Transfer was achieved by dipping the glass into the subphase and slowly pulling it out. By repeating this step several times multiple layers could be achieved, which were structured into

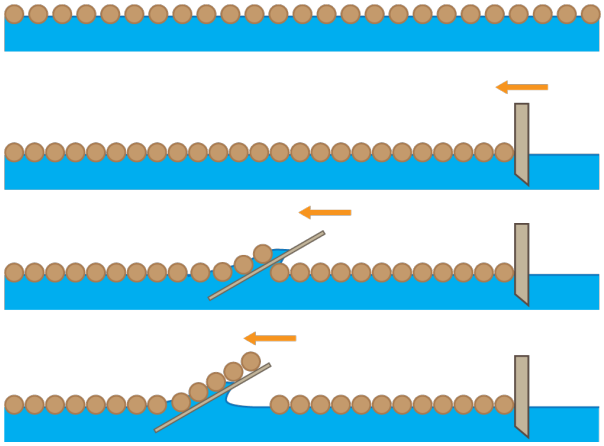

Figure 2.3: Schematic drawing of the Langmuir-Blodgett method.

a *hcp* crystal. Images of both the single and multilayer crystals are shown in figure 2.4. Long range ordering was observed for surfaces of 100 μm^2 in size, but some local defects and grain boundaries were still present.

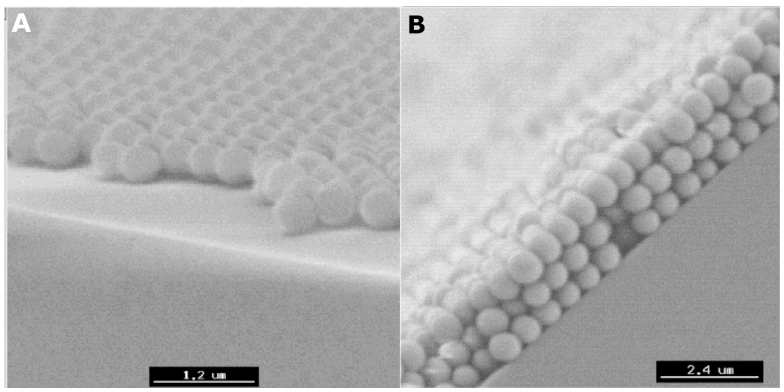

Figure 2.4: SEM images of the colloidal crystals produced by the Langmuir-Blodgett method. **A**) A monolayer of colloidal crystals manufactured by the method. **B**) Multiple layers of colloidal crystals by performing the procedure several times. Adapted from [14].

The techniques has its limits in terms of particle size and functionalization. As some functionalization causes silica particles to end up on the liquid side of the subphase under increasing pressure, preventing transfer to the substrate. A coupling agent was used to retain the film on the interface, but this resulted in an unordered crystal on the substrate.

Crystal damage can easily occur in Langmuir based processes due to capillary forces, as when a substrate is scooped in or the water level is lowered it can result in particles adhering to the walls, causing stresses within the crystal. A method developed by Lotito and Zambelli[36] prevents these stresses. In their method a monolayer composed out of 200 nm PS spheres is formed on the air-water interface within a floating rubber ring. By lowering the water level gently at a controllable rate, to prevent the occurrence of turbulent flows, the monolayer transferred onto a substrate which was placed underwater. In this fashion, square samples up to about 6.45 cm^2 and circular samples with a diameter of up to 10.15 cm cm were fabricated. By combining particles of two different sizes so called binary colloidal crystals were produced, in which smaller spheres filled the interstices of the larger ones. However, these crystals showed to be more defect prone than their non-binary counterparts. Figure 2.5 shows an image of this setup, working principle and sem images of the binary crystals.

Another method developed by Hatton and co-workers[37] combined a sol-gel precursor, tetraethoxysilane (TEOS), with Poly(methyl methacrylate) (PMMA) particles, with a diameter between 250 and 400 nm suspended in deionized water. The addition of the silica gel caused the particles to stick together better, forming temporary ”glue-like” connections. A substrate was put into the suspension,

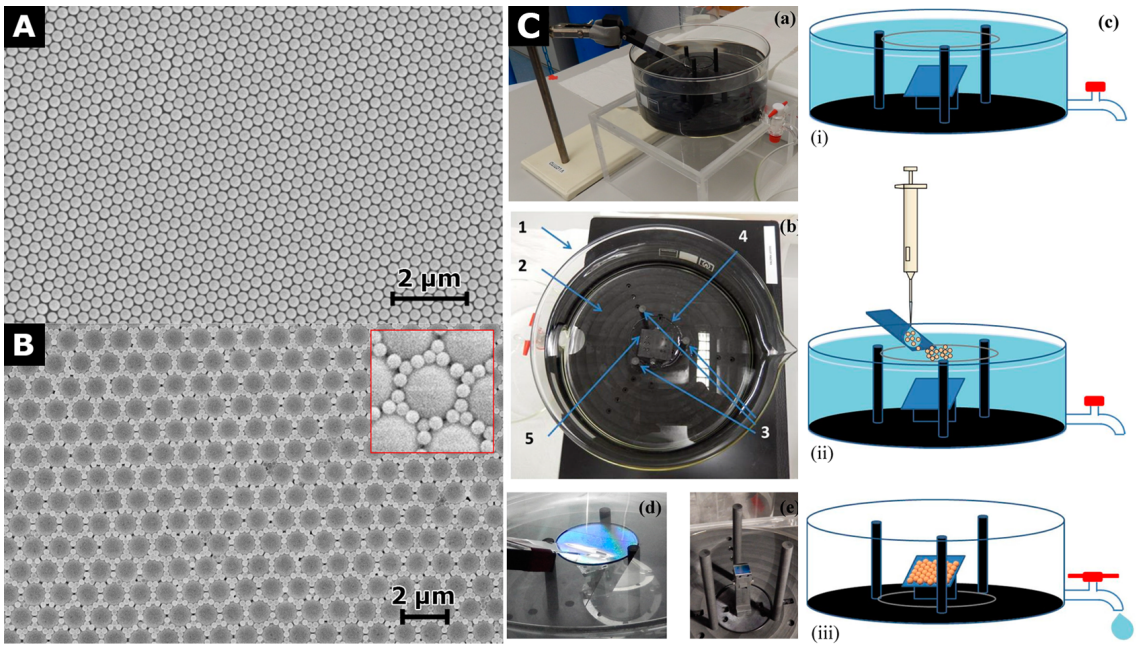

Figure 2.5: Pictures and schematic drawing of the setup and resulting binary crystals. **A**) Hexagonally close packed crystals. **B**) Binary crystals, formed from a suspension with two distinct particle sizes. **C**) Demonstration of the setup. A colloidal monolayers forms on the air-water interface and the water level is lowered, allowing the transfer of a colloidal crystals onto the interface. Adapted from [36].

around which a meniscus formed due surface tension causing transfer of the particles. By increasing the temperature to 65 °C the depositing meniscus evaporated and slowly travelled down the substrate, until the suspension was fully evaporated after 1 to 2 days. The final crystals consisted of 18 to 20 layers, with an additional benefit that the formation is independent of the shape or curvature of the substrate.

Droplet Deposition

Generating colloidal crystals by evaporating droplets of colloidal suspensions is a popular self-assembly technique due to its simplicity and speed. However, it is a method which remains difficult to control as flows within the droplets caused by rapid evaporation lead to non-uniform patterned surfaces. Large numbers of particles end up either near the edge or in the centre. This is popularly known as the coffee stain effect. An analysis performed by Bhardwaj and co-workers[38] showed that the effect can be overcome by altering the pH value of the suspension.

In their experiments, titanium dioxide particles with a diameter of 25 ±2 nm were suspended in water, with a volume fraction of 2 %. Droplets of 4 to 6 nL of this suspension were then dispersed and allowed to evaporate in dry air. By adding either hydrochloric acid or sodium hydroxide the pH value of the suspension was lowered or increased, respectively. The effect of which is that the adhesive forces are either attractive, at low pH values, or repulsive, at high pH values. This causes particles to form in a well defined ring at high pH values, but deposit themselves over an uniform surface at low pH values. However comparing experimental to numberical data revealed discrepancies, the influence of which they suspensed was the van der Waals forces between particles and the change in adhesive forces over time, as the pH value changes during evaporation.

Droplets of colloidal suspension can be deposited by using an ink-jet method, as demonstrated by Ko and co-workers[15]. They prepared a colloidal ink with 330 nm silica particles at 5 wt % fraction, which was almost seven times more viscous than water at room temperature. Droplets of 189 ±6 pL were then deposited onto several different substrates with varying contact angles. The influence of which has a high impact on the formation of the final colloidal crystal. For a high contact angle, the final colloidal crystal was hemispherical in nature and close packed, with a packing factor up to 77 %. While for low contact angles the packing density could be as low as 24 %, with flat disk-like randomly structured aggregates and a well ordered monolayer at the edge. By looking at the mechanics of evaporation the resulting structures can easily be explained. For flat droplets, with a low contact

angle, the evaporation mainly takes place at the edge. Such that new particles are drawn by capillary forces from the thicker section of the droplet which pin on the contact edge. However for spherical droplets, on the hydrophobic surface, the degree of evaporation is uniform over the surface, resulting in a close packed aggregate.

Majunder and co-workers[39] established a simple method in which they observed an alcohol saturated atmosphere to increase the contact angle and reduce the evaporation rate. Silica particles with diameters between 3 and 10 µm were resuspended in water at a 0.25 % volume fraction. Samples were then placed in a petri dish with four compartments, of which three of the four were filled with ethanol and remaining with a colloidal droplet.

As the ethanol evaporated the entire dish became saturated by ethanol vapour, infiltrating the droplet and causing a flow that recirculated the colloidal particles away from settling. Secondly, the absorption of alcohol by the droplet causes the droplet's contact angle to lower and wetting to increase, increasing the area for the particles to settle. Without the ethanol vapour particles settled after around 10 to 15 minutes, while in an ethanol saturated atmosphere the particles were still circulating after 40 minutes. After removal of the alcohol atmosphere aggregations in form of a ring at the edge were still observed.

2.3.2. Physical

Methods described as physical are considered to rely on self-assembly where a template, force or shear drives the formation of the colloidal crystal. These kinds of self-assembly methods generally have a high throughput and make use of well established manufacturing techniques. Therefore, this makes them foremost candidates for large-scale industrial application.

Spincoating

Spincoating is widely used in the semiconductor industry to create uniform layers of photoresist onto wafers for lithographical etching. After a solution is dispersed onto the spincoater, the substrate is rapidly accelerated causing centrifugal forces. This will causes mass to be ejected and results shear which thins the liquid film. The minimal thickness of which is dependent on the balance between adhesive forces and the shear. Ultra thin films down to several tens of nanometres can be reached, depending on the used solution[40].

A spincoating technique was developed by Jiang and co-workers that allows rapid production of colloidal crystals out of silica particles. Where they varied the particle diameters from 2 µm down to 100 nm. Commercially available monodisperse silica particles suspended in ethanol were purchased, which they centrifuged to separate the particles from the ethanol. They were then resuspended into the viscous, non-evaporating and non-volatile monomer ethoxylated trimethylolpropnae triacrylate (ETPTA), to which a photointiator (Darocur 1173) was added to enable UV curing.

Silicon substrates were primed with 3-acryloxypropyl trichlorosilane (APTCS) to prevent peeling of the cured ETPTA. On these substrates 600 µL of the suspension was dispersed and fully spread by manual manipulation. To achieve a thin films, two spincoating steps were performed. First the wafer was spincoated for half a minute at 200 rpm until a six armed monochromatic diffraction star appeared, which is due to there being a *hcp* crystal lattice. In the second step, the spin speed is accelerated at 2000 rpm/s to a final spin speed, depending on the desired film thickness. After spincoating, the wafer was transferred to a nitrogen filled chamber where the ETPTA was polymerized by UV light.

Oxygen plasma etching was used to liberate the silica particles from the polymer matrix. Etching only affects the polymer and also prevents the formation of defects in the colloidal crystal, such as cracks. Five minutes of plasma etching was needed to fully remove a 30 µm thick layer of ETPTA, however shorter etching time also allows partial liberation of particles. After the removal of the polymer matrix SEM Imaging showed that the crystals had a *hcp* structure. However, the top most layer was found to deviate, being non-close packed (*ncp*) with a centre-to-centre distance of $1.41D$, where D is the particle diameter.

The *hcp* structure can be explained by the following observations. Shear plays a dominant role in the crystallization, causing layers of the crystal to be slide over each other during the spincoating. Electrostatic repulsion had little effect on the formation, as adding salts to the dispersions had negligible effects. Vertical packing is dependent on a pressure gradient normal to the spun film, with the highest intensity at the substrate. The researchers believed that the photo-polymerization step also plays a

role in the final crystalline structure. As the ETPTA film shrunk towards the substrate during curing [41].

Using the previously described method proved to be very difficult for creating colloidal monolayers, as experimental reproduction was poor. Discontinuous islands of disordered colloids were found with surface areas as large as 1 mm^2. Therefore a second study was performed aimed towards producing monolayers. Silica spheres with a 315 nm diameter in ETPTA were deposited onto a silicon substrate, priming it with APTCS which also lowered the contact angle of the suspension from about 60 degrees down to 10 degrees. Which was required to completely wet the substrate in order to obtain an uniform monolayer. One major change was the angular spinspeed being much lower, at 200 rpm/s instead of 2000 rpm/s. With the initial spin speed set to 200 rpm the speed was increased in five steps up to 8000 rpm, with the spin speeds being held constant for several minutes in between.

Using this stepwise method, monolayer polycrystalline colloidal crystals were found with a domain size smaller than for the multilayered crystals. However, a centre to centre distance of $1.41D$ was observed, similar to the particles on top of the multilayered colloidal crystals. Over fifty samples were prepared and all resulted in monolayer crystals.

The technique is simple and fast, with the sample preparation time around half an hour. However, the self-assembled monolayers remain quite fragile[42].

Mechanisms, Limitations and Optimization of Spincoating

Even though colloidal crystallization by spincoating is a promising technique, it is limited by defects. Many of which are the result of improperly tuned parameter, such as spinning speed and acceleration[36].

As most colloidal suspension are commercially provided in evaporating solvents, Toolan and co-workers[19] sought to better understand the balance between shear forces, generated by the spincoating, and the attractive capillary forces caused by evaporation. As adhesive forces are dominated by the convective particle flux, the capillary forces will interfere with the growth of the crystal. To study these interactions they observed the spincoating of the crystals before evaporation of the dispersant. This was performed by spinning dispersions at 1250 rpm and observing the samples with a stroboscopic microscopy. In their experiment they used 5 µm PS particles which were dispersed in both water and ethanol in at various concentrations.

With a low mass fraction the particles initially spread out in a loose and random order due to shear thinning, where they are mainly seen to be moving in clusters. A few seconds later evaporative thinning dominates the shear thinning of the spincoating, which causes a radial outflow away from the centre. Ordering in the crystal takes place due to capillary effects, where wetting fronts push the particles away. However, if the shear forces are too high gaps can appear in the crystal as clusters detach from each other. After 16 seconds the morphology becomes fixed, except that any gaps which formed earlier grew in size as they filled with fluids.

A high mass fraction resulted in close packed structures forming earlier and small multilayer crystalline regions being separated by defects, opposed to incomplete monolayers found at lower mass fractions. Therefore, evaporation of the dispersant was shown to play a dominant role. For the ethanol dispersions no radial outflow was observed and a densely packed monolayer forms after just 1.5 seconds, on top of which a layer of disordered particles forms, due to the rapid evaporation.

By applying statical experimental design Cheng and co-workers[43] managed to optimize and identify the most important parameters for producing colloidal monolayers. Through their optimization of a two-step spincoating process they produced defect free surface areas larger than 0.003 mm^2. What they identified is the relative humidity of the environment plays a large role in the final quality. This was explained due to the mechanisms behind the formation of colloidal monolayers, which they fabricated by spincoating 1.5 µm silica particles suspended in ultrapure water at 25% wt. As the water film is less thick than the silica particles being spun, capillary forces between the particles cause them to become closely packed. As particles travel, unoccupied sites cause water to evaporate and lead to convective flow which pull in new particles, causing crystal growth. However, if the humidity is too high there will be very little evaporation and longer spinning speed times are necessary. Diffusion of particles can also occur when there is too much water, which leads to defects.

Surface Structuring and Confinement

By modifying the surface of a substrate certain conditions can be generated that precisely steer particles into global minima. An example of this a technique which is based on modifying a substrate by a

holographic technique, which was applied for colloidal patterning by Ye and co-workers[44]. A thin polymer film, containing azobenzen, was treated such that a sinusoidal pattern was formed in the film. Subsequently, the film was deposited vertically into a vial containing an aqueous suspension of PS spheres which was heated to 55 °C. Slow evaporation, as described in the section on deposition techniques, lead to the self-assembly by a meniscus. After the main body of liquid had evaporated from the surface, capillary forces resulting from slowly evaporating liquid within the surface structures drew any particles close by into the final formation.

Varying grid spacing and particle size allowed different crystalline structures to be created. A ratio between the two was defined as $x = d/p$, where d is the particle diameter and p the period of the holographic wave. In figure 2.6 all crystal lattice can be seen which were found by varying x.

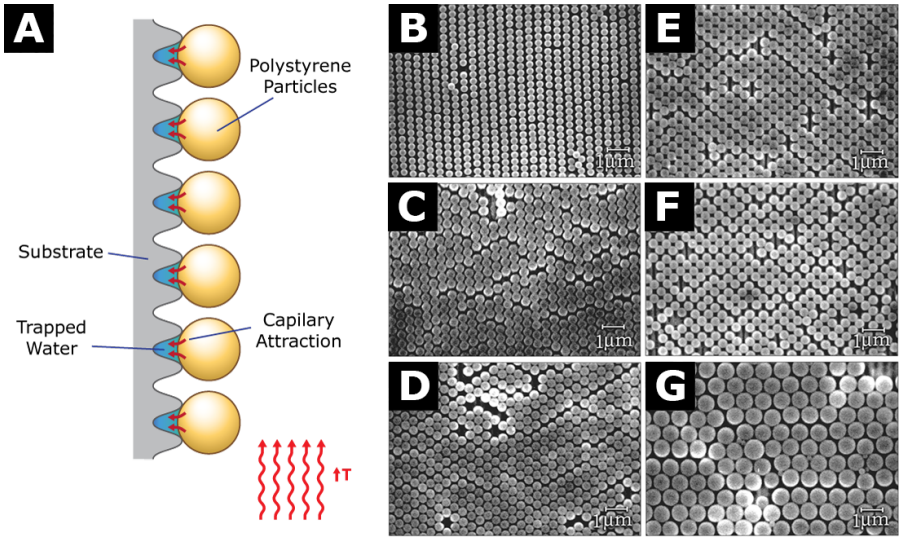

Figure 2.6: SEM images of colloidal patterns resulting from template driven self-assembly. **A**) Schematic drawing of the modified substrate and the capillary attraction exerted on the colloidal particles under heat induced drying. **B**) Stripe structure, (x = 0.74). **C**) 2D centered-rectangular lattice, (x = 1.05). **D**) 2D hexagonally close packed lattice, (x = 1.15). **E**) 2D centered-rectangular lattice, (x = 1.33). **F**) 2D centered-rectangular lattice, (x = 1.4). **G**) 2D hexagonal latice, (x = 2.0). Adapted from [44].

Trapping particles is a popular option and can also be performed on particles below 100 nm, as shown by Xia and co-workers[45]. Substrates were patterned by photolithography such that physical grooves and holes were created which could trap the particles during spincoating. Nano grooves and holes were etched into a silica surface with dimensions of less than 200 nm, trapping silica spheres, of around 80 nm in size and smaller, into the etched features. Altering the pH value of the aqueous colloidal suspension by either adding hydrocholoric acid (HCl) or an ammonia solution (NH4OH) altered the final position. When pH values were above 7 the silica spheres would get negatively charged and stick to the non-patterned surface more easily.

Trapping techniques were shown to effectively work on the nanoscale as well by Asbahi and co-workers. Nanostructures were fabricated by e-beam lithography and cleaned with UV ozone to enhance solvent wettability. Several different nanostructures were produced including trenches, posts, rectangular holes and comb-like structures. Of which the dimensions were determined in such a way that the evaporation of the suspension could be precisely controlled, and the final particle location could be influenced. Particles were synthesized and encased by oleylamine ligands with a 12 nm diameter and then suspended into hexane. The structured substrates were then dipped into the colloidal suspension after which they were slowly pulled out (0.1 to 0.5 mm min^{-1}). A thin meniscus consisting out of fluid and particles formed and evaporated until the van der Waals attraction was so strong that it prevented further evaporation. Depending on the fluid this value is around 5 to 30 nm, which is thin enough such that the heat flux through this area can be considered zero, and the liquid film will possess the same temperature distribution as the substrate, even when it is superheated. Secondly, the van der Waals attraction generates a disjoining pressure which causes the particles to be pushed into locations where the pressure is lowest, which for rectangular shaped cavities happens to be the corners. By exploiting this, several patterns are created, as shown in figure 2.7.

Untreated surfaces lead to particles gathering in hexagonal clusters, with holes appearing due to

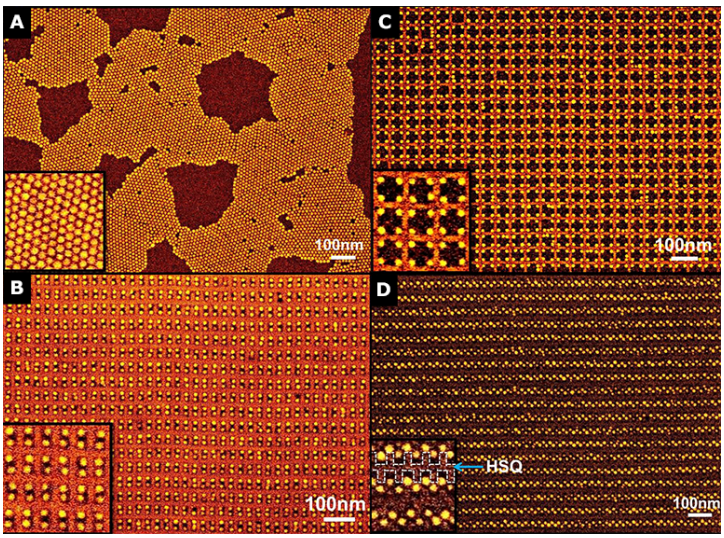

Figure 2.7: SEM images of colloidal patterns resulting from template driven self-assembly. **A**) Hexagonal lattice structure on an untreated surface. **B**) Array of two particles trapped in a single rectangular square. **C**) Array of squares with a particle trapped in each corner. **D**) Zig-zag pattern of particles trapped within a comb-like structure. Adapted from [46]

.

evaporative forces. For smaller features the final results are fairly defect prone. However, when the aspect ratio between particle and dimensions of the structures is increased, the number of over and under occupied sites increases as well. Statements are made that the film does eventually dry out, even though the evaporation was assumed to be contained by the van der Waals interaction. It is likely that some evaporation does occur which is not accounted for in the model, as it is based on Young-Laplace equation. Which assumes the fluid to be continuous[46, 47].

For well defined structures it is possible to predict and influence the self assembly process by minimizing the interaction energy between particle and substrate. Silvestre and co-workers[48] were able to predict and experimentally verify the energy minimization, and subsequent interaction, of a colloidal particle suspended in a liquid crystal interacting with a similar sized pyramid. Microfabrication methods were exploted to graft an epoxy pyramid onto a glass substrate, which was then placed in the liquid crystal 4-pentyl-4-cyanobiphenyl (5CB). The composition of the energy of the liquid crystal and surface potential led to an energy well at the tip of the pyramid. Silica and Melanin particles were placed in the liquid crystals and their position in relation to the pyramid were tracked by a fluorescent imaging technique.

Unfortunately, some of the particles were trapped slightly off the tip, indicating that the predicted energy well was off-centre. Surface irregularities of the pyramid, with respect to the model, were the most likely perpetrator. Steric effects were not discussed but might be influential in terms of large scale self-assembly[49, 50].

Shear and Gravity Assisted

A doctor blade is a device commonly used to print highly uniform films in the printing industry and used as well to create ceramic coatings. A perpendicular blade moves closely along a substrate, leaving only a thin film of the initially deposited material. Yang and co-workers[51] extended this technique to produce close packed colloidal crystals. An amount of 1 mL of silica particles suspended in ETPTA, with a 20-50% volume fraction, was deposited on one side of the blade. Then the blade was moved with a controlled speed and a thin layer was deposited in a disordered fashion. However, the layers themselves were each closely packed, such that there was only long range ordering in two dimensions. The disordered structures are a result of the shear force which, for viscous fluids, has a linear profile expressed as

$$\tau = -\mu \frac{\mathrm{d}v}{\mathrm{d}h} \tag{2.3}$$

Where μ is the viscosity of the suspensions, v the speed of the blade and h the thickness of the

film. Leading to a shear of an unequal magnitude for each layer, which has a direct limit on the usable particle size. Particle sizes smaller than 200 nm require a more viscous suspension agent to order the particles. Although the method is simple it is also very sensitive to dust and debris, which easily damaged the colloidal crystals and appeared clearly in the SEM images.

2.3.3. External Fields

In this section several methods are outlined in which external fields, magnetic or electric, play a dominant role in the final structure of the colloidal crystal. Since these fields are generally well understood they can offer a large degree of control on the final structures. As well as allowing the formation of three-dimensional structures.

Electric Field Driven

Self-assembly with electric fields on polystyrene ellipsoids was performed by Crassous and co-workers[52], by suspending them in a composite microgel in water which were then placed between glass slides separated at 120 µm coated with indium tin oxide (ITO). Blocking any passage of the electric field, except through the uncoated part. An uniform alternating field at 160 kHz was applied, to prevent particles from being attracted to the electrodes. Without the field, the particles were fully subject to Brownian motion. A field of at least $E \approx 25\text{kV m}^{-1}$ was used to overcome this, after which the particles align in its direction after which they form long string-like sheets due to electrostatic interaction, which eventually self-assemble into tubular structures. However, if the oblate radius of the ellipsoids was too low or the electric field too weak the suspension would only produce close packed aggregates. Half a minute was required for the tubes to form, although not all particles participated equally. After the electric field was turned off, the structures disassembled and the ellipsoids drifted randomly.

While the previous method shows the flexibility of self-assembly, the final result is unstable. With the deformation of the particles highly influencing the final structures. Yet particles don't have to be altered or functionalized in any way to be able to be influenced by an electric field, which was shown by Wu and co-workers[34]. By using the right concentration of salt and an oscillating alternating electric field, the interactions between particles can be carefully tuned. Polystyrene particles were synthesized and suspended in deionized water and trapped in-between two slides. By varying the salt concentration, formations of molecular like structures appear, as the forces that usually balance the dispersion are distorted by the applied field. In this fashion, several oligomers were created, including triangular aggregations such as pentagonal and hexagonal rings, honeycombs and islands. Both the salt level and field frequency impact the structure of the oligomers, albeit in different ways. If the salt concentration is too high a close packed monolayer formed, but a high frequency resulted in a decreased inter-particle distance. Again, these formations are unstable and highly sensitive to Brownian motion, volumetric effects and particle concentrations.

Electric fields can also be used to modify the colloidal crystals fabricated by spincoating. Such a modified method was developed by Bartlett and co-workers[53], where a non-uniform alternating electric field was added that rotated synchronous to the chuck, influencing the outward flow of the suspension. The addition of the field breaks the axial symmetry originating from the shear thinning and changes the orientation of the colloids. They suspected that their methods could be scaled down such that nanocolloids can be used, however no experiments had yet been performed.

Magnetic Field Driven

Demirörs and co-workers[54] showed that they could create colloidal arrays from particles that are both attracted (paramagnetic) and repelled (diamagnetic) by a magnetostatic field[25]. On top of a permanent magnet they placed a nickel grid, embedded within a spincoated PDMS flat composite structure, that focused the magnetic field into a predefined shape, which they dubbed virtual moulds. Particles were either trapped or expelled from these moulds, depending on their magnetic properties. Functionalization was performed on the surface to be able to attach amine functionalized particles. As the magnetostatic effect on small particles is very small, the most influential paremeters are the magnetic susceptibilities of the particles and dispersing medium. By tuning these, both paramagnetic and diamagnetic particles could have the same magnitude of force exerted on them, allowing a wild variation of patterns to be created. By taking advantage of the decay of the magnetic field, bridge-like structures were formed. Which form when the gravity and the magnetic force repelling diamagnetic particles balance each other. By applying a second layer on top the magnetic field was extended into an

hourglass shape, such that diamagnetic particles could be trapped in-between the fields in an egg-like shape. Several examples of both the 2D and 3D structures that can be created through this method are shown in 2.8.

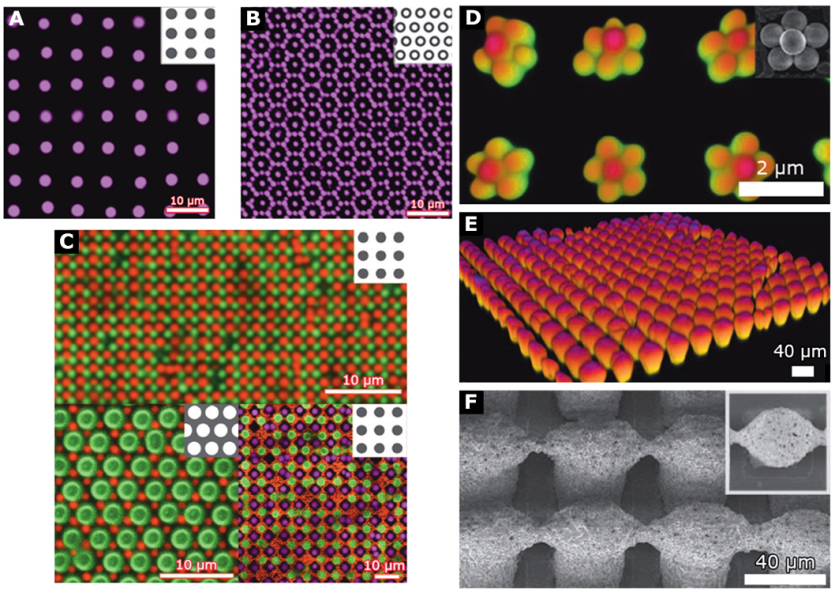

Figure 2.8: By using particles with different magnetic properties and of varying sizes, a myriad of patterns can be created with the same nickel-PDMS grid. **A**) Paramagnetic particles 2.85 µm in size assembled at the intersections of the nickel grid. **B**) Diamagnetic particles 1.2 µm in size assembled in a hexagonal pattern. **C**) Several grids created by combining paramagnetic and non-magnetic particles of different sizes. **D**) An assembly of colloidal molecules, formed out of particles larger than the grid spacing. **E**) Bridge-like structures formed by levitating particles. **F**) Egg-like structures formed in-between two magnet-grid sandwiches Adapted from [54].

2.3.4. Chemical

By altering the chemistry of a surface or template it is possible to control the interaction of chemical compounds. These kinds of interactions, while large in scale, can also be used to drive the self-assembly of colloidal particles. Therefore, an overview is given in this section where the resulting colloidal crystals are controlled or greatly influenced by chemical interactions.

Template Functionalization

By modifying the substrate onto which particles are deposited it is easy to self-assemble large amounts of particles. Li and co-workers[23] came up with a simple technique where they functionalized a normally negative silica surfaces with amine groups which turning the charge positive. By then introducing silica nanoparticles, of roughly 67 nm in size, they were able to create aggregates of particles on the surface. However, the functionalized monolayer is very sensitive to any impurities and degrades if contaminated. Using a colloidal suspension of 90% ethanol and 10% with a particle weight fraction of 2.04% the highest surface coverage was achieved. By adding salt to the suspension the screening length was reduced with which a maximum surface coverage of 84.2 % was observed. However no real close packed ordering was found which they concluded could not be achieved with electrostatic attraction alone.

Patchy Particles

By only functionalizing part of the particles, so called Janus particles, unique structures can be made. Chen and co-workers[55] funcitonalized only the poles of spherical particles to be hydrophobic, in order to make 'Kagome' lattices. When these spheres are suspended in deionized water they will try and reduce their wetting surface as much as possible, causing the poles of two particles to approach as close as possible. As the electric repulsion between the treated particles is not insignificant, salt was added to the colloidal suspension to reduce the electrostatic repulsion. This way the hydrophobic poles could approach each other close enough to form lattices, as seen in figure 2.9. To avoid agglomeration

onto the substrate, and hindering self-assembly, it was negatively charged, electrostatically repelling the lattice.

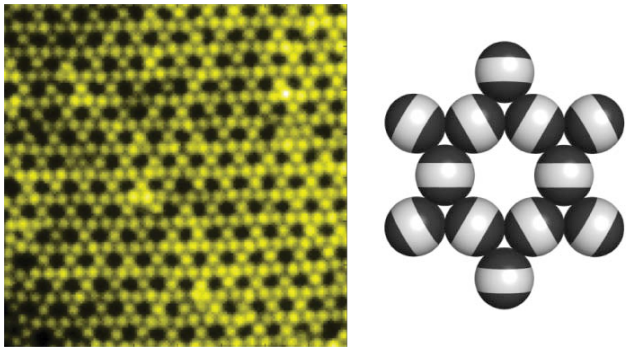

Figure 2.9: Fluorescence image of the kagome structure and a schematic representation of the particle-particle adhesion. Adapted from [55]

Although promising, the method is very slow since it can take up to ten hours for just 70 % of the particles to achieve the desired structure. This is partially explained due to transient nature of some of the lattice structures, as Brownian motion influences the shape. A follow up study[56] was performed, where the angle of deposition of the patches was further improved by introducing an etching step. Allowing functionalized patches at defined angles resulting in different lattice structures.

DNA Directed

By coating colloids with DNA they can be given a structure that diverts from the thermodynamically minimal position commonly found for untreated particles, as discussed before. The advantage of using DNA is that it can be activated and deactivated, effectively allowing programming of the self-assembly process. Di Michele and co-workers[57] functionalized streptavidin coated PS particles, with a size of 500 nm, such that single-stranded DNA (ssDNA) was attached in a shell around the particle. When activated the single-stranded DNA will combine into double-stranded sequences, causing particles with matching strands to be connected to one another. This process is commonly known as hybridization. They showed that it is also possible to have several different DNA strands with varying activation temperatures, allowing the formation of different structures by changing the temperature. Another major advantage of this technique is that DNA interactions can be thermally reversed.

However, as DNA is in the size of nanometres it is difficult to use programmable strands on microparticles. Therefore, Wang and co-workers[58] developed a technique in which they functionalized both silica and polymer particles with a large shell of ssDNA, up to 115,000 strands per particles, for particle diameters up to 3.5 µm. Using 1 µm particles they managed to create a three dimensional colloidal crystal that exhibit a *ccp* structure. And by combining particles of different sizes and complementary DNA strands they managed to create crystalline structures resembling those found in metalloids and fullerenes. However, the synthesis of large crystals remains difficult. As DNA has a very specific activation temperature and will not hybridize except unless this is reached. Lowering the temperature in turn decreases the amount of diffusion, which leads to formation of larger crystals. Therefore, the temperatures in the crystallization process have to be properly tuned. One major cause of defects within the DNA techniques are steric effects and misalignment of local crystals.

2.3.5. Modifying Colloidal Structures

As the minimum energy configurations of colloidal crystals are usually close packed, the potential applications are limited. Therefore, it may be desirable to modify the crystals into patterned or more spaced topographies. Modifications of the crystals can be performed in several ways. By using a technique called micro contact printing (μcp)[59], a PDMS stamp is used to selectively pick up particles from the substrate. Through mechanically stretching the substrate the inter-particle spacing can be increased anisotropically. Isotropic spacing can be achieved by the PDMS with a non-polar solvent such as toluene. However particles don't readily adhere to PDMS as it has low surface energy. Application of an adhesive monolayer onto the PDMS can make it 'sticky'[11]. Another option is to either partially cure or to treat the PDMS with oxygen plasma etching, as it is viscous when unpolymerized[55].

2.4. Polymer Micro and Nanostructures fabricated through Colloidal Self-Assembled Structures

As self-assembly methods are simple, cheap and flexible, they are ideal candidates towards creating sub-micron features in polymers. Preventing having to resort to complicated techniques and machinery, such as lithography. This section sets out to show polymers structured by patterns created through self-assembly. As well as where potential opportunities are available to further improve on them.

2.4.1. Surface Structuring

Several different polymer nanostructures were fabricated by Trujilo and co-workers[60] by combining a colloidal mask with the Initiated Chemical Vapour Deposition Technique (iCVD)[61]. The colloidal mask, which was fabricated out of self-assembled monodisperse PS nanospheres, acted as a geometrical constraint for the polymer patterning. Before deposition of the polymer, a silane coupling agent was applied to the substrate to improve adhesion. With the mask attached to the surface, the polymers were deposited using the iCVD technique. Wherein the pre-polymer vapours are guided past the hot filaments which initiates a free radical polymerization process, removing the need for a curing agent. As this makes the method non-wetting, it allowed the polymer to infiltrate into the interstices and graft layers starting from the substrate. Resulting in a consistent morphology, as the deposition, at a rate between 30 and 200 nm/min is not influenced by any capillary effects. As polymers are not required to be soluble, and the operating temperature of iCVD is relatively low, polymers which are usually excluded by other CVD techniques can be used.

Lastly, the colloidal mask was removed by placing it in a solution of Tetrahydrofuran (THF) and ultrasonicating it for 10 minutes. To ensure all colloids were actually removed, the sample was placed in a fresh solution of THF for at least 8 hours. A schematic overview of the method is shown in figure 2.10.

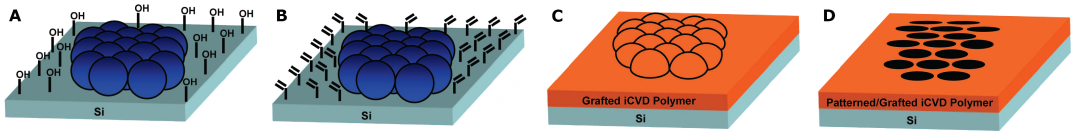

Figure 2.10: The four main steps of the method illustrated. **A**) Surface after hydroxylation and colloidal mask application, **B**) application of vinyl-silane coupling agent, **C**) application of polymer film through iCVD method, **D**) patterned film after removal of colloidal mask through treatment with Tetrahydrofuran (THF). Adapted from [60].

Several different polymers were grafted in this fashion, with widely varying properties. From superhydrophobic pPFDA films, pHEMA films which, when cross-linked, can absorb large amounts of water and swell up to 55% in volume and pPFM films which are able to immobilize biomolecules. Reducing the particle size of the colloids in the mask in turn reduces the dimensions of the features. By using 80 nm particles a minimal feature size of 25 nm could be achieved.

A variation to this method was developed by Diao and co-workers[62] which they named Nanoparticle Imprint Lithography. Commercially acquired monodisperse colloidal silica suspensions were dispersed onto a substrate leading to the formation of hexagonally close packed monolayers. By sintering the OH groups of both substrate and particle were broken, resulting in the silica particles and substrate forming covalent bonds, creating the ”imprint mould”. A pre-polymer mixture, made out of polyacrylic acid (monomer), divinylbenzen (crosslinker) and polymerization initiator IRGACURE 2022, was then sandwiched in-between the imprint mold and a glass slide treated with a coupling agent. The prepolymer mixture was cured by subjecting it to ultraviolet light, after which the mould was lifted off and spherical pores were found in the polymer film. With diameters from 300 nm down to 15 nm. In a similar fashion they synthesized iron oxide nanoparticles and used them to make hexagonally shaped pores. The method and its results are shown in figure 2.11.

2.4.2. Fabrication of Patterned PDMS Stamps

Choi and co-workers[63] developed an easy method to produce stamps which could be used with soft lithography techniques to reproduce patterns of colloidal crystals, assembled through a Langmuir-Blodgett method, into acrylate films. After drying of the crystal chloromethysilane was vapour deposited on top, to further strengthened and stabilized it against mechanical stresses.

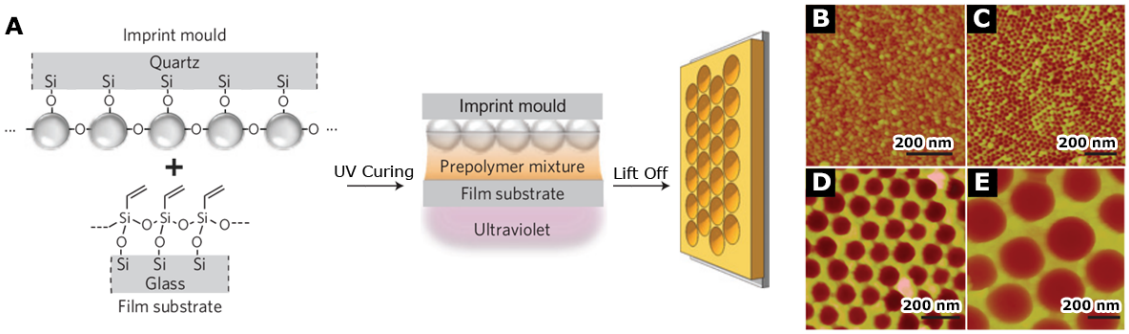

Figure 2.11: Structure and interaction of two polymer films. **A**) Schematic drawing of production of structured polymer films through a colloidal imprint mould and transparent quartz substrate. AFM images of the pores produced through the imprint method of; **B**) 15 nm, **C**) 40 nm, **D**) 120 nm, **E**) 300 nm particles. Adapted from [62].

Three variations were presented which allow the fabrication of a PDMS stamp. In the first method the PDMS was deposited on top of the crystal, allowed to infiltrate and then cured. By peeling it off, the infiltrated PDMS was mechanically separated from the top layer. Then, a thin layer of acrylate was spincoated on another glass slide into which the PDMS stamp was pushed and cured with UV light. Removal of the stamp revealed the structure and allowed for reuse. In the second method the colloidal crystals were infiltrated with a PEDOT/PPS solution and cured, after which the top layer was etched off with oxygen plasma, leaving behind the pattern which conformed to the bottom of the removed PS spheres. On top of this a PDMS stamp was developed, which produces patterns inverse to the first stamp. The last method involves two steps of self-assembly. On top of the first acrylate pattern a new colloidal self-assembly step is performed, resulting in a spaced monolayer of smaller PS particles, onto which a new PDMS stamp was developed.

2.4.3. Sensing Films

A colloidal imprinting process was developed by Yang and Park[64] which allowed the detection of the herbicide atrazine. A PDMS master mould was developed that was pressed into PS films to produce trenches of 650 and 300 nm. These films were then dipped into colloidal suspension of PS particles, which were slightly smaller than the width of the trenches, resulting in close packed zigzag patterns of colloidal particles. Lines of colloidal particles could be produced by dipping the substrate into the colloidal suspension with the trenches perpendicular to the interface. Lattices with a wave-like non-close packed structure could be produced by using particle sizes almost twice as large as the trench width. Heating the colloids just above the glass temperature at 130 °C caused them to melt and anneal. Allowing for more uniform zig-zag patterns.

PDMS negatives were made of the colloidal structures to create films for atrazine sensors. The surface of which were then modified such that chemical bonds that allowed for binding of atrazine molecules. Atrazine uptake was verified by putting the films onto a quartz crystal microbalance sensor which allows the measurement of the resonance frequency, and as more atrazine is chemisorbed the frequency shifts upwards. Due to the large surface area of the structures created through colloidal imprinting, the films were shown to be more sensitive to atrazine than either planar films or even films with circular posts. The film only showed a significant response to mixtures with atrazine in them and not to its tested analogues.

2.4.4. Replication by Hot Embossing

Hot embossing is a microstructuring technique in which a thermoplastic polymer is heated above it's glass temperature, a patterned master mould is pushed into the polymer and the temperature is reduced. After the polymer is cooled well below it's glass temperature, the master is removed and a negative of the pattern of the master is left behind in the polymer[65]. Feature sizes within the range of 0.1 to 10 µm can be created through this process in a cycle time of around 10 minutes[5].

However, to the author's knowledge, there has been no research on using self-assembled monolayer colloidal crystals or masks as a master mold within a hot-embossing technique. A similar approach by the name of Nano Imprint Lithography has been developed with colloidal stamps to fabricate sub-micron

cavities within Polystyrene films[66] and UV curable polymers[62].

Because hot embossing is a highly conformal technique, any imperfections in the master mould will also be copied into the target[67]. Which suggest that a monolayer crystal, with a polymer matrix which is thinner than the particle diameter, would ideally be the most suitable for pattern replication.

2.5. Summary and Discussion

In this chapter a short overview of all relevant topics regarding to colloidal crystal fabrication has been presented, including a section on the applications in which they have been used. At this time a large collection of techniques exist which are attractive, in terms of fabricating large area colloidal crystals with differing sizes. Secondly, the variation in fabrication times differs largely from technique to technique. A full overview of the specifications can be found in appendix C.1.

Currently monolayer colloidal crystals have been used in only a handful of replication techniques as masks, with hot embossing not having been tested so far. The main demand for a replication by hot embossing is that the master mould is stable under heat and pressure, which limits the self-assembly techniques that can be used to make a colloidal crystals which can be used as a master.

Therefore, any transient self-assembly technique, such as one employing fields, are not directly suitable as master moulds. Secondly, any colloidal crystal that are not produced with adhesion towards the substrate, such as a polymer matrix, will need treatment that improves the adhesion from the colloidal crystal to the substrate.

For a comprehensive overview of self-assembly techniques and their usage in replication techniques, please see our upcoming publication: Surface Self-Assembly of Colloidal Crystals for Micro- and Nano-patterning in Advances in Colloid and Interface Science.

3

Polymer Embedded Colloidal Crystals Fabricated by Spincoating for the use in Hot Embossing

3.1. Introduction

As established in section 2.3, there are a large amount of self-assembly techniques available that differ in terms of colloidal crystal size, quality and fabrication speed. But so far very little research has been performed where colloidal crystals were used as the master in a hot embossing or nanoimprint lithography process. The research in which the colloidal crystals were used directly to replicate features has so far been quite promising, as demonstrated in section 2.4.

Therefore in this section the research performed towards using colloidal crystals directly in a hot embossing step is discussed. Based on a paper in which ETPTA (ethoxylated trimethylolpropnae triacrylate), a photocurable monomer, was used as a matrix for multilayer[41] and monolayer[42] colloidal crystals, by self-assembly through spincoating. The reason for which being that the colloidal crystals are manufactured within a process that takes less than an hour, and directly traps the crystals in a matrix such that they are fixed, making them suitable for hot-embossing.

In this chapter the experimental steps are described towards fabricating the colloidal stamps, the fashion in which their quality is evaluated and improved is described and the results of the imprinting with these stamp is discussed.

3.2. Fabrication of Colloidal Stamps

In this section the approach towards manufacturing the colloidal stamps, verification and effectiveness of imprinting in a hot embossing technique are presented and discussed. A schematic drawing of the steps described can be seen in figure 3.3.

3.2.1. Preparation of ETPTA Base

First a substrate was required to spincoat the colloidal crystal onto, as cured ETPTA shows very little adherence to either glass or silicon[a]. Thin films will easily detach when temporary submerged in DI water. Either light manipulation by laboratory pliers or soft bursts from an air gun were enough to detach the film. Therefore, a coupling agent was used to improve adhesion of ETPTA to the substrate. A primer that is suitable with acrylates, the silane coupling agent KR-513[68], was used to anchor the ETPTA film onto the substrate.

In order to apply the primer silicon wafers were cut into square pieces ranging from 2x2 to 1x1 cm, either by using a wafer cutter or diamond pen, and then cleaned in acetone and isopropanol. Subsequently, the wafers were dried on a hotplate at 175 °C for 5 minute before being allowed to

[a] A fabrication of a base ETPTA layer was necessary as the primer left an uneven surface on the wafer, making it unsuitable for flat single layer crystals. For a detailed look see appendix A.3.

cool down in a fume hood on a piece of aluminium foil. After cooling, 100 µL of the coupling agent was dispensed onto the cleaned wafers while they were present in the spincoater, rotating at a speed of 1000 rpm. After deposition the speed was increased to 3000 rpm and held for 60 seconds, the spincoated wafer was then transferred to a hotplate at 175 °C where the coupling agent was cured for 5 minutes, before being left to cool down again.

The ETPTA base layer was fabricated by pipetting the ETPTA prepolymer from the container and adding the photointiator Darocur 1173 at a 4% weight fraction to the mixture, after which it was thoroughly mixed by hand and vibromixer. The concentration of the photointiator was determined by the desired layer thickness, which for film below 20 µm is 2 - 4 %[69]. A study by Jančovičová and co-workers [70] also shows that a maximum conversion could be achieved by a concentration of around 3 % for a 10 µm layer of the urethane acrylate oligomer Craynor 925, which had been covered with polyethylene foil to reduce the oxygen inhibition. Initiator concentrations which are too high can prevent the radiation from penetrating properly and leading to an uneven gradient in the curing film. The needed amount of prepolymer mixture was determined by measuring the substrate and pipetting 12,5 µL cm^{-2} onto the primed substrate. A cover-slip was then placed on top of the film, such that the pre-polymer mixture was sandwiched in-between the two glass pieces and up to three of these samples were exposed to UV radiation for 2 minutes. Because of the low-adhesion of ETPTA to glass, the cover-slip was easily removed after curing by gently lifting it off by means of a pair of laboratory pliers. A schematic drawing of the curing stage is shown in figure 3.1.

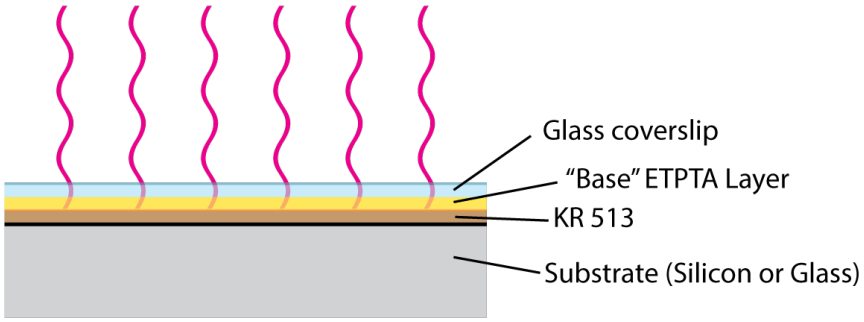

Figure 3.1: A schematic overview of the fabrication of the ETPTA base layer. With the uncured ETPTA sandwiched in-between the primer and the coverslip.

3.2.2. Preparation of the Colloidal Crystals

Colloidal suspension were prepared by creating a pre-polymer mixture with 6% wt Darocur 1173 added. With a high precison scale roughly 0.15 to 0.20 grams of dry unfunctionalized silicon particles, 2.47 µm in diameter, were then deposited into a eppendorf tube. After which the necessary amount of the pre-polymer mixture was added, such that the weight fractions were 10% wt silicon particles, 4 % wt Darocur 1173 and 86 % wt ETPTA[b]. The suspension was then mixed by placing it onto a vibromixer until the solution was entirely opaque. After which it was ultrasonicated for 5 minutes to prevent coagulation of particles, before being mixed one last time on the vibromixer. The mixture was then left to rest such that it could be checked for sedimentation, which was not seen to occur in any of the suspensions prepared. A micropipette was used to draw 25 µl and pipette it onto the ETPTA base, after which it was spread by tilting the substrate such that the surface was covered as much as possible. In order to maintain an equal concentration for all depositions, the suspensions were mixed with the vibromixer for roughly 10 seconds at high speeds before drawing it with the micropipette. The pre-crystalline suspension were then placed into a spincoater and then spincoated in two steps. First a speed-up step was performed bringing the speed up to 500 rpm and held for 30 seconds after which the speed was increased to 1000 rpm with both steps having an angular acceleration of 200 rpm/s.

This protocol was partially based on the research by Jiang and co-workers[42] who prepared non-close packed colloidal crystal monolayers embedded into an ETPTA matrix, in which six seemingly

[b]The required values were calculated by entering the measured weight of the silica particles into the python script provided in section 3.5.1.

arbitrarily determined steps were used. However they did note that a lower acceleration led to higher quality crystals. As well as the research on colloidal crystal spincoating with evaporative media in which Cheng and co-workers[43] showed that, within a two-step spincoating method, the first spincoating step and a low relative humidity were the most important. However, as the ETPTA is not evaporative, the first spincoating step is of less critical importance as the menisci between the particles are non-evaporative and thus don't exert a force pulling the particles together.

After the spincoating of the colloidal crystals, the colloidal stamp construction is complete. There, just before exposure, a glass coverslip is gently placed on top of the layer with the spincoated crystals, to reduce the influences of oxygen quenching. Subsequently the stamps are cured one by one by exposing them to the hot UV lamps for 2 minutes, after which they are retrieved and the coverslip is gently lifted off by a pair of laboratory pliers.

3.2.3. Post-Treatment

Because of oxygen quenching, and non-total conversion of the monomer, a thin film of uncured ETPTA was still present on top of the crystals. Therefore, the stamps were cleaned by placing them into a beaker filled with DI water which was then ultrasonicated for 1 minute. After which the stamp was removed and dried by putting it onto a hotplate at 125 °C for 5 minutes, before removing it and allowing to cool down to room temperature on a piece of aluminium foil. The comparison between a sample which has been treated this way and one which is not submitted to post-treatment can be seen by the naked eye, but the difference becomes even more obvious when imaging it by SEM, as can be seen in figure 3.2.

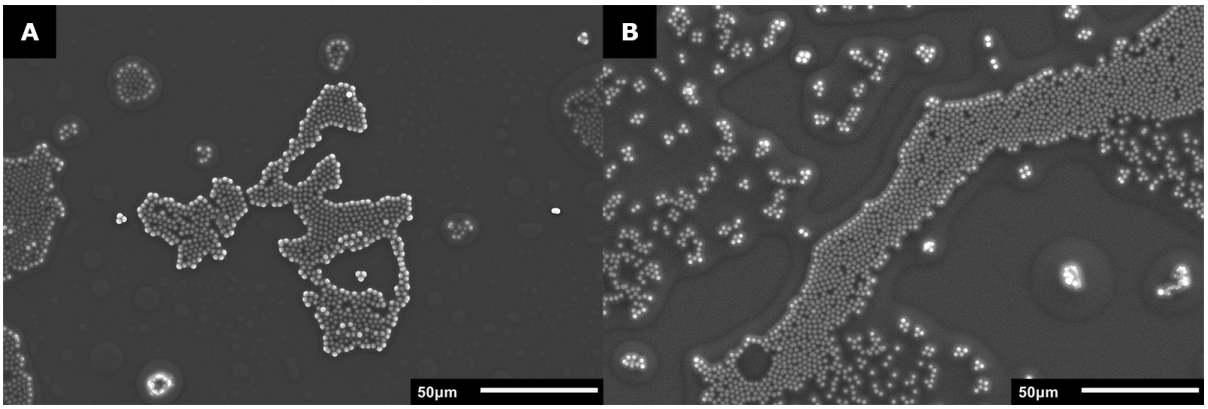

Figure 3.2: Comparison of the crystals after cleaning by means of SEM imaging. **A**) Crystals after cleaning in DI water and ultrasonication. **B**) Crystals without a cleaning procedure.

After the post-treatment the number of contaminants and thick layers of ETPTA are significantly reduced, at the cost of a large amount of the particles. This is probably in a large part thanks to low amount of conversion of the pre-polymer mixture to cured ETPTA due to oxygen quenching and any particles which stick to the coverslip upon removal. To verify this the crystal ought to be cured within a nitrogen or carbon dioxide purged environment, in a vacuum or under a laminate and compared in a similar fashion[71].

3.2.4. Summary and Discussion

This section presented an overview of the steps required to fabricate a colloidal crystal that could be used within a hot embossing process, and explained which considerations went into the choices. Any considerations not presented within the main text are referred to in the corresponding sections in appendix A. Currently the fabrication of the colloidal stamps requires a three layer construction, where an ETPTA base layer is adhered to a silanized silicon wafer which was cut to size, as the ETPTA has very little weak adhesion to the tested substrates. However, because priming the substrate leaves a non-uniform layer of the coupling agent, a base layer of ETPTA was fabricated which serves as substrate for the colloidal crystal, as discussed in appendix A.3. Then on top of this layer the colloidal crystal is spincoated and a coverslip is gently placed on top before curing the ETPTA for 2 minutes with UV light, after which it is cleaned by ultrasonicating it in DI water, to remove any uncured polymer and

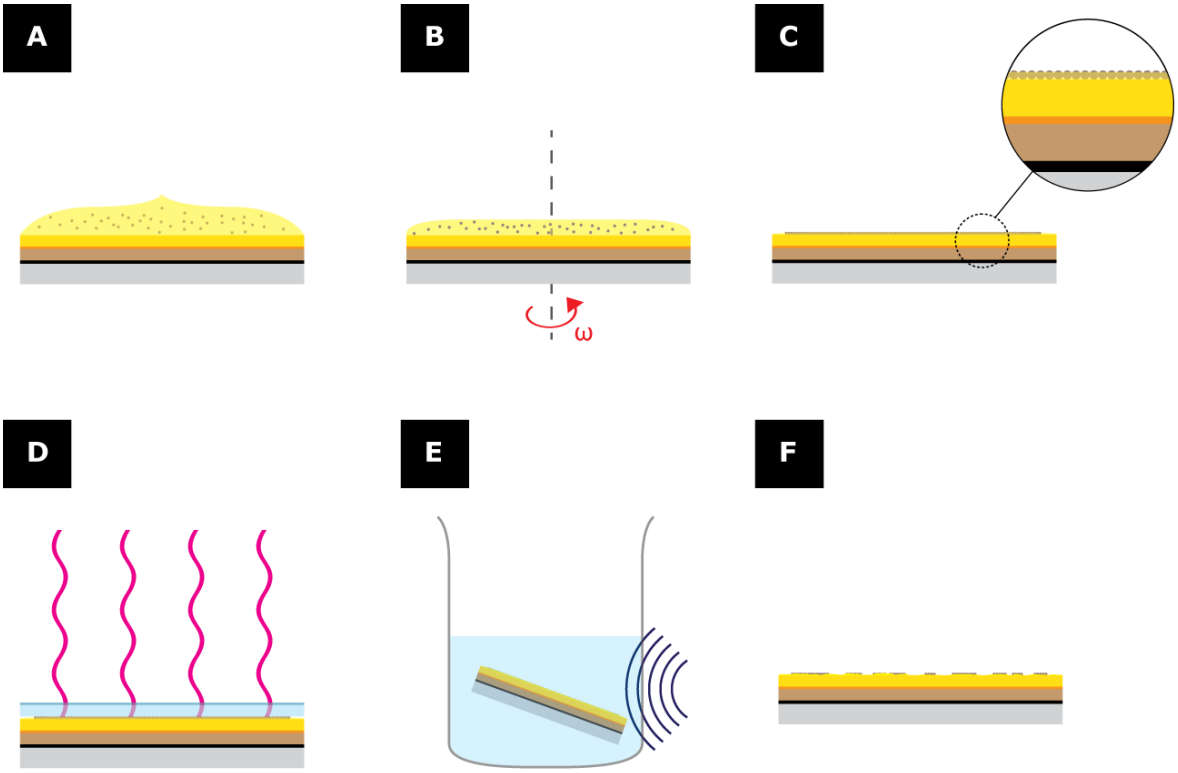

Figure 3.3: A schematic overview of the steps described in the protocol. **A**) A droplet of the colloidal suspension is deposited onto the ETPTA base and spread out. **B**) The colloidal suspension is spincoated, spreading the particles over a large area and thinning the polymer matrix. **C**) After the spincoating has finished the particles are covered partly in the polymer matrix. **D**) A coverslip is placed on top of the crystal and the polymer matrix is cured by UV radiation. **E**) The coverslip is removed and the colloidal crystals is put into a beaker filled with DI water and ultrasonicated for 1 minute. **F**) Any uncured polymer is removed and the crystals that remain on the surface form the colloidal stamp.

contaminants. This resulted in a colloidal stamp, where colloidal crystals were encased in ETPTA on top of an ETPTA substrate.

3.3. Colloidal Crystal Quality and Improvement

The verification of colloidal crystals has been performed in several ways in literature, such as but not limited to: packing density[72], fast fourier transformations (FFT)[73] and ordering parameters[74]. With the fabrication procedure established in the last section, the approach and results of a qualitative investigation now follows on the factors that influence the final form of the colloidal crystals.

3.3.1. Sample Imaging

The effects of spincoating an evaporative suspension have in the past been investigated by capturing the formation of the crystals by spectroscopy[19]. Revealing that the evaporation rate, particle concentration and spin-coating parameters all have significant influence on the formation of the colloidal crystals . However, no experimental research could be found on the effect of spincoating spin speed (rpm) and particle weight concentration (% wt) for non-evaporative media, such as polymers. Therefore, the effects of rpm and weight percentage were investigated in a series of experiments.

The crystals were sputtered with a coating of gold-palladium to make them conductive and then imaged with the SEM[c]. Out of all the imaged crystals, the ones with the largest amount of closely packed microspheres and the fewest defects were chosen for further processing, such that the best 3 crystals were used for the data processing.

[c]As the sputtering of the samples prohibits further alteration other imaging methods were tested. However, either interferometer or AFM measurements did not result in sharp enough images for further processing.

3.3.2. Ordering parameter

In order to make a qualitative measurement of the crystal quality a method has to be determined that is able to effectively measure the quality of the crystal. The parameter used in this case is the ordering parameter[d]. Where by using image recognition techniques the particles or their centers are detected[e] and a triangular grid is constructed by Delaunay triangulation. Wherein the particles are connected to their closest neighbours by centre-to-centre lines, an example of which is shown in 3.4. To remove any outliers the average magnitude of all centre-to-centre distances is calculated and lengths above 4/3 of the mean are cut off as these often indicate lines connecting points which are very far away from one another.

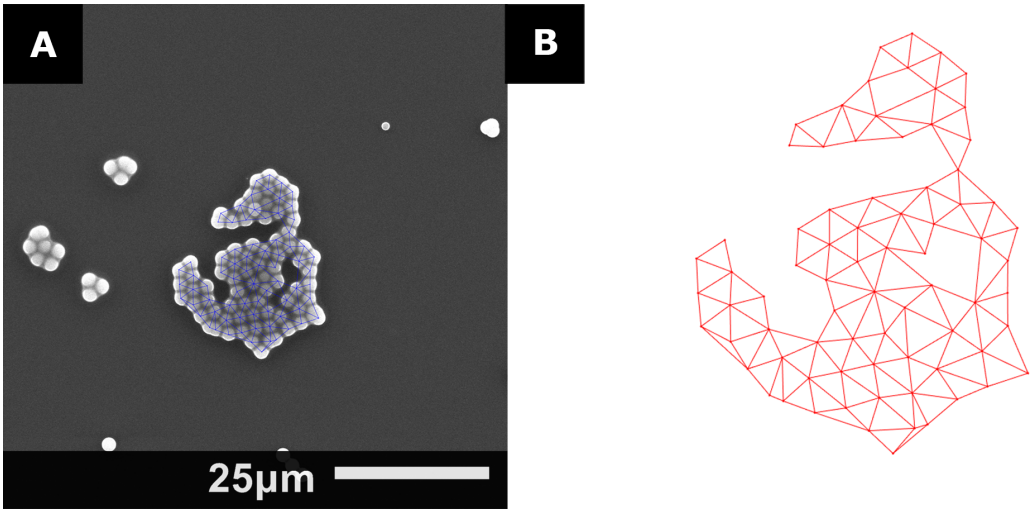

Figure 3.4: Image of the triangulation as found by the Delaunay algorithm. **A**) The tessellation overlaid on the SEM image that was analyzed, showing that the particle detection algorithm sometimes skips over certain particles and that the grid connects particles which are not directly connected. **B**) A close-up of the triangulation separated of the SEM image.

An ideal crystal is taken as a hexagonally packed lattice, such that every single particle has 6 neighbours all with the same center to center distance. Which will lead to a mesh with triangles in them in which every single corner has an angle of 60 degrees. By taking the grid found by Delaunay Triangulation. The angles between the particles can be calculated through the the law of cosines[75] expressed as,

$$\begin{aligned} a^2 &= b^2 + c^2 - 2bc\cos\alpha\,, \\ b^2 &= a^2 + c^2 - 2ac\cos\beta \text{ and} \\ c^2 &= a^2 + b^2 - 2ab\cos\gamma\,. \end{aligned} \tag{3.1}$$

Where a,b and c are the distances between the particles and α,β and γ are the angles opposite to the lines, respectively. As the coordinates are output by the grid build by the image recognition software, and the neighbouring particles are provided by the Delaunay algorithm, all angles can be evaluated by this law. When the angles are known they can then be used the modified six-fold symmetric ordering parameter, defined as

$$\Psi_6 = \frac{1}{N}\left|\sum_j^N e^{6\mathrm{i}\theta_j}\right|, \tag{3.2}$$

to determine the resemble of the detected crystal to the ideal. Wherein N is the total number of angles, θ_j is the angle between three particles. Such that, when all the angles between all particles are exactly 60 degrees, the ordering parameter is 1. Any defects and the accuracy of the imaging software reduces this factor[f].

[d] FFT transformations were also applied on the SEM images of the crystals but didn't result in usable information, as the ETPTA, defects and picture quality all influenced the retrievable information.
[e] More information on the used image recognition techniques can be found in appendix B.1.
[f] This approach deviates from the standard expression of the local bond order parameter, which evaluates each particles number

3.3.3. Influence of RPM

With the ordering parameter the quality of the crystal can be determined. The first parameter that was checked was the spincoating speed of the second spincoating step. All samples were manufactured in the same way, except that per 3 samples the spin-speed of the second step was increased, such as is displayed in table 3.1.

Samples	Speed Step 1 (rpm)	Speed Step 2 (rpm)	Step Times (s)
1, 2, 3	500	1000	30/120
4, 5, 6	500	2000	30/120
7, 8, 9	500	3000	30/120
10, 11, 12	500	4000	30/120
13, 14, 15	500	5000	30/120

Table 3.1: The parameters used in the spincoating spinspeed tests.

Then the samples were imaged in the SEM at a 500x times (or 1000x if necessary) magnification and converted into a point grid[g]. As described before, the number of participating particles and the order parameter of the selected crystals were computed. These data points are represented in terms of a boxplot[76] which presents the non-gaussian distribution of the results of the experiments. The data is divided into quartiles, with 50% of the data represented by the box and the other 50% by the whiskers. This allows the filtering of any (suspected) outliers, which are outside the last interquartile range. The boxplot of spincoating speed versus the order parameter (equation (3.2)) is displayed in figure 3.5 **A** and that of the spincoating speed versus number of participating particles is displayed in figure 3.5 **B**.

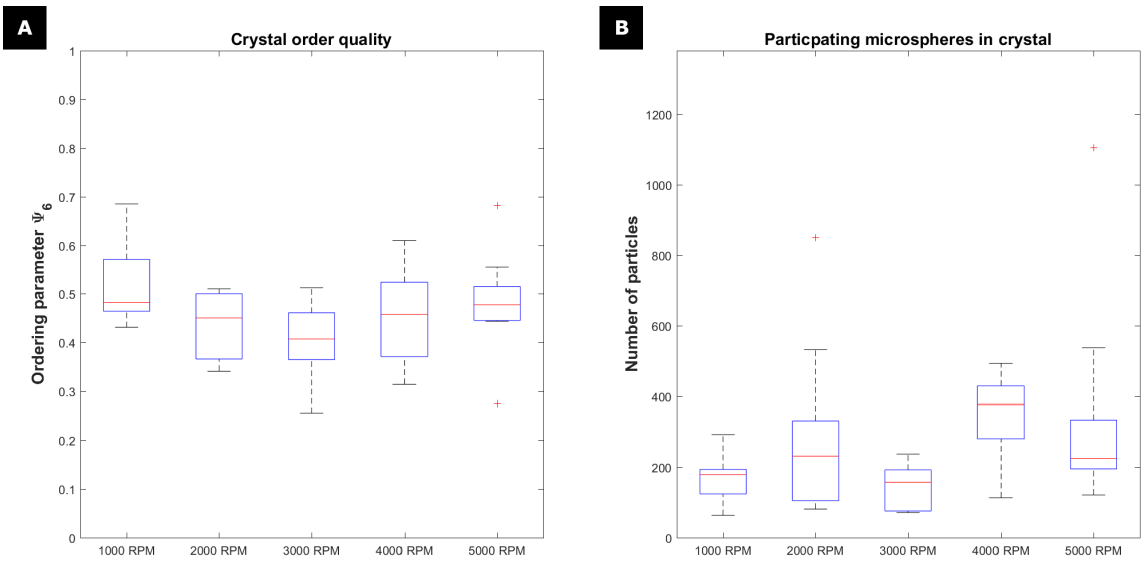

Figure 3.5: The plots resulting from the spincoating spin speed experiment. **A**) The order parameter as per equation (3.2) versus the variation of the second spincoating step speed, with measurement points 1000, 2000, 3000, 4000 and 5000 RPM. **B**) Number of particles versus the second spincoating step speed, with measurement points 1000, 2000, 3000, 4000 and 5000 RPM.

Both plots show no clear relation towards an increasing or decreasing ordering or number of particles. Meaning that at least the second spincoating speed has very little influence in the final formation

of neighbours and then calculates the angles and the ordering parameter locally, before taking the mean of these parameters to evaluate the global ordering parameter. The difference being that it takes a different, slightly more complex, approach to implement. A short explanations on how this influences the order parameter is provided in appendix B.2.2

[g]The center detection algorithms used to identify this point grid are presented in appendix B.1.

of the crystals. However, the SEM images of the stamps do show a change in the morphology of the polymer matrix, shown in figure 3.6.

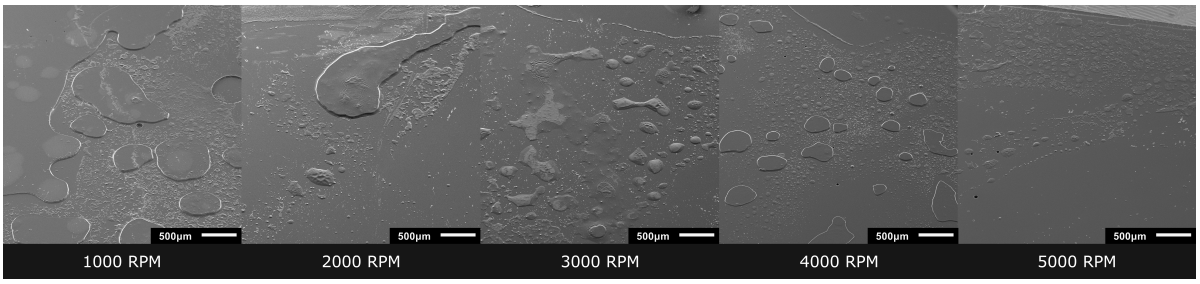

Figure 3.6: The change in the morphology of crystals concentration per spincoating speed. With the layer of ETPTA becoming visibly thinner and particle depositions becoming spread out.

From the images a change in morphology is seen where at low spin speeds there are large islands of polymer where particles are trapped inside, with cluttered particles loosely deposited in-between. But at high spin speeds the islands are smaller and more dispersed, which is likely due to higher shear forces spreading the polymer thinner. The shear stress within a non-evaporating film spread by spin-coating[77] can be described as

$$\sigma_{rz} = \rho\omega^2 r\,(h - z)\,, \tag{3.3}$$

where σ_{rz} is the film shear stress, ρ the fluid density, ω the angular velocity, h the film thickness and z the height coordinate. Which shows that the shear stress increases quadratically with the spincoating speed.

3.3.4. Influence of Particle Concentration

After the experiment with the spin speeds, the second parameter that was investigated was the particle concentration. The RPM experiment was carried out with a 10% wt solution and in this experiment 5% and 20% wt concentrations were tested. For this set of experiments the settings of having a first step at 500 RPM for 30 seconds and 5000 RPM for 120 seconds were used, as it resulted in a thinner polymer layer and doesn't influence the size of the crystals and their order, as shown in the previous experiment. The experimental parameters that were varied in this test are shown in table 3.2.

Samples	Concentration
13, 14, 15	10% wt
25, 26, 27	20% wt
28, 29, 30	5% wt

Table 3.2: An overview of the fabricated and imaged samples including their concentrations. The spincoating steps were performed at 500 RPM for 30 seconds and 5000 RPM for 120 seconds.

Using the same approach as used in the RPM experiment the concentration versus the order parameter and number of participating microparticles are found, plotted in figure 3.7 **A** and **B**, respectively.

Again, the concentration of the particles has no real influence on the order quality of the crystal. However, the concentrations does have a noticeable effect on the number of particles within a crystal. While the 5% and 10% wt concentrations don't show a major difference in terms of crystal size, it increases significantly once the concentrations reaches 20% wt.

Lastly, the influence of the particle concentration upon the polymer matrix was qualitatively observed by taking SEM images at 45 degrees and looking at the change in the morphology, as shown in figure 3.7.

3.3.5. Influence of Particles

However, a experiment that was readily available was to study the influence that the particles had on shaping the polymer matrix. A sample was prepared as usual, except that after the fabrication of the

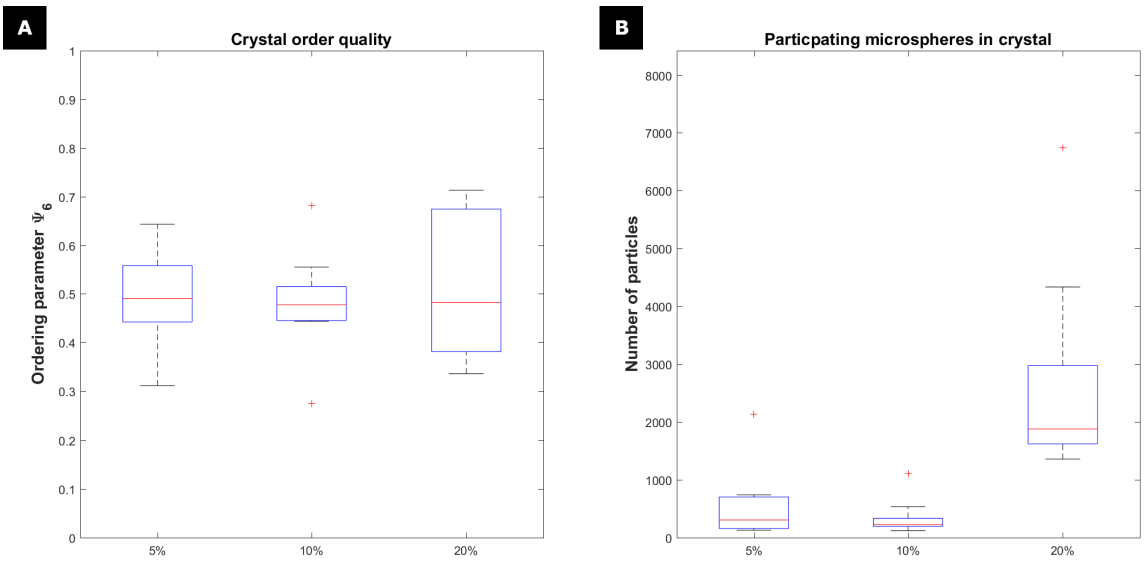

Figure 3.7: The plots of the concentration experiment. (**A**) The order parameter as per equation (3.2) versus the particle weight concentration in the suspension, with measurement points 5% wt, 10% wt and 20% wt. (**B**) Number of particles versus the particle weight concentration in the suspension, with measurement points 5% wt, 10% wt and 20% wt.

base a solution without particles was spincoated on top of the base ETPTA layer. Again the spincoating was performed in two steps, at 500 rpm for 30 seconds and 5000 rpm for 120 seconds. This layer was then covered with a coverslip, cured and cleaned as per the previously established protocol. The images of the resulting structure were captured by SEM and are displayed in figure 3.9.

When comparing figure 3.9 to figure 3.8, it is clear that the particles are influential in shaping the way the spincoated ETPTA is distributed and cures.

Two factors are suspected to be at play. Either the particle concentrations affects the shear stress distribution in the film during spincoating, or the particles could affect the way the ETPTA cures. The first could potentially be determined by developing a numerical solution for a non-evaporating colloidal suspension, an approach which has been used for evaporating suspension[78]. For the latter the thermal flows can be mapped by infrared spectroscopy[70], in which the transmittance of the materials is compared before and after curing. By comparing these the total conversion ratio can be determined.

3.3.6. Summary and Discussion

This section presented and discussed the findings of the two main experiments that were performed. That is, determining the influence of the spincoating speed and particle concentration on the quality and size of the resulting colloidal crystals trapped in a polymer matrix.

What can be seen is that for lower particle concentrations there are only small islands of particles suspended within the ETPTA, but as the particle concentration increases the islands become bigger and at one point join each other. This is likely the influencing factor in why the crystals in the 20% wt are larger in terms of participating particles than for lower concentrations. However, the particle weight fraction at which point this occurs and if this behaviour continues at even higher concentrations is hitherto unknown.

A likely explanation for the change in morphology of the crystals is that steric effects become more dominant as the particle concentration increases. Interparticle electrostatic effects were considered to be of minimal contribution by Jiang and co-workers[41], as this effect was tested by adding tetrabutylammonium chloride to the suspension, which had minimal effect on the crystal quality. A way in which this effect could be investigated would be by employing the technique by Toolan and co-workers[19], in which the formation of crystals was imaged by spectroscopy and inspecting the change in the resulting inverse FFT transformations.

A description of the ordering parameter and the method for analyzing the samples was discussed as well, however detailed information on the image and data processing is provided in B. The main

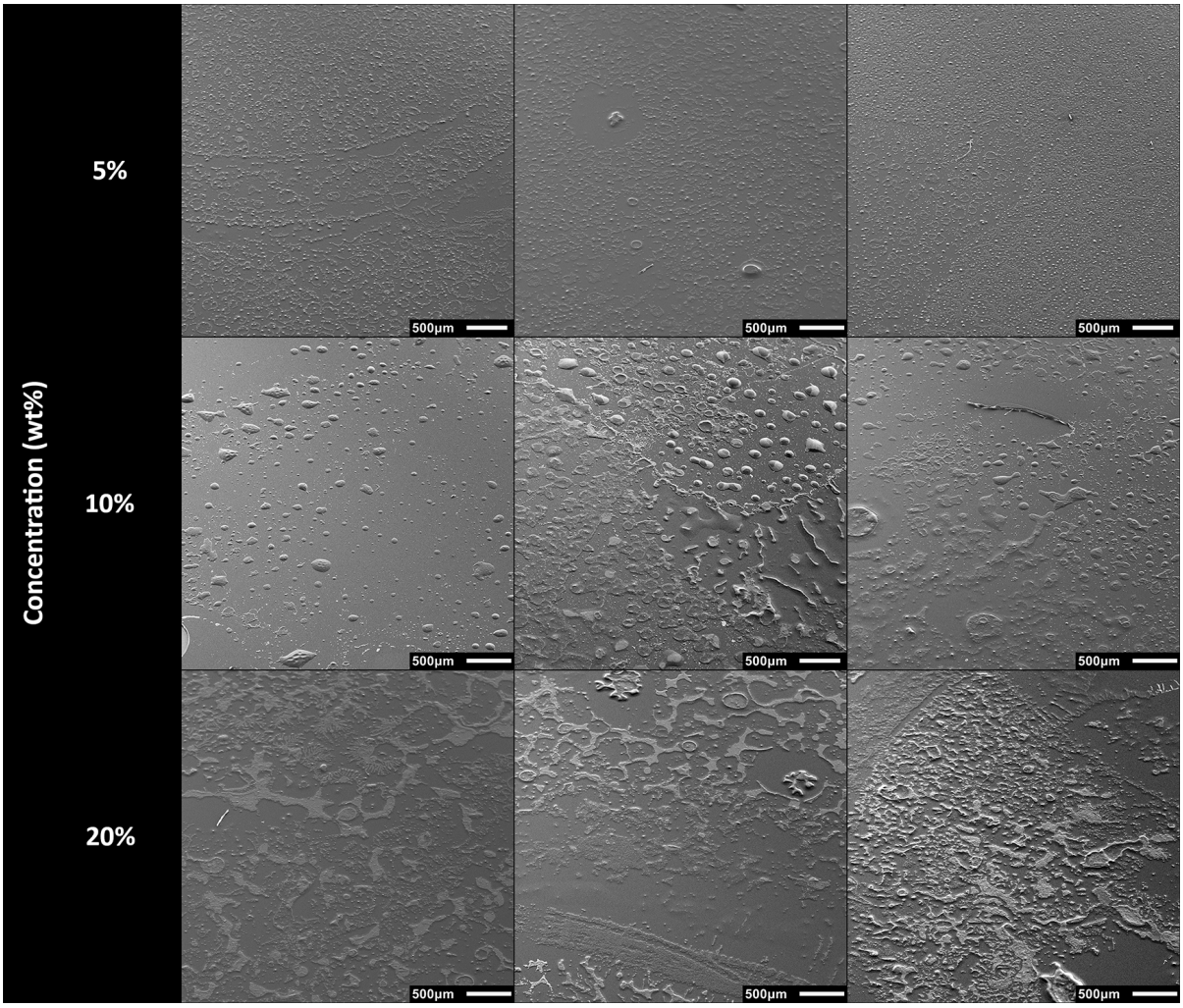

Figure 3.8: SEM images captured at 45 degrees providing an overview of the change in morphology from a 5% wt to a 20% wt particle fraction. One picture at the same magnification was selected for every single sample.

findings of the experiments were that the second spincoating speed has little influence on the size and quality of the crystals, but does influence the surrounding polymer matrix. In fact, the concentration of the particles within the colloidal suspension had a large effect on the crystals size, but again did little to improve the quality.

One last important finding was that without particles much larger uninterrupted depositions of ETPTA remain on the surface, which suggest that the particles play an important role in either the shear stress distribution of the pre-polymer or curing rate during UV exposure.

3.4. Imprinting of colloidal crystals

The viability of using the colloidal stamps within a hot embossing replication step is one of the main aims of this thesis. So far this type of fabrication technique has seen very little research, as was discussed in section 2.4.4. This section presents the results of the experiments in which the colloidal stamps were hot-embossed into a sheet of thermoplastic TOPAS.

3.4.1. Hot Embossing Experiments

The thermoplastic TOPAS 8007, which is a copolymer with a glass temperature of around 70 °C[79], is used as a hot embossing target. The process of which is composed out of several steps. First, the colloidal stamp, prepared as described in section 3.2 with a 10 % wt ratio and submitted to post-treatment, was loaded together with the TOPAS film which served as a target, as shown in figure 3.10

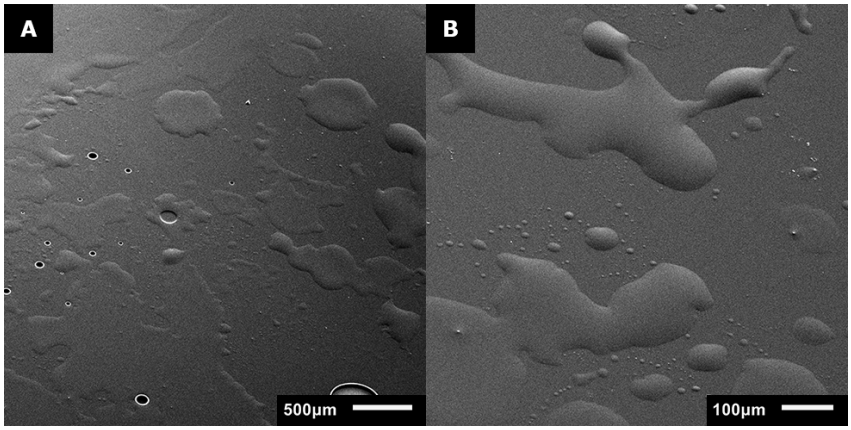

Figure 3.9: SEM Images under 45 degrees of a sample with ETPTA spincoated on top of a layer of ETPTA and then cured and post-treated. **A**) Overview picture of the structure of the cured ETPTA. **B**) Patch at 100 times magnification of the cured ETPTA.

B. Then the temperature of the hot embossing tool was heated up and the stamp and target were compressed into each other.

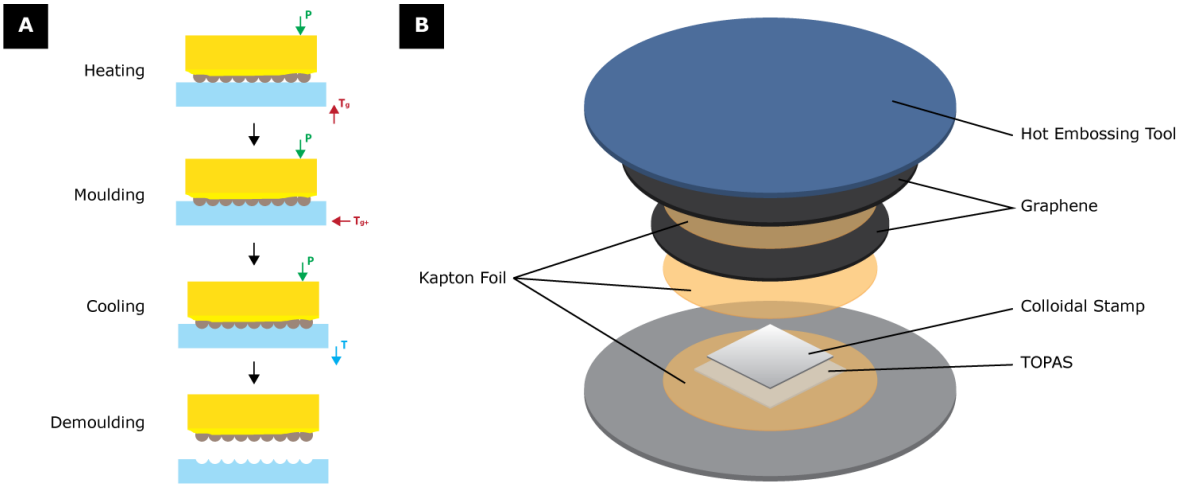

Figure 3.10: Fabrication throught Hot Embossing. **A**) The four main fabrication steps of hot embossing. The Hot Embosser is heated up past the glass temperature of the material and the stamp is pressed into the target. After the cycle time, the target is allowed to cool and finally the mould is removed. **B**) An illustration of the 'sandwich' that is constructed for the hot embossing procedure

The minimum temperature that needs to be used at this stage is the glass temperature of the TOPAS film. However, any temperature higher than that will result in a less viscous flow and thus a more conformal imprint[80]. For this reason the hot embossing tool was heated up to a temperature of 100 °C instead and a pressure of 3kN was applied onto the sandwich at 1 kN min^{-1} for a total operation time of 8 minutes. Then, the hot embosser was convectively cooled down and the pressure removed after the chamber temperature reached 55 °C. The sample was removed once the temperature reached around 35 °C and then allowed to cool down to room temperature. Afterwards, the stamp was peeled from the TOPAS film by use of laboratory pliers.

After the stamp was removed the TOPAS targets were prepared for SEM imaging, a collection of which are shown in figure 3.11.

In these two samples there are multiple instances of colloidal crystals leaving imprints or completely transferring into the TOPAS film. Secondly, the multilayered crystals that were also observed in the colloidal stamps are also transferred but leave very disorganized structures. As the morphology of these is not on a flat plane, the depth of the imprint in the TOPAS film is therefore inconsistent. Because of these findings an investigation followed how the imprint quality could be improved.

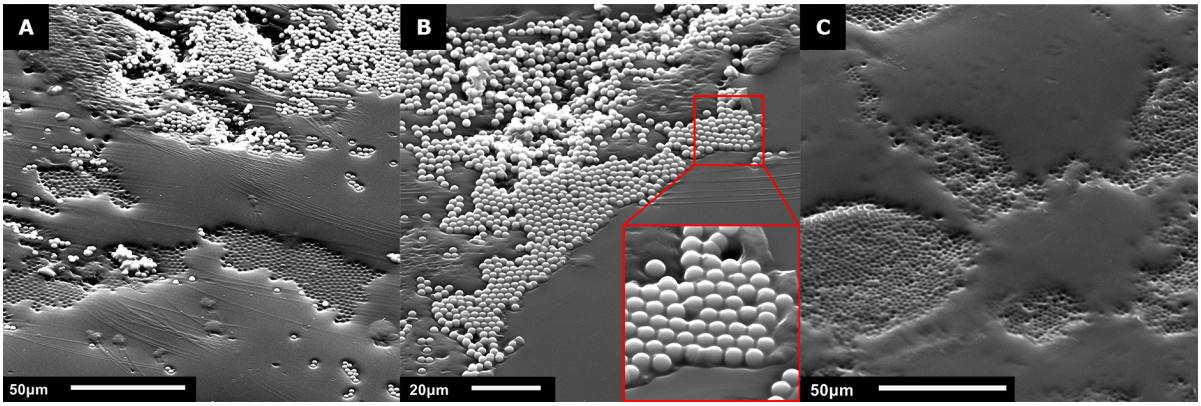

Figure 3.11: SEM Images of the first hot embossing samples. **A**) Imprints of colloidal crystals are left behind, with some of them including the crystals themselves. **B**) Some colloidal crystals transferred completely into the target, a close-up is included in which the polymer matrix can be seen. **C**) The quality of the colloidal crystal imprint varies a lot. In this image a multilayer crystal was imprinted, resulting in an uneven height distribution.

3.4.2. Influence of Stamp Cleaning

In general, before the hot embossing procedure every single colloidal stamp was cleaned, as described in section 3.2.3. However, the effect of which on final result of the hot embossing was unknown. Therefore, two stamps were fabricated similar to the ones in the main hot embossing experiments except that they were submitted to post-treatment.

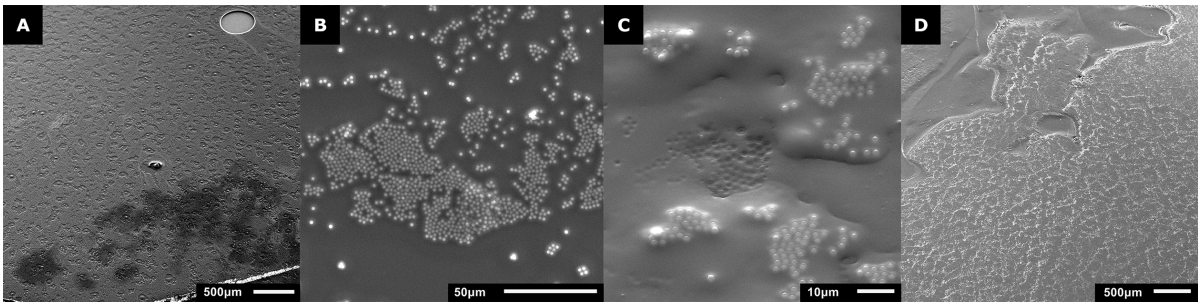

Figure 3.12: SEM images of the stamp and target without post-treatment. **A**) Zoomed out image of the stamp without post-treatment. **B**) Close-up of a stamp without post-treatment, with a large amount of loose particles scattered around a crystal. **C**) A deposition of the polymer matrix and colloidal crystals surrounding an imprint on the target TOPAS. **D**) A zoomed out image showing a large amount of particles and polymer transferred to the target TOPAS.

In figure 3.12 **A** and **B** the stamp with a large amount of particles, mostly loosely collected around larger crystals, is shown. When comparing this to figure 3.6 and figure 3.8 shows a much larger amount of particles still on the surface, even if they are not directly participating in the crystal formation. This suggests that a rather thick layer of the ETPTA does not cure, even when the stamps are cured under the coverslip, as in the previously attained stamps only small islands remain. Secondly, in figure 3.12 **C** and **D** a large amount of particles is seen to transfer onto the target TOPAS and the imprints of the particles that did not transfer having concentric rings, which are not seen in figure 3.11 **A**. This results indicates that in order to have a clean transfer of the colloidal crystals, any polymer which is not fully cured must be washed off in a post-treatment step.

3.4.3. Post-treatment of the Target

As the pre-cleaning of the colloidal stamps had actually a positive effect on the embossing a post-treatment step for the targets themselves was tested instead. After removal of the stamps from the TOPAS targets they were put into a beaker filled with ethanol[h] and then ultrasonicated for 5 minutes. After which they were removed from the ethanol and allowed to dry for 10 minutes at room temperature. The choice for ethanol as a rinsing agent was based on the fact that it is more volatile than water, and

[h] A small test was run to see if the ethanol damaged the TOPAS in any way as is presented in see appendix A.5

thus evaporates much faster. Secondly, the ETPTA mixture readily dissolves in ethanol and is thus suitable for removing any of the pre-polymer mixture if it was till present[81].

Next the TOPAS targets where then imaged by SEM[i] to be able to compare them to the non-cleaned targets, which are shown in figure 3.13. Comparing figure 3.13 with figure 3.11 shows that a large amount of the particles is removable, even for a worst case scenario such as in figure 3.13 **B**.

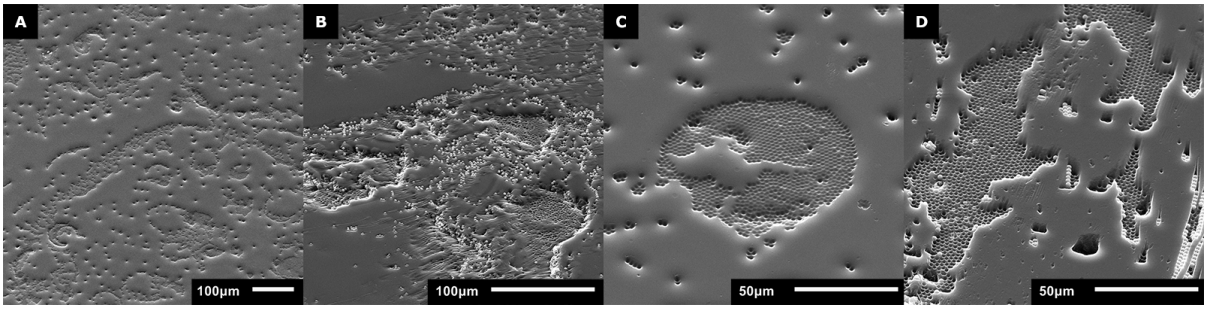

Figure 3.13: SEM images showing the effectiveness of the three targets which were treated with the ethanol and ultrasonication post-treatment. **A**) Overview of one of the targets in which the treatment was successful. **B**) Overview of another target in which sliding probably trapped some of the particles and they are geometrically locked. **C**) Picture of a perfectly cleaned colloidal crystals imprint. **D**) Again, due to sliding, some particles got trapped and were unable to be removed.

3.4.4. Summary and Discussion

Within this section the results of the replication experiments were presented, where the colloidal stamps were imprinted into a TOPAS film using a hot embosser. The crystals had the tendency to transfer into the target material, which results in the stamp being one-time use only. However, the benefit of using this techniques is that because the polymer matrix is in-between the particles it barely influences the final imprint pattern.

The colloidal stamp is currently one-time use only. As the silicon substrates have the tendency to break, or the crystals have the tendency to delaminate. Secondly, it was shown that cleaning the target with ethanol and ultrasonication resulted in the removal of a large amount of the particles. As for two out of the three samples tested almost all of the particles were able to be removed from the target. For the third the cleaning treatment was only partially successful, however there are markings which suggests that sliding between the stamp and target may have caused some of the particles to become trapped.

Therefore, the adhesion of the colloidal stamps remains a problem, but the imprint quality at this time of the monolayer is promising for future research.

3.4.5. Future Recommendations

Hot embossing directly with a colloidal stamp has been shown to be possible. However, some aspects of the fabrication technique still need development.

The adhesion of the and area of the colloidal stamp stands to be improved. This can either be done by replacing the material of the polymer matrix, or by optimizing the curing conditions. Such as curing the colloidal crystals in a vacuum or nitrogen purged environment. However, this could influence the maximum achievable crystals quality. The differences between crystals achieved between the coverslip method and one with oxygen deprivation can be evaluated with the method presented in section 3.3.2. Potentially this can eliminate the post-treatment step or reduce it's influence.

Alternatively, reduction in adhesion between the colloidal stamp and target material could also help with the reusability of the stamps and the transfer of particles. By applying an anti-stiction layer the adhesion of the colloidal stamp could also be significantly reduced[82].

Further research into other more easily to cure polymer matrix materials that are suitable for a hot embossing environment should also be considered. Which could also potentially help advance the understanding into the quality of spincoated colloidal crystals in non-evaporative dispersion media.

[i] Other imaging method were tested to see if it was possible to register the action the cleaning had on the targets. However both optical and interferometer measurements were unable to distinguish any difference in the morphology before and after cleaning, at the same locations.

3.5. Experimental

The polymer ETPTA (Trimethylolpropane ethoxylate triacrylate, average M_n ~428) and UV curing agent DaroCur 1173 (2-Hydroxy-2-methylpropiophenone) were purchased from Sigma-Aldrich and used without purification. P-type Silicon wafers 4 inch (500 µm thick) and 2 inch (230 µm thick) in diameter were purchased from the Kavli Institute of Nanoscience Delft. The Shin-Etsu Oligomer Acrylate KR-513 was attained from EVG. Dry silica particles, with a median size of 2.47 µm, were purchased from Bangs Laboratories, Inc. Suspension composed of ETPTA and 20%, 10% and 5% wt silica particles and 4% wt Darocur 1173 were prepared in Eppendorf tubes or vials, by weighing all component with a Scaltec SBC 33. Menzel-Gläzer Coverslips with a thickness of < 190 µm were used out of the box. A POLOS SPIN150i-NPP Single Substrate Spin Processor was used to spincoat 25 µl of the suspensions onto the ETPTA films synthesized on the wafers. In order to cure the ETPTA a Dentalfarm Photopol Light was used. Ethanol, Aceton and Isopropanol were all purchased at reagent quality from Sigma-Aldrich. SEM images were captured by a Jeol JSM-6010LA Scanning Electron Microscope, with acceleration voltages ranging from between 10 kV to 20 kV. Microscopic images were captured by a Motic BA310Met Microscope using a 2 MegaPixel Moticam USB Camera.

3.5.1. Dataset

For the dataset used in the experiments, please consult the digital version of this thesis which includes links to figshare, where the files are hosted.

- Edited SEM images of the colloidal crystals for the analysis of spincoating speed and concentrations
- SEM Images of colloidal stamp imprints in TOPAS
- SEM Images of colloidal crystals with triangular meshes overlaid
- Raw SEM .tiff files of the colloidal crystals and overview images
- Concentration Script - Python
- Scripts for Colloidal Crystal Analysis - Matlab

4

Reflection

In this chapter a reflection is provided on the thought process within designing the experiments, what new knowledge has been gained and how any future scientific experimental work can be improved.

4.1. Experimental Design

The main goal of this thesis was to fabricate colloidal crystals that could be used in a hot embossing technique. As was demonstrated in section 2.3 a large amount of techniques exist, in which the selection is limited by the demands of the hot embossing process being that it requires a master that will not break or deform under heat and pressure. Therefore, a proof of concept experiment was performed first in which the colloidal stamps were fabricated by a simple spincoating self-assembly technique, as described in appendix A.1. The reason for the choice of a spincoating technique fell down onto the availability of equipment, speed of the fabrication and the resulting crystals that were fabricated in literature.

The selected method for spincoating involved a polymer that was used to trap colloids in a hexagonal non-close packed lattice on four inch wafers, both for multilayers[41] and monolayers[42]. However, one aspect that was lacking from these publications was that the spincoating steps was quite arbitrary, with up to six spincoating steps applied, of which the motivation and significance was unclear. Secondly, while there have been papers which investigated the change in morphology and influence on the crystals quality during spincoating, there were non for non-evaporating fluids. Therefore, the experiment with the spincoating speed was performed to see to which extend this parameter influenced the final outcome of the crystal quality and size.

At the same time the goal was still to eventually use these colloidal stamps in a hot embossing process. Therefore, a protocol first needed to be established that was suitable for hot embossing. To develop this protocol some simple tests were run to identify any problems that needed to be solved.

First of all, the polymer ETPTA which was used in paper is not a very commonly used acrylate, which meant that not much data was readily available on the material. This lead to an oversight as the polymer suffers from a phenomenon called oxygen quenching during curing, where the polymerization is retarded by molecular oxygen in the atmosphere. However, before it was clear that this was the case several experiments had been performed by varying the photoinitiator weight fraction, using the same photoinitiator from a different lab and testing several different UV sources. Eventually it became clear that this is in fact a well known problem, one that is often solved by curing within a purged atmosphere, as had been done in the original paper. After enquiry at several different labs on campus it became clear that this kind of equipment was not available, which left two possible options. Either to dedicate time to building a setup to be able to cure the polymer in a nitrogen atmosphere, or to find an alternative way of curing. This led to several experimental trials to find alternative ways of curing including using vacuum, using glucose oxidase as described in appendix A.2.2 or just simply cutting off the oxygen by means of a cover slip. The last option was deemed to be the simplest and suitable for the fabrication of the colloidal stamps, of which the results were presented in appendix A.3.

Curing films of ETPTA with a coverslip saw a low adhesion behaviour on glass, as was mentioned in the paper, which was improved by use of a silane. However, the application method of the agent used

by use of q-tips was deemed to be unsuitable, as any non-uniform layer will influence the morphology of the monolayer crystals.

One problem with the coverslip method was that it mostly works for flat distributions of the polymer, which the addition of spincoating and the silica particles distorted. This makes it a less effective method than curing it by oxygen deprivation, but did allow to simply cure the colloidal crystals. A post-cleaning step was required to remove a large amount of polymer which had not fully cured. This means that the resulting crystals of the self-assembly are influenced by the coverslip placement and cleaning steps. As an improvement a vacuum or nitrogen filled chamber ought to be used to cure the crystals without any outside interference. PDMS was briefly investigated to see if it would make for a suitable matrix material as described in appendix A.4, but was not used in the end as it is too viscous to spread thinly and uniformly enough. Because the desired layer should be thinner than the particle diameter of 2.47 µm. Techniques are available for diluting PDMS into hexane and spincoating it such that films of a few hundreds of nanometer[83] can be fabricated, which might make it worth a second look.

In order to evaluate the colloidal stamps a lot of methods were tested, but the problem with most of them was that the features could not be properly mapped. Optical microscopes are only able to capture a single focal plane, which results in most of the features being out of focus. An interferometer is not able to distinguish features that are underneath another surface, such as an overhang or a sphere. Using an AFM resulted in some very blurry images, and without a clear definition of which area had been imaged, leaving only the SEM as a viable imaging technique. However, because the crystals were non-conducting they had to be sputter-coated with a conductive layer, rendering it impossible to perform comparison images on single samples to check the influence of post-treatments. Which meant that a larger amount of samples had to be created in order to check these influences.

Once the crystals were imaged however they still needed to be analyzed. The first choice was to do this by Fast Fourier Transform (FFT) of the SEM images in WSxM, however this resulted in transformations that were too ill-defined to retrieve any information about the ordering and separation distance. Particle detection and evaluation of the angles between them by the ordering parameter, as proved in section 3.3.2, provided an qualitative measurement.

As the algorithm used to evaluate the colloidal crystals is not suitable for the imprints, it is currently very hard to find details when imaging the targets from an incident angle. Therefore, all the SEM images were taken at a 45 degree angle, distorting the true distance due to perspective resulting in the particles becoming 'squashed' and throwing off the algorithm. This could potentially be fixed by using a correction factor, but time did not allow further investigation into this.

4.2. Timeline Comparison

A rough estimation of the length of the phases from the start of the experiments until they ended is presented in figure 4.1, without taking into account the time that was spend finishing my obligatory courses and any holidays.

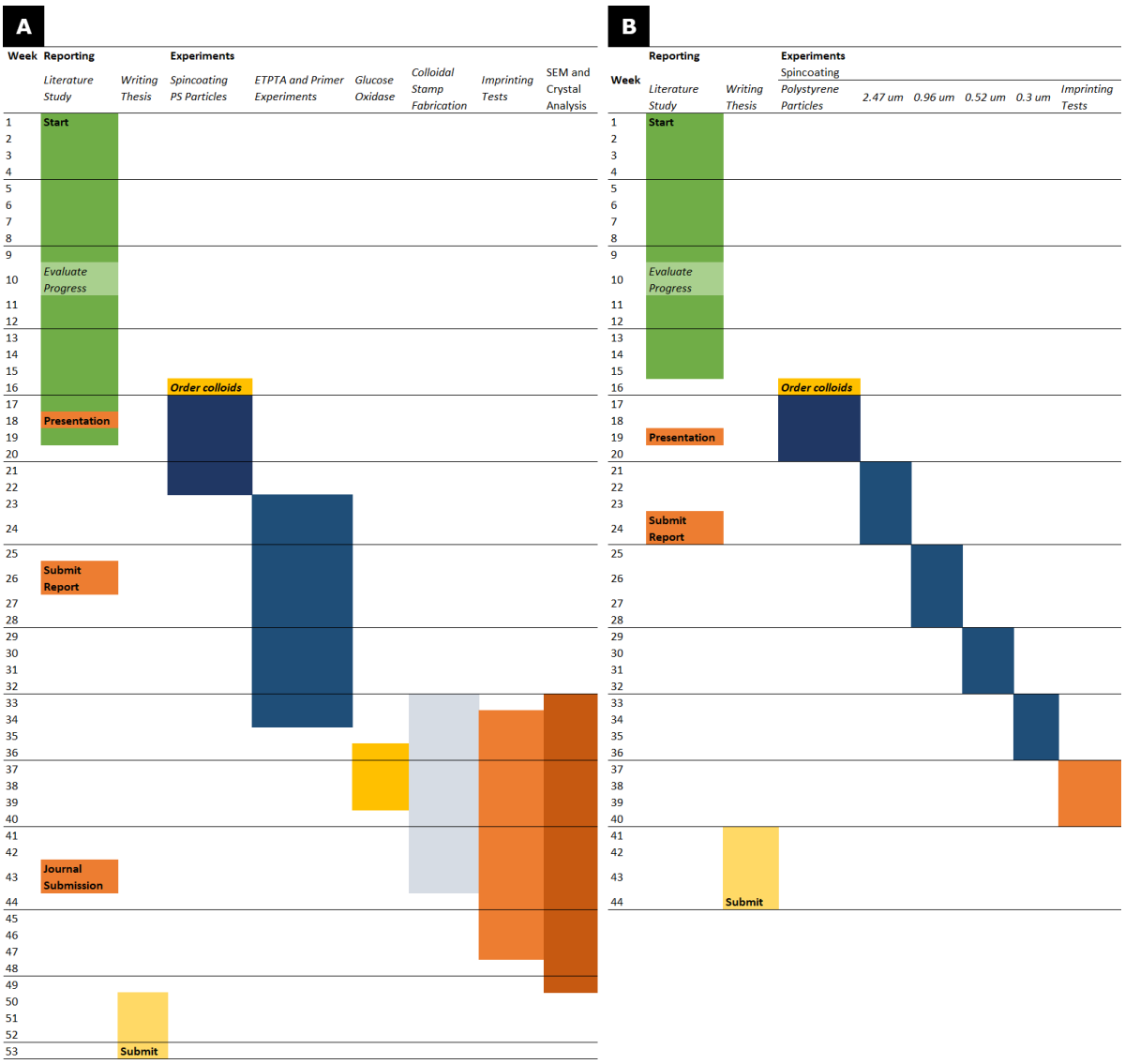

Figure 4.1: Comparison of the time spend versus planned. **A**) Actual timeline. **B**) Time planned to be spend on experiments.

The initial plan was to also test the effect that particle size has on the quality and size of the colloidal crystals. However, because of the curing issues with the ETPTA this became an issue with a lower priority and instead time was invested into solving this problem. Revealing also an assortment of new problems that had to be fixed, as described in detail section 4.1. Another part that took much more time than expected was the analysis of the crystals, mostly because only the SEM turned out to be a viable instrument for the crystal analysis. Secondly, the identification of particles became more work than expected as there is no general consensus within literature for a single verification technique, and because an algorithm is not publicly available.

4.3. Contributions

This project does not exist within a vacuum, therefore it is important to look at environment in which it exist. Originating from a research initiative which was started to discover the effects of surface morphology on the crystallization of salts which make up kidney stones. However, the surfaces required for this research are currently manufactured externally and are costly and complex to produce. Therefore, the idea was proposed to use the self-assembly of colloids to produce masters which could replicate these types of surfaces in-house through hot embossing. Due to this research this can now be achieved.

The main takeaway from this research is that it is possible to use self-assembled colloidal crystals as a pattern to make imprints into the TOPAS material. Other achievements within this project have been the characterization of polymer embedded crystals. As well as the development of a simple technique for curing and processing colloidal crystals by means of ubiquitous laboratory equipment, e.i. the coverslip. Lastly, the parameter space for self assembly by spincoating is reduced, due to the spincoating speed having very little influence on the crystals quality. Therefore, this research results directly in expanding the toolset of the polymer microfabrication group as a whole.

Within the Micro and Nano Engineering group this research could be used within future self-assembly or microstructuring projects, with a potential expansion towards non-polymeric materials.

Within the scientific community this works expands the research on spincoating colloidal crystals within polymeric suspensions, on which very little research has been performed. Furthermore, there are currently no publications which specifically treat the usage of monolayer colloidal crystals to replicate patterns through hot embossing.

4.4. Personal Points of Improvement

Let me start out by saying that I have learned a lot in this past year. From having next to no experience with experimental work, I managed to get hands on and I learned about what it means to perform experimental work in a scientific way. Which includes rigorous verification of results through measurements and qualitative and quantitative means. The last part is exactly what I struggled with because it was something I had to learn. As I have very little background in practical laboratory work I sometimes didn't know how to move forward. I think therefore that making a detailed experimental plan, with the parameters that I want to test and which results I want to obtain and in which fashion would help a lot with finding the right direction earlier on. Even though the goal of my research was clear, the direction in which to go was not. Leaving me with a lot of options which, without a clear way to approach it, sometimes left me overwhelmed. This is of course part of scientific experimentation, as you never know what exactly is going to work. But I do think working with a more structured approach could help me in preventing repeating failed attempts and streamlining my research.

Secondly, although I was aware of this, at the start of my research I kept a shoddy logbook. Even though I did store all my measurements neatly, the steps taken towards the results of some of my experiments were sometimes missing or incomplete. This has led me to having to do some experiments again or having to spend a lot of time later trying to piece everything together. For my main experiments I did manage to resolve this and I kept good track of my steps and often wrote down everything on the respective petridish I was using and in my logbook, which helped a lot in avoiding confusion.

Lastly, I had the tendency during this project to aim at technology readiness level that was higher than could possibly be achieved within the scope of this project. Although this has also been my main drive within the project, it also made me not want to settle for less. Such that I initially rejected results in favour of trying to achieve even 'better' ones. This last point has been the major lesson I learned, because although it drives me to advance, rigorously evaluating my results helps me in guiding the direction of my research.

A

Experiments

A.1. Proof of Concept

In order to identify the requirements for a colloidal stamp a proof of concept experiment was carried out. In this experiment aqueous polystyrene particles with a median size of 5 µm, provided by Fluka (now Sigma-Aldrich), were deposited onto silicon wafers. With the domains arbitrarily determined by cutting the silicon with a diamond pen. The solution was ultrasonicated for 5 minutes in a xxxx ultrasonicator to prevent particles clumping together. Silicon wafer pieces were treated in a Diener Femto Plasma cleaner for 2 minutes at 60 watt to reduce hydrophobicity of the surface. Droplets of 100 µl were dispensed onto the cleaned surface and then spincoated at 500, 1000 or 2000 rpm for 60 seconds. The difference in terms of the final crystal can already clearly be seen by eye as in figure A.1.

Figure A.1: Samples which have been plasma cleaned and spincoated with 100 µl of the aqueous polystyrene solutions. From left to right; 500 rpm, 1000 rpm and 2000 rpm spincoated for 60 seconds. All samples are around 1 cm^2.

Similar samples were inspected by SEM imaging after sputtering a conductive gold layer on top, revealing *hcp* structures and multilayers of varying thickness, as shown in figure A.2.

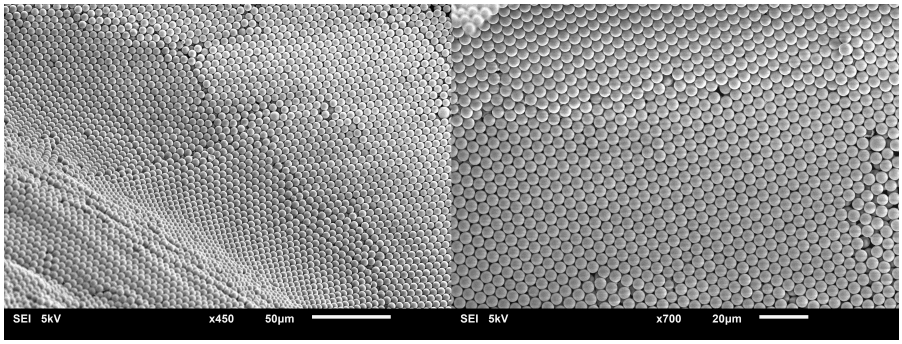

Figure A.2: Images of silicon spincoated with 5 µm polystyrene beads showing the quality and sudden change in layer thickness

Generally the adhesion between silica particles and a silicon surface is not strong enough to withstand a hot embossing procedure. As the adhesion can be overcome by a simple soft lithography

technique. Which was demonstrated by Yan and co-workers[59] where they modified a colloidal crystal by crafting a PDMS stamp with which they selectively picked up rows of silica particles. This method was used as an inspiration to evaluate the effectiveness of a PDMS stamp in a hot embossing process.

Firstl two colloidal crystal were prepared at a spinspeed of 2000 RPM. Then in a 10 cm petridish a prepolymer mixture of PDMS was prepared by combining it with a curing agent at a 10:1 ratio. An oven was heated to 60 °C and the PDMS was placed within the oven for 1 hour. After an hour the PDMS was removed and cooled down to room temperature. One of the sample was placed with the crystal facing the PDMS and pressed into the target until it visibly deformed, before releasing the pressure. A second sample was pressed multiple times into the PDMS at different locations before being completely removed. This sample was then placed into the oven again and cured for another 3 hours. The difference between the two methods could be visually distinguished. The stamping method left very few particles on the PDMS surface, with multiple stamping sites seemingly retaining little to almost no particle transfer. In figure A.3 a visual comparison of the two methods can be seen. Where for the stamping method the site with the highest retention was shown.

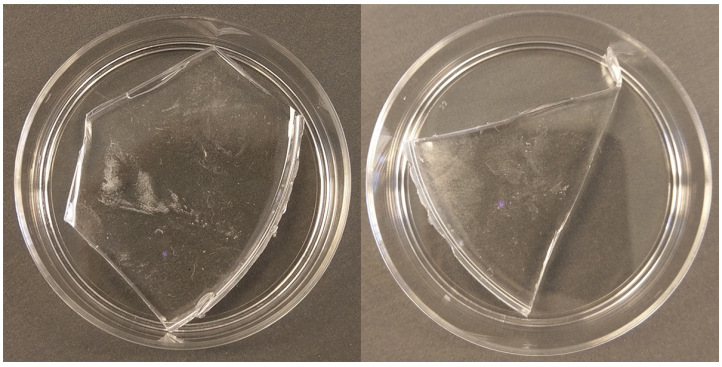

Figure A.3: The difference in particle transfer can be clearly seen with the naked eye. The colloidal crystal which was pressed into the material and left there during curing (left) resulted in a high particle retention on the PDMS surface. While the stamping of the crystal onto the PDMS left few particles (right).

The piece of PDMS with the highest particle retention was cut out from the filled petridish and imaged with a Bruker White Light Interferometer. This revealed two distinct features as can be seen in figure A.4. Firstly, a large amount of particles were attached to the surface, shown by the peaks. The shape of these particles can not be imaged because they are round, however their presence and crystalline structure can be observed. Secondly some of the particles had left an imprint but had not detached from the colloidal crystal.

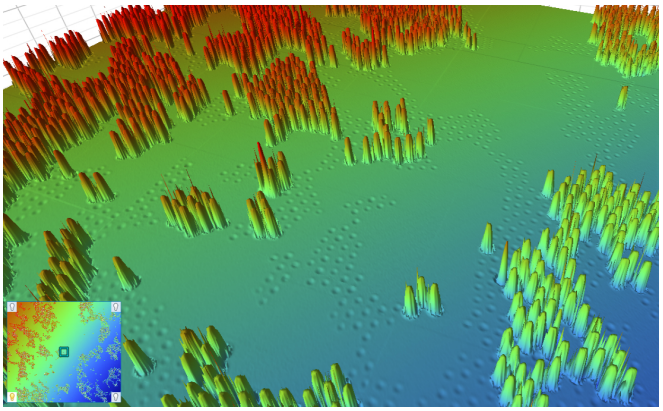

Figure A.4: The presence of polystyrene particles and imprints left behind by particles which did not attach to the PDMS stamp can be observed.

As a final part of the proof of concept test, this stamp was used in a hot embossing test to examine the replication of the features. This was carried out by placing it in a hot embosser and pressing the PDMS stamp into a thin film of TOPAS. This film was then sputter coated with a 15 nm layer of

paladium-gold to make it conductive and then imaged by SEM. Figure A.5 shows two distinct features on the surface. A large amount of particles which were attached to the PDMS stamp had transferred into the TOPAS, meaning that the particles poorly adhered to the PDMS. Which shows that particle adhesion to the stamp is important for two reason. Firstly, the transfer of particles damages the target material and no replication is attained. Secondly, the stamp is not reusable and a new stamp would have to be synthesized for every single polymer replication.

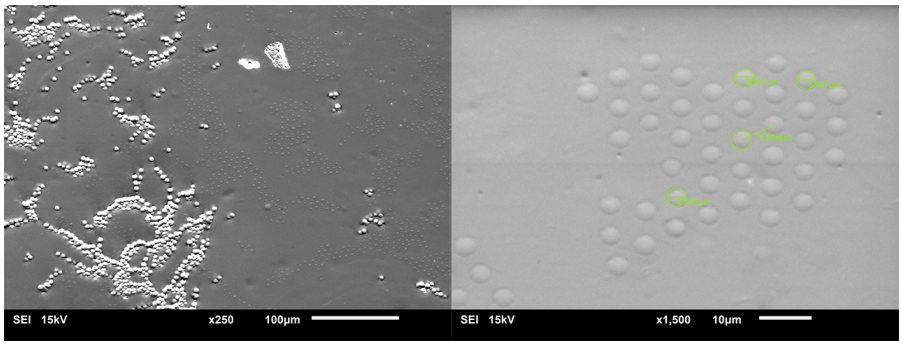

Figure A.5: SEM images showing both polystyrene particles and domes left behind by the PDMS master.

However, the site were the particles were imprinted into the PDMS transferred very well and resulted into dome-shaped structures. The height of the dome can be calculated by means of the schematic drawing in figure A.6.

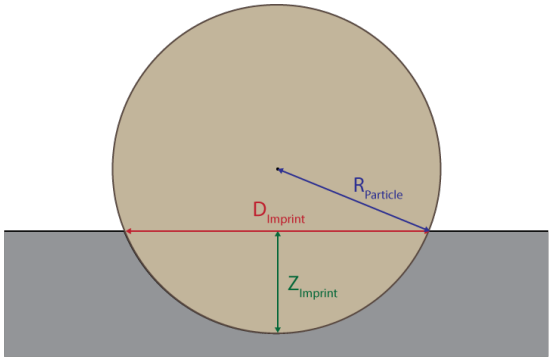

Figure A.6: Schematic overview in order to calculate the imprint depth. With the dimensions of the particle radius (R_{Particle}), the measured imprint diameter (D_{Imprint}) and the imprint depth (Z_{Imprint}).

Using the known particle size and measured imprint diameter, as measured by the SEM, the imprint depth (or height of the domes) can be calculated by means of equation (A.1).

$$Z_{\text{Imprint}} = R_{\text{Particle}} - \sqrt{R^2_{\text{Particle}} - \frac{1}{2}D^2_{\text{Imprint}}} \tag{A.1}$$

With a value for D_{Imprint} of 3.467 µm the imprint depth is 310.120 nm, roughly $\frac{1}{16}$th of the entire sphere.

A.2. Methods for Curing ETPTA

Curing of the ETPTA (Trimethylolpropane ethoxylate triacrylate) monomer proved to be difficult, as for thick droplets a thin layer of the monomer remained uncured. For thin layers the effect was even worse as the monomer barely cured and could be washed off in water. However, it was unclear what the layer was composed of, as it could be either uncured monomer or excess curing agent. Therefore, a XRD analysis was carried out on three separate silicon 501 wafers, onto which ETPTA, Darocur 1173 and a mixture of the two was spincoated. The latter was cured in a Photopol Light[84] UV curing unit

for 2 minutes, such that it was exposed to two 75 W UV lamps with a peak wavelength at 490 nm. Figure A.7 shows the results as measured by a Bruker-AXS D5005 diffractometer, wherein materials which are composed of the same atoms, should have the same peak width. The XRD pattern suggests that the liquid ETPTA and cured ETPTA share more similarities than the Darocur film. However, because the samples were not homogeneous, due to partial coverage on the samples, it was difficult to draw a definitive conclusion.

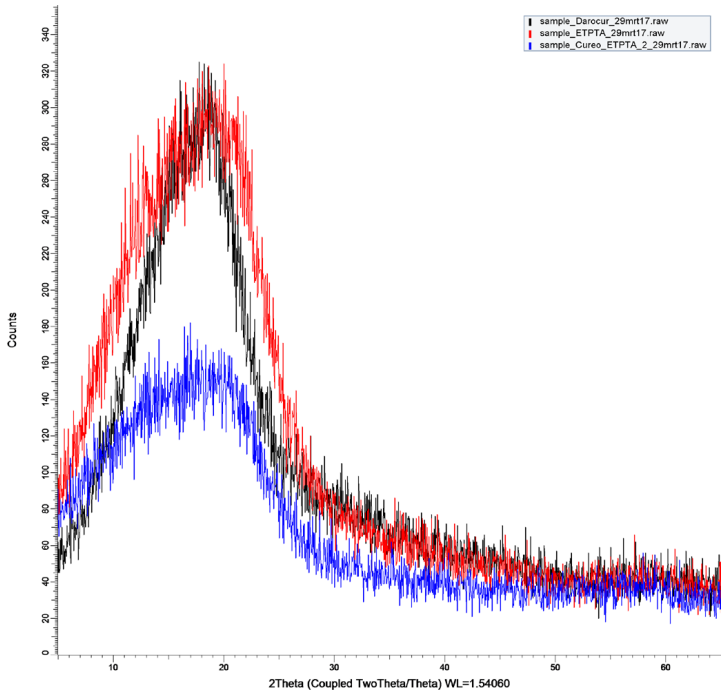

Figure A.7: XRD analysis of three silicon 501 wafers, showing the data found for the monomer ETPTA, the photoinitiator Darocur 1173 and (partially) polymerized ETPTA.

Therefore, this analysis did not yield an answer to the partial polymerization of the ETPTA. Therefore I contacted the author of the paper; Peng Jian, Professor of Chemical Engineering at the University of Florida. He suggested that the problem I experienced had to do with atmospheric oxygen inhibiting the curing of the ETPTA. Literature revealed that this is in fact the result of certain curing agents, especially type II photointiators, where oxygen will absorb the radicals of the photocuring agent. This forms so called peroxyl radicals, which do not participate in the polymerization of the polymerizing monomer[71]. Jiang and co-workers[41] used a vacuum chamber which was back-filled with nitrogen to circumvent this problem. Unfortunately, this kind of equipment was not available in labs across the university campus and an alternative had to be found to cure the ETPTA monomer.

A.2.1. Coverslip Method and Base Fabrication

A very simple way of curing the ETPTA is by depriving it off oxygen by sandwiching it in-between two glass slides, as this cuts it off from molecular oxygen and prevents quenching. This revealed a new problem as when the ETPTA was cured through this sandwich structure, the film was easily peeled from the substrate. Therefore, a primer was spincoated onto the glass before a layer of ETPTA was spincoated on top of it. As a primer the silane coupling agent KR-513 was used, which is designed to function with acrylates in mind. This method is far from ideal as now the ETPTA layer comes into contact with the coverslip. Therefore, an alternative method involving the protein Glucose Oxidase was investigated.

A.2.2. Glucose Oxidase

A method developed by Oytun and co-workers[85] prevents oxygen inhibition during the curing of poly(ethyleneglycol) diacrylate (PEGDA) by adding the protein glucose oxidase(GOx). In this process a mixture of glucose, water and glucose oxidase is used to convert the glucose into gluconolactone

and hydrogen peroxide by capturing molecular oxygen. This prevents the oxygen from interfering with the polymerization of the monomer, without the need of removing ambient oxygen. The method was successfully implemented into a composite hydrogel developed by Sydney Gladman and Coworkers[86], where they embedded cellulose fibrils into the monomer N-isopropylacrylamide. This composite hydrogel was used to 3D print polymer structures which deformed anisotropically after a swelling agent was added.

Therefore an experiment was performed to see if it was possible to create a colloidal suspension consisting of ETPTA, water, glucose oxidase and glucose. Freeze dried Glucose Oxidase from Aspergillus niger was purchased from Sigma Aldrich. Instead of glucose, white cane sugar donated by Sodexo was used. As cane sugar is made up out of sucrose which is a combination of glucose and fructose[87]. The reaction should be similar to that of glucose with glucose oxidase, in which two hydrogen atoms are scavenged from glucose, displayed in figure A.8.

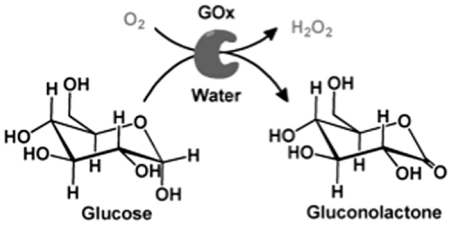

Figure A.8: Reaction of glucose with glucose oxidase and molecular oxygen, adapted from [85].

By the chemical formulas for Fructose ($C_{12}H_{22}O_{11}$) and the reaction provided by figure A.8, the final result should logically be,

$$C_{12}H_{22}O_{11} + O_2 \xrightarrow{\text{GOx}} C_{12}H_{20}O_{11} + H_2O_2 \tag{A.2}$$

The chemical formula of the final product can be be found online, however no information could be retrieved on what the final product of this reaction would be. In order to test the effectiveness of the method with ETPTA the following recipe was used, based on the one used for the PEGDA monomer.

First the ETPTA mixture was prepared as in section 3.2.1, with a concentration of silica particle at 20% wt and ETPTA at 80 % wt. Then cane sugar was dissolved into water and added to the ETPTA mixture. After which it was mixed on thoroughly on a platform shaker and subsequently ultrasonicated for 5 minutes, until an uniform white suspension was present. Finally the Glucose Oxidase was measured and dissolved in water, after which it was added to the ETPTA and aqueous sucrose mixture and vigorously shaken. Finally, 25 µL of the suspension was pipetted onto precleaned and, with a diamond pen, bisected pieces of microscope glass, which had been rinsed in ethanol and DI water before being baked at 150 °C for 5 minutes. A two step-spincoating procedure was used, first the spinspeed was set to 300 rpm for 60 seconds after which it was increased to 1000 rpm for 120 seconds, with both steps having an angular acceleration of 200 rpm/s.

Depending on the water concentration, some suspension were seen to take on hydrophobic behaviour of the water. Therefore, some of the glass slides were post-treated by submitting them to oxygen plasma at 60 W for about 1-2 minutes, in order to change the behaviour of the droplet with the slide. Secondly, varying concentrations of water and ETPTA were tested, while keeping the sugar and glucose oxidase weight the same, in order to allow the ETPTA to dominate the water. The tested recipes of interest are displayed in table A.1.

After curing the samples were subjected to a post-treatment, which involved dipping the samples in ethanol and subsequently in DI water. After which they were transferred to a hotplate at around 125-130 °C, where they were left for 5 minutes, before being allowed to cool down to room temperature. The reason this step was performed because even with addition of Glucose Oxidase not all available monomers will be polymerized, as noted in the PEGDA experiments. To verify this for the ETPTA, the conversion can be calculated by,

$$C(\%) = \frac{\Delta H_t}{\Delta H_{\text{theory}}} * 100\,. \tag{A.3}$$

Material	Recipe 1	Recipe 2	Recipe 3
ETPTA (ml)	0,1	0,2	0,1
SI Weight (mg)	22,2	44,4	22,2
ETPTA Weight (mg)	88,8	177,6	88,8
Water (ml)	0,05	0,02	0,05
Water Weight (mg)	49,91	19,964	49,91
Gox (ml)	0,05	0,02	0,01
Concentration (mg/ml)	2,5	6,25	12,5
Gox Weight (mg)	0,125	0,125	0,125
Water Content Weight (mg)	49,785	19,839	9,857
Sucrose (mg)	1,25	1,25	1,25
Total Weight (mg)	212,07	263,178	172,142
Concentrations (wt%)			
Water	47,01	15,12	34,72
Gox	0,06	0,05	0,07
Sucrose	0,59	0,47	0,73
ETPTA	41,87	67,48	51,59
SI-P	10,47	16,87	12,9

Table A.1: Tested recipes with used volumes, weights and concentrations

Where ΔH_t is the reaction heat as measured at time t and ΔH_{theory} is the amount of heat theoretically required for complete polymerization. To measure ΔH_t the researchers used Photo-Differential Scanning Calorimetry, to measure the heat flow over time and use it to determine the conversion rate[88]. This technique should be viable for detecting the conversion rate in the ETPTA mixture as well, which will provide more in-depth information on the effectiveness of the method for the fabrication of colloidal stamps with the ETPTA monomer.

What follows is a table with a selected number of samples fabricated which were subjected to further investigation.

To examine the structure of the colloidal crystals, an microscope was used to image two spots on sample 1-4. However, two problems were identified through this method. Firstly, the microscope focuses on a single plane, such that multilayer crystals are only partly in focus. This results in inconsistent images which are only marginally suitable for a qualitative analysis, as can be seen in figure A.9.

Secondly, an interferometer was used to try and map the structure of the colloidal crystal. However, as can be seen in cA.10, the resolution is not sharp and enough and the structures are ill-defined. As

Recipe	Sample	Plasma Treatment
Recipe 1	Sample 1-3	No
	Sample 1-4	Yes
Recipe 2	Sample 3-2	Yes
	Sample 3-4	No
Recipe 3	Sample 4-1	Yes
	Sample 4-2	No

Table A.2: The samples which are used to discuss the results in this section, including the used recipe and indication of if they were plasma treated.

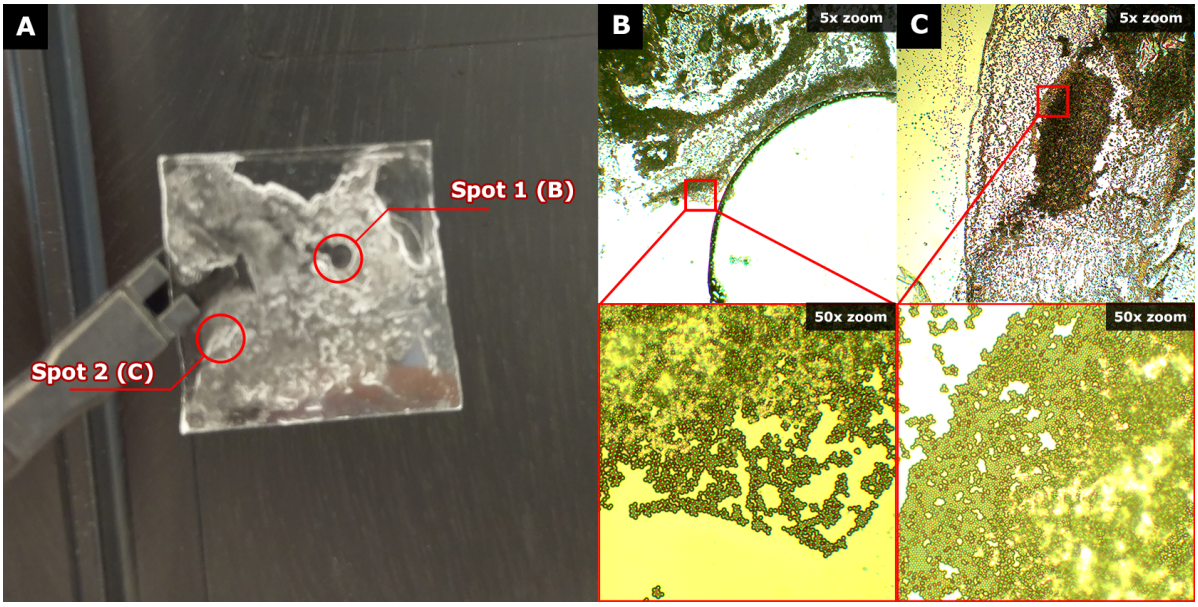

Figure A.9: Microscopy images of sample 1-4, as per table A.1, before post-treatment with ethanol and DI water. **A**) Photograph of sample. **B**) Microscopic images of spot 1 captured with 5x and 50x objective lenses. **C**) Microscopic images of spot 2 captured with 5x and 50x objective lenses.

the particle size is known, with a nominal diameter of 2.47 µm, the features should be clearly defined at the micron scale. However, as can be seen in figure A.10 **C**, at this scale, there is no clear indication of where one particle ends and one begins. This kind of behaviour was observed before in the proof of concept phase, as seen in figure A.4, where because of the spherical nature of the particles, there are no sharply defined edges for the interferometer to cut off. Since in this case the particles are not only on top of the substrate but also partially embedded, the distinction between particle and matrix becomes even less clear.

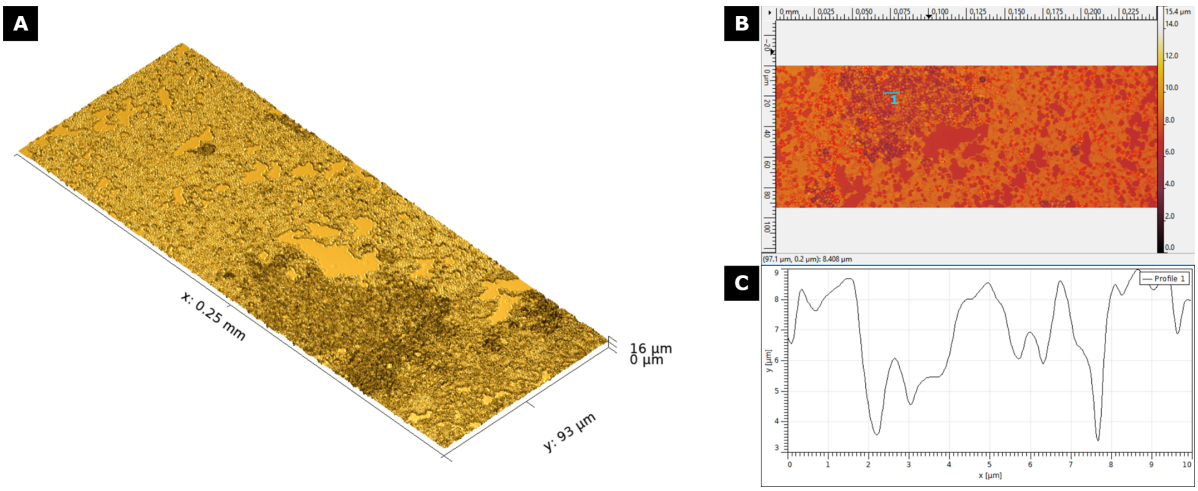

Figure A.10: Interferometer measurements of a slide which has been pre-treated with plasma after which it was spincoated with recipe 1, as per table A.1. **A**) 3D Topography of the sample at a 50x magnification. **B**) Top-down view of the topography at 50x magnification. **C**) Profile measurement of a line on the topography.

Therefore, the samples were sputter coated conductive layer and were then imaged by SEM, resulting in the images shown in figure A.11.

Figure A.11 shows that for the mixtures with water an oxygen plasma treatment is necessary in order to avoid huge deposits of silicon particles which are glued together. An observation made in the lab was that with suspensions which had a low amount of water but a higher concentration of GOx and sugar, such as recipes 2, was that they poorly mixed. This is clearly observed in the SEM images

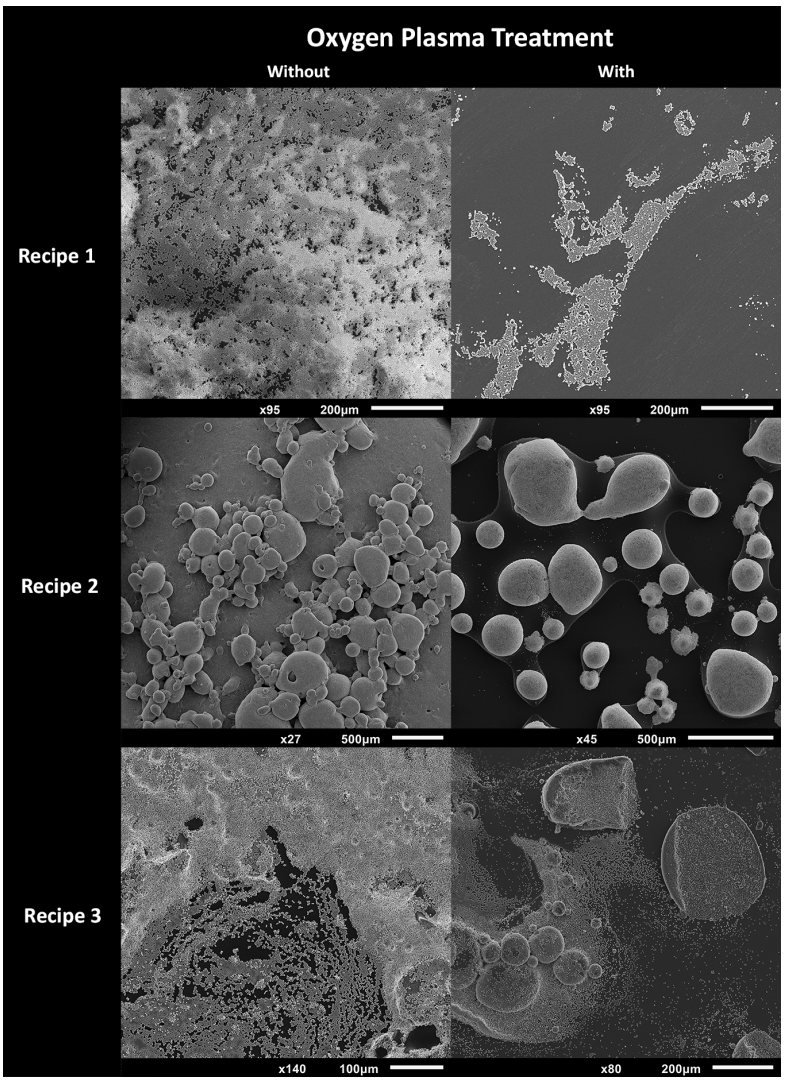

Figure A.11: Comparison image created out of images captured with the Scanning Electron Microscope (SEM), displaying the tested recipes and indicating if oxygen plasma treatment was applied or not.

as well, as the silicon particles form clumped structures. The combination of recipe 1 and the oxygen plasma treatment seems ideal for the formation of crystals, however the one main obstacle is that with the addition of water an evaporative mechanism is now reintroduced into the crystals formation. While the usage of the ETPTA as a suspension and matrix material was chosen in order to avoid the having an evaporative element in the self-assembly.

However, as the resulting crystal was a monolayer with a close packed structure, hot embossing tests were performed to evaluate the effectiveness of these kinds of stamps. Therefore, a stamp was fabricated with the suspension of recipe 3 and then hot-embossed at a temperature of 110 °C and pressure of 1000 N. Unfortunately this resulted in the crystal transferring detaching from the glass substrate into the TOPAS, as can be seen in figure A.12.

To verify the result both the stamp and the sample were imaged with the SEM, the results of which are displayed in figure A.13. As can be seen, other than some surface damage, there are no visible traces of ETPTA on the subtrate or any presence of silicon particles.

Because of this result, it was further investigated why the adhesion of the sample was so low as that it could transfer into the TOPAS. With a new recipe, based on the recipe 1, where the silicon particle concentration was lowered to 10% and the GOx was concentrated more while still maintaining the 100 µl total water volume. The further concentration of the GOx made it slightly easier to handle, as the amount of GOx needed for the lower concentration suspension was very difficult to measure.

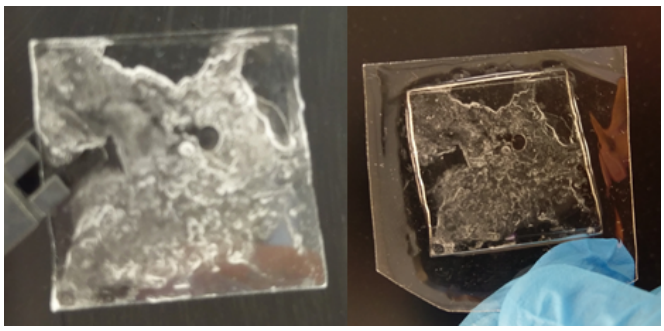

Figure A.12: Photographs of the sample after preparation and the resulting imprint in TOPAS after hot embossing.

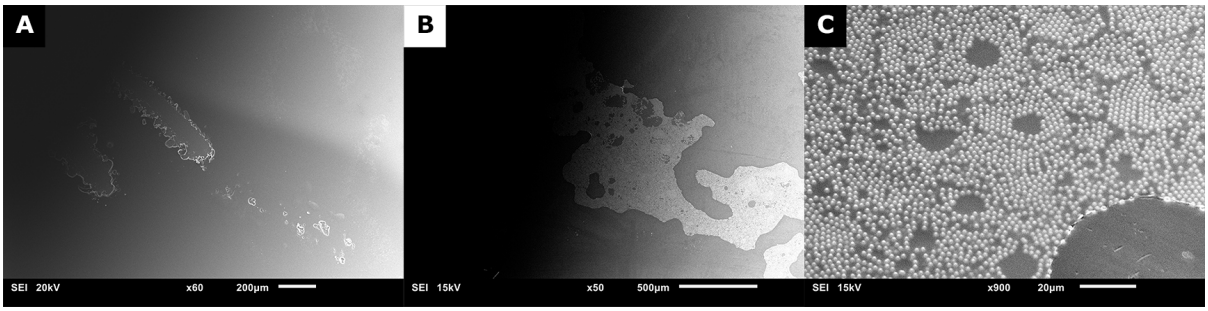

Figure A.13: SEM Images of the stamp fabricated with the GOx suspension. **A**) SEM Image of the colloidal crystals substrate after stamping, with the crystal fully removed and only some remaining surface damage. **B**) SEM image of the target with the colloidal crystals visibly embedded into it. **C**) Close-up of the embedded crystal.

The new suspension was then spincoated and cured as per the previous steps and then cleaned by ultrasonicating it in ethanol for 5 minutes, after which it was rinsed in water and placed on a hotplate at 135 °C. However, after 2 minutes the crystal started peeling from the ETPTA base after 2 minutes, showing that there is some issue with the adhesion of the crystal.

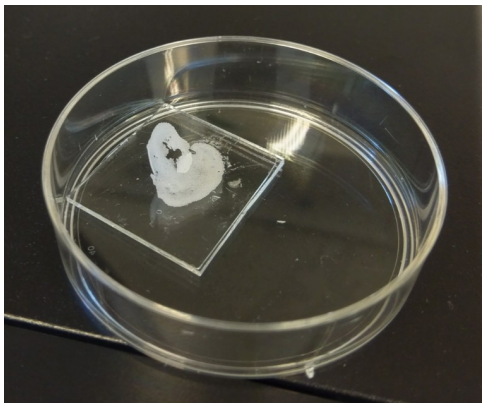

Figure A.14: Photograph of the sample after ethanol treatment and heating on a hotplate, the film is visibly seen peeling away from the ETPTA base.

After this final experiment the test with the Glucose Oxidase were discontinued.

Summary and Discussion

As the ETPTA monomer suffers from oxygen quenching, which inhibits the polymerization of the entirety of the monomers, an alternative was sought to cure it fully. Therefore a method which included Glucose Oxidase and sugar, to harvest molecular oxygen, was incorporated into the spincoating self-assembly method. However, the concentrations of the liquids proved to be very influential, as concentrated suspensions lead to clotting. Secondly, an oyxgen plasma treatment of the ETPTA base was necessary to make the substrate less hydrophilic and to allow a spread out coverage. Lastly, the current iteration

of the recipe leads to the film releasing from the substrate under conditions with increased temperature and pressure, such as in the hot embosser. At this stage it is, not yet, a viable technique for synthesis of colloidal crystals which are suitable for imprinting by hot embossing. Therefore, the method of curing ETPTA by placing a coverslip on top of the films and crystals will be used.

A.3. Influence of ETPTA Base on Surface Roughness

In this section a small comparison is made to check the influence of the primer on the fabrication of the colloidal stamp. Secondly, the quality of the ETPTA base structure is checked to see if it provides a flat enough surface for the colloidal crystals

A.3.1. Surface Roughness of ETPTA Spincoated onto Primer

Spincoating ETPTA directly onto the KR513 primer resulted in a very wavy surface finish. To evaluate a sample was produced and image per interferometry, after which the surface roughness parameters were determined in Gwyddion. The results are provided in table A.3.

Sample	R_a(µm)	R_{rms}(µm)
1-1	7.699	8.908
1-2	5.403	6.482
1-3	8.538	9.036
Average	7.213	8.142

Table A.3: Table with the found surface roughness parameters for ETPTA directly spincoated onto the primer.

This shows that the roughness is in fact. on average. roughly a magnitude of 2.9 and 3.3 higher than the particle diameter for the arithmetic (R_a) and root mean square (R_{rms}). respectively. Secondly, by looking at the profile of these spots, as shown in figure A.15, it is clear that the surfaces are not smooth at all. Therefore a layer of ETPTA was fabricated on top of the spincoated primer.

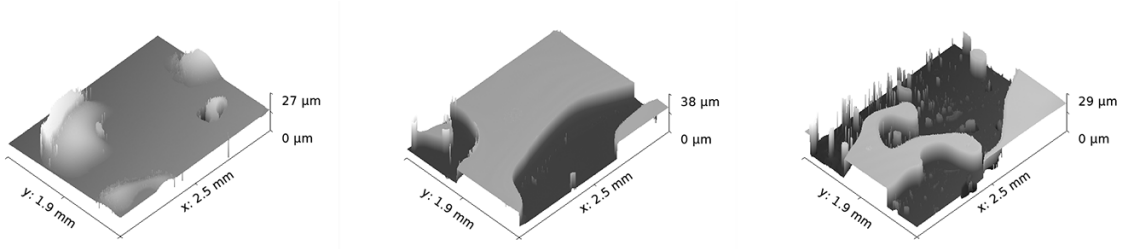

Figure A.15: Images of the surface structures found of the three imaged spots on the ETPTA directly spincoated onto the KR513 primer.

A.3.2. Surface Roughness of ETPTA Base

To check how smooth the surface of the ETPTA base is three of these structures were imaged by interferometry, with four spots evaluated per samples. Some samples contained defects, such that certain parts were masked to avoid their interference in the analysis. Table A.4 displays the found values using Gwyddion, including the measured area. In order to provide a fair comparison, a normalization factor was determined per,

$$R_{norm} = \frac{A_{meas}}{A_{avg}} R_{meas}\,, \tag{A.4}$$

where A_{meas}. A_{avg} and R_{meas} are the measured area. average area and measured roughness, respectively.

These results show that the surface is much smoother if the ETPTA base is fabricated on top of the primer, than by spincoating directly onto the primer. For completeness, in figure A.16 the three roughest surfaces are shown, which other than some small defects, have surfaces with very little observable waviness.

Sample	R_a(µm)	R_{rms}(µm)	**Area** (mm^2)	**Normalized** R_a(µm)	**Normalized** R_{rms}(µm)
1-1	0.202	0.462	3.478	0.180	0.412
1-2	0.516	0.604	2.898	0.384	0.449
1-3	0.263	0.809	3.485	0.235	0.723
1-4	0.422	0.607	3.714	0.402	0.578
2-1	0.260	0.416	4.032	0.269	0.430
2-2	0.590	1.001	4.729	0.716	1.214
2-3	0.568	0.869	4.077	0.594	0.909
2-4	0.237	0.306	2.898	0.176	0.227
3-1	0.500	0.646	3.486	0.447	0.578
3-2	0.038	0.050	4.661	0.045	0.060
3-3	0.038	0.052	4.661	0.045	0.062
3-4	0.104	0.154	4.661	0.124	0.184
Average	0.312	0.498	3.898	0.302	0.486

Table A.4: Table with the found surface roughness parameters for the investigated samples

A.4. PDMS as an Alternative Polymer Matrix

Because currently used polymer matrix material requires an environment free of oxygen to properly cure, alternative materials were considered. However, one main criteria was the material should be able to withstand a temperature above the glass temperature of TOPAS. One of these, which was readily available, was PDMS. As PDMS is very viscous (5.1 Pa s[89]), which is more than 500 times as viscous as water[90]. This directly influences the maximum thickness of a spincoated film, as per equation (3.3).

However, the spincoater is limited to a maximum spin speed which limits the maximum shear force. Therefore a simple test was carried out to see if it was possible to achieve a film less thick than the particle size. The PDMS was made less viscous by adding more curing agent, at a weight ratio of 3:1 instead of the standard used 10:1 ratio. The PDMS mixture was prepared and thoroughly mixed after which it was put into a desiccator and pumped down to remove the air bubbles which entered the PDMS during mixing.

About 100 µl of the PDMS was then dispensed using an Eppendorf micropipette onto the glass slide, after which the slide was put into the spincoater and spun at either 2500, 5000, 7500 or 10000 rpm for 90 seconds. The slides were then cured in an enclosed oven for about 4 hours at a temperature of 80 °C, to ensure complete curing. For each spin speed two samples were prepared in the same fashion.

After curing the samples were then imaged by use of a white light interferometer, by using a green light narrowband wavelength, resulting in a height map of each sample. Three spots were imaged of each sample such that a total of 6 measurement points, all taken at points where the edge of the PDMS was, were retrieved per spin speed. Then using the analysis program Gwyddion a height profile was extracted. Then the mean thickness was calculated in a script written in matlab displayed in appendix A.4.1. A few of the profiles and the calculated mean thickness of the profiles are displayed in figure A.17.

In this fashion the average height of the samples was calculated and use to find the average thickness of the spincoated PDMS samples. A boxplot of the thickness versus the spincoating speed is displayed in figure A.18.

From these results it is determined an average film thickness is found of 1.4988 µm when spincoating at 10000 RPM, which would make it suitable for trapping the particles. However, when spin speeds are increased the profiles become very rough, with the waviness increasing[91]. This profile will also then be replicated into the target material, and as mentioned in section 2.4.4, a flat monolayer crystal is required to achieve a conformal imprint. However, this waviness might be a result from the fact that PDMS is transparent, which makes it harder to image with interferometry. Further verification is therefore required, such as through SEM imaging.

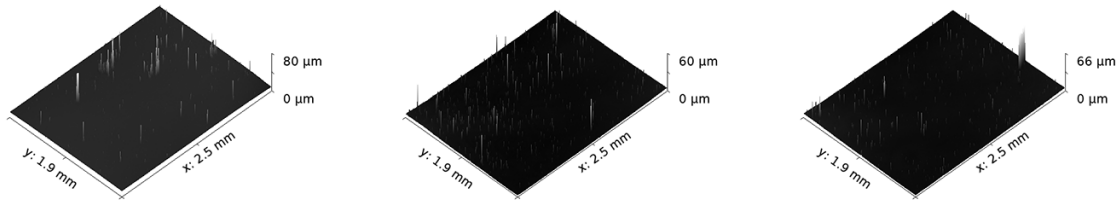

Figure A.16: 3D surface images of the surfaces with the roughest surfaces. From left to right: samples 1-3, 2-2 and 2-3.

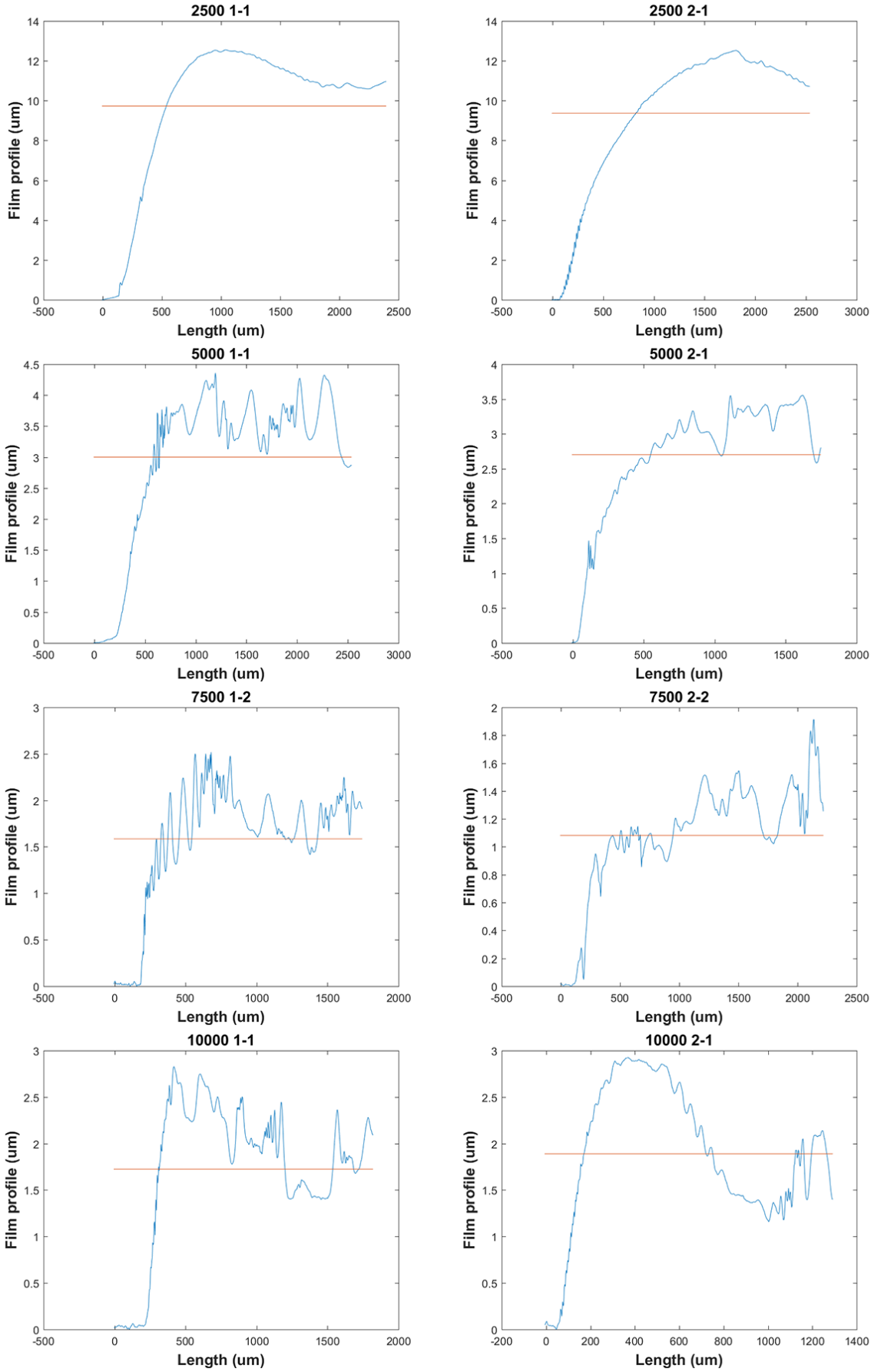

Figure A.17: An overview of some of the profiles extracted from the PDMS films and the mean plotted in them in red. The sample numbering is defined as spinspeed-sample-spot.

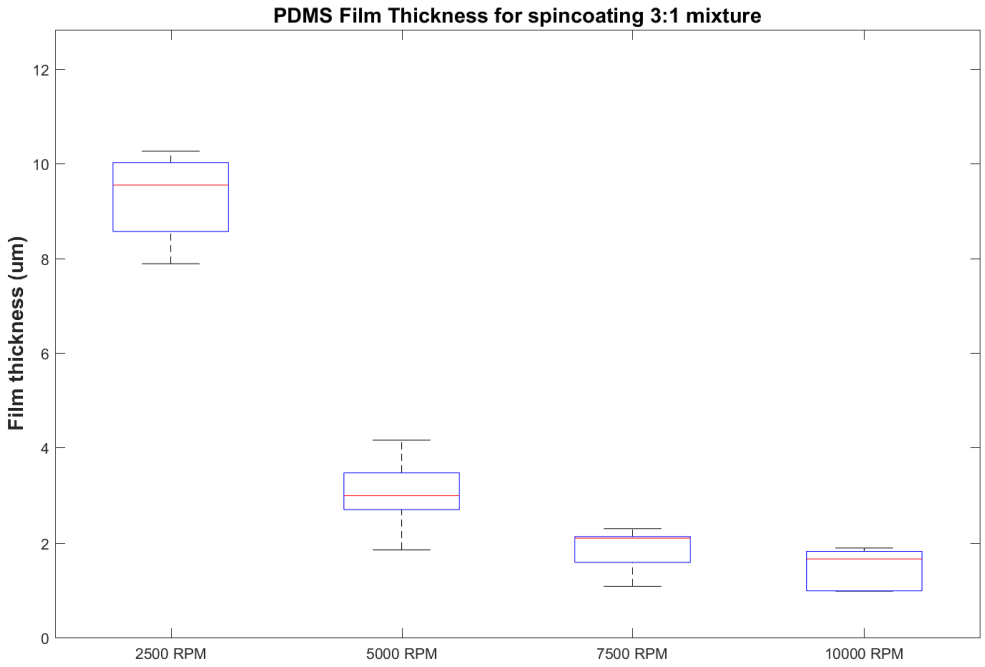

Figure A.18: A boxplot of the influence of the spin speed on the thickness of the PDMS film.

A.4.1. Matlab Script for PDMS evaluation

```
clear all
clc

M = {'2500 1-1.txt','2500 1-2.txt','2500 1-3.txt',...
'2500 2-1.txt','2500 2-2.txt','2500 2-3.txt',...
'5000 1-1.txt','5000 1-2.txt','5000 1-3.txt',...
'5000 2-1.txt','5000 2-2.txt','5000 2-3.txt',...
'7500 1-2.txt','7500 1-3.txt','7500 1-4.txt',...
'7500 2-2.txt','7500 2-3.txt','7500 2-4.txt',...
'10000 1-1.txt','10000 1-2.txt','10000 1-4.txt',...
'10000 2-1.txt','10000 2-2.txt','10000 2-3.txt'};

for j = 1:1:length(M)
clear V_filt
v = load(M{j});
floor = min(v(:,2));
V = v - floor;
[r,c] = find(V == max(V(:,2)));

avg_v = sum(V(:,2))/length(V);
no = length(V);
red = linspace(avg_v,avg_v,length(V(:,2)));

figure('Visible','Off')
figname = strrep(M{j},'txt','png');
titlename = strrep(M{j},'.txt','');
plot(V(:,1)*(10^6),V(:,2)*(10^6))
hold on
plot(V(:,1)*(10^6),red*(10^6))
title(titlename,'interpreter','Tex','FontSize',14,...
'FontWeight','bold')
ylabel('Film profile (um)','interpreter','Tex','FontSize',14,...
'FontWeight','bold')
xlabel('Length (um)','interpreter','Tex','FontSize',14,...
'FontWeight','bold')
saveas(gcf,figname)
hold off

data(j,1) = avg_v;
data(j,2) = no;
end

data = data*(10^6);

%Specify window settings
w = 1600;
h = 1000;
sz = 2/3;

```

```
figure(j+1)
set(gcf, 'Position', [100, 100, w*(sz), h*(sz)])
boxplot([data(1:6,1),data(7:12,1),data(13:18,1),data(19:24,1)],...
'positions',[2500,5000,7500,10000],...
'Labels',{'2500 RPM','5000 RPM','7500 RPM','10000 RPM'})
ylim([0 max(data(:,1))*1.25])
ylabel('Film thickness (um)','interpreter','Tex','FontSize',14,...
'FontWeight','bold')
title('PDMS Film Thickness for spincoating 3:1 mixture','FontSize',14,...
'FontWeight','bold')
saveas(gcf,'PDMS_plot.png');
```

A.5. Effect of Ethanol on TOPAS

A small experiment was performed to see if ethanol had any effect on TOPAS films in the short or long term. Three samples were prepared: one which was not treated, one exposed to ethanol for 5 minutes and the last film was exposed for over 24 hours. Only the film that was exposed for 24 hours showed a change that could be observed by microscope as shown in figure A.19. This could mean that the ethanol could damage the microstructures over the long term. To measure this, surface roughness measurements ought to be performed with a fine enough resolution.

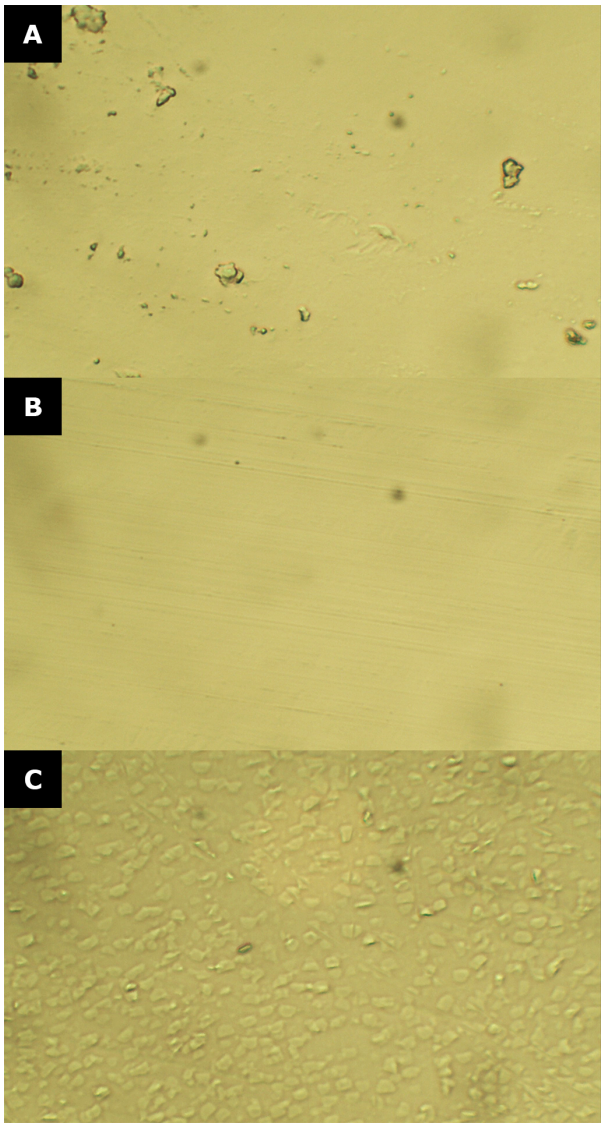

Figure A.19: Microscopic images at 50x magnification observing the influence of ethanol on pieces of TOPAS film. **A**) TOPAS film without any treatment, including some contaminants. **B**) TOPAS after rinsing and exposure for 5 minutes. **C**) TOPAS left for over 24 hours to ethanol exposure. Significant damage has occured to the topas film, which could damage any microstructures on the film.

B

Data Processing

B.1. Crystal Image Analysis

Because the number of particles in a single SEM image can be huge, it is not trivial matter to detect most, if not all, of these without losing information on the structure of the crystal. In the end two different image recognition techniques were used to detect the particles within the crystals, both will briefly be discussed in this section.

B.1.1. Particle Detection by Circular Hough Transform

A Circular Hough Transform (CHT) is a reliable way to find the centers of a circular object[92], which functions as follows. Starting from a circular shape, a circle with a user defined radius is drawn from this point. The points in which the highest number of circles meet is then chosen as the center of the circular object. A schematic description of this is shown in figure B.1, from which it is clear that the closer the radius is to that of the detection circle, the closer the detected centre will be to the actual centre of the particle.

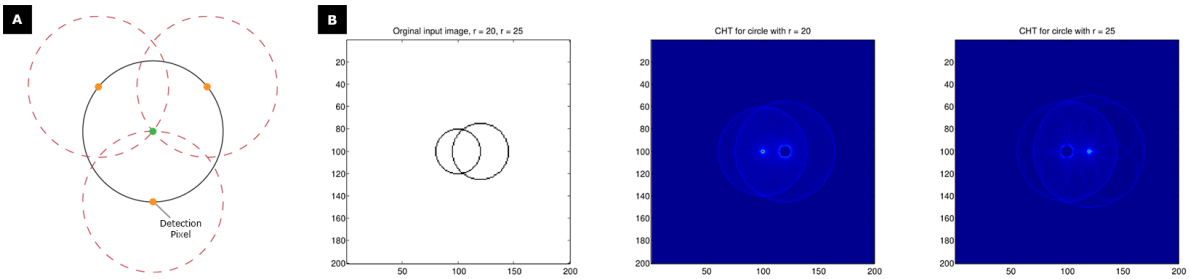

Figure B.1: Example of the of the Circular Hough Transform (CHT) algorithm. **A**) Schematic image of the centre detection. Circles are drawn from the detection pixels and the centre is determined where they intersect. **B**) An example of the influence of the detection radius. The closer the detection radius circle is to that of the circle which is to be detected, the higher the confidence of the location of the circle becomes. Adapted from [92].

Using the CHT algorithim build into Matlab through the CircleFinder application[93], the particle centres are detected and saved in terms of x and y coordinates. An example of how this detection is performed is shown in figure B.2.

However, the problem with the algorithm is that particles which are fuzzy or not bright compared to the background, are rarely detected.

B.1.2. Particle Detection by Crocker-Grier Algorithm

Therefore, an algorithm by John Crocker and David Grier[94] (CG), which can detect particles from low resolution video material, for some of the SEM images. This detection is performed through filtering of the images through certain convolution kernels, such that fuzzy particles are turned into bright spots which indicate the centres. An example of it's usage is displayed in figure B.3.

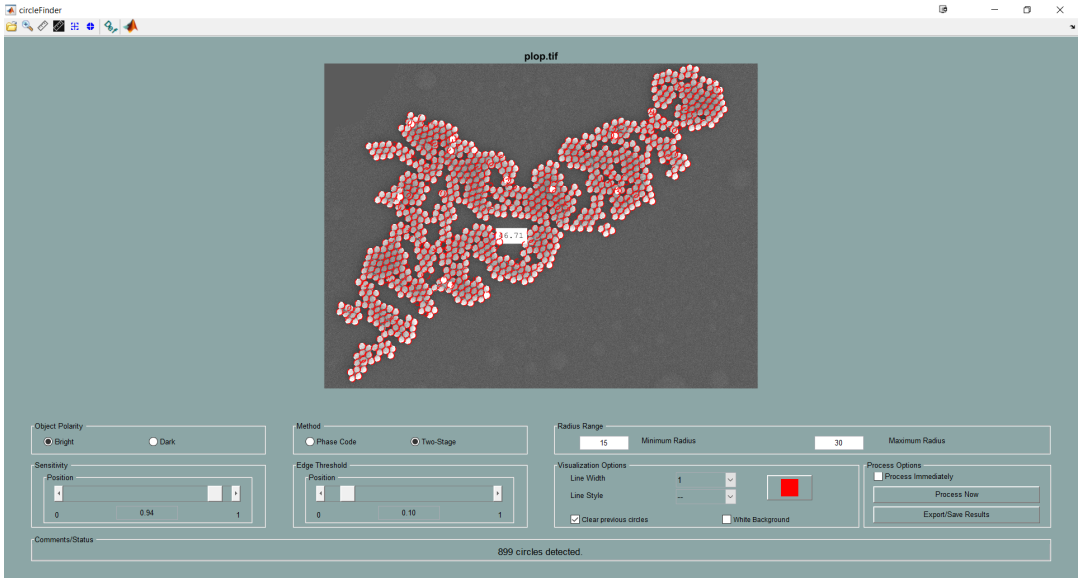

Figure B.2: Image of the CircleFinder application as provided by Mathworks. The particles are detected by the red circles drawn around them.

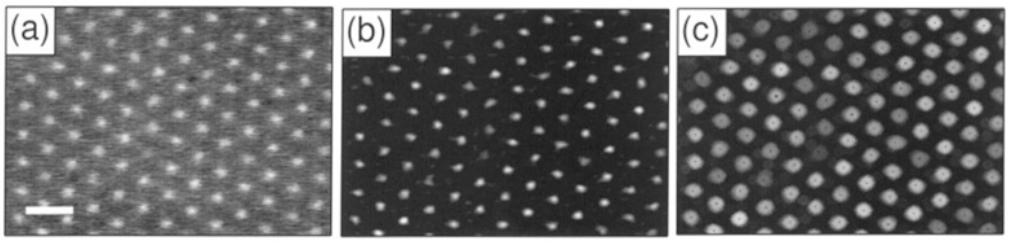

Figure B.3: Images of the image transformation. **A**) An image of a colloidal crystals with scale bar 2 µm. **B**) The image as filtered with the convolution kernel. **C**) By dilation the particle centres are revealed as black dots. Adapted from [94].

The centres are retrieved by taking the local brightness maxima and refinement by only keeping the upper 30th percentile as a particle location. The implementation within Matlab was performed by Maria Kilfoil[95], and was incorporated within an algorithm which processed a set of SEM images.

As both algorithms function differently in terms of particle detection, a comparison of some SEM images using both methods is provided in appendix B.3.

B.2. Method for Evaluating Colloidal Crystal Lattices

Using the coordinates from the particle detection algorithm the lattices can be evaluated. In order to do this Delaunay Triangulation[96] is employed. Within this algorithm a triangular mesh is found in which all the angles are reduced to their smallest values possible that can be achieved within a triangular shape. The points which need to be connected in this fashion are found by drawing a circle a circle such that the centre is an equal distance from each point. A schematic image of this can be seen in figure B.4.

By using the set of coordinates and using the built-in Delaunay Triangulation in matlab a triangular mesh is retrieved. For each triangle the vector lengths are then determined by taking the norm[75] as,

$$|\mathrm{v}| = \sqrt{x^2 + y^2}\,, \tag{B.1}$$

where x and y represent the distance between the two measured points. The angles and ordering parameter are then calculated as explained in section 3.3.2.

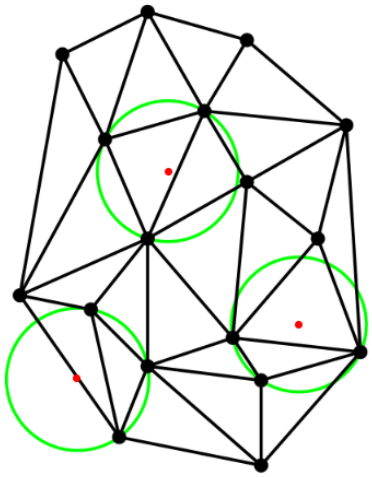

Figure B.4: An example of a Delaunay Triangulation, where the green circles intersect the particles and the red dots represent a point equidistant to each point on the circle. Adapted from [96].

B.2.1. Verification

To validate the method a test pattern was made which is exactly hexagonal. The patterns were then detected using the HCT algorithm and a mesh was generated as show in figure B.5. By evaluating all the angles an order parameter was found of 0.9988, while for an ideal pattern the value should be exactly 1. However, some operations will lead to numerical errors which could lead to the small discrepancy found in the order parameter.

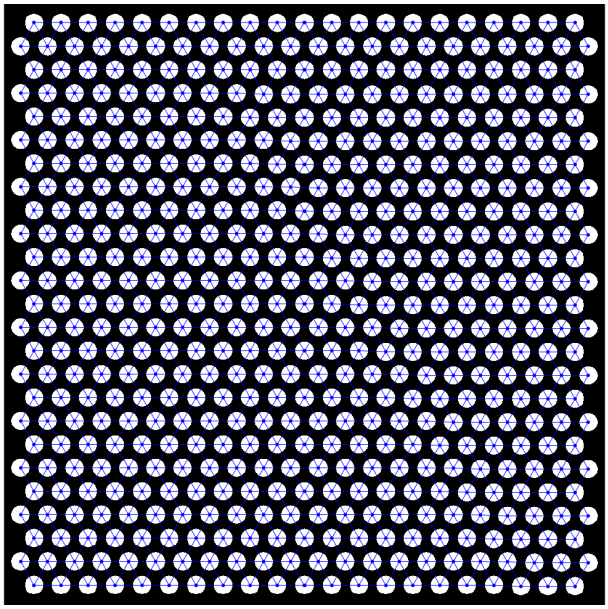

Figure B.5: Ideal hexagonal pattern with the Delaunay mesh overlaid on top of it.

B.2.2. Order Parameter

The local bond order parameter[97] is a very powerful tool to determine how well a particle fits within a local symmetry,

$$\Psi_l^j = \frac{1}{N_j} \left| \sum^{k} e^{6i\theta_{jk}} \right|, \tag{B.2}$$

where the N_j is the number of neighbouring particles and the angles between particle j and the k particles are used to determine the order. Providing a lot of information about the crystallization of the particles. For already formed colloidal crystals this is order is then summed and average, resulting in an order for the entire lattice. However, due to this approach not all angles are evenly weighted. Considering that N_j is the total amount of particles, this means that for the entire lattice not all angles are weighted the same. For example when there is one missing particle from the six-fold symmetry a N_j factor of 1/5 is found, while for an extra particle a N_j factor of 1/7 is found. Meaning that the missing particles angles weigh heavier against the ordering than an extra one. However, since the distance between particles is not taken into account, this penalization seems arbitrary. Weighing the number of angles, as is done in equation (3.2), suggest a more fair evaluation of colloidal crystals. However, a comparison using both ordering parameters on different crystals structures would be needed show how large the influence on the order parameter actually is.

B.3. Comparison and Evaluation of Particle Detection Results

Because the algorithms function completely differently compared to one another, it is necessary to compare their results to see if they can be used interchangeably. Such that the datasets achieved with the two different algorithms can be fairly compared to one another. The results of a random collection of crystals are determined and presented in table B.1.

Sample	**No. CG**	**Ψ_6 CG**	**No. CHT**	**Ψ_6 CHT**	**Difference No. (%)**	**Difference Ψ_6 (%)**
1-3	151	0,566	152	0,564	0,662	0,373
6-1	83	0,540	82	0,506	1,220	6,801
7-1	121	0,309	122	0,472	0,826	52,718
11-3	283	0,471	292	0,384	3,180	22,587
12-2	107	0,335	113	0,332	5,607	1,116
15-3	147	0,552	144	0,555	2,083	0,580
Average					2,263	14,029

Table B.1: Comparison table of the Circular Hough Transform (CHT) and the Crocker-Grier (CG) algorithm, of the number of detected particles (No.) and the order parameter (Ψ_6).

s

As far as the detection of particle numbers goes the difference is minimal. However a worrying trend can be seen in the difference between the two sets of the crystals, where there is an 25 and 52 % difference in the detected crystal quality. Even though the difference in the number of detected particles is less than 5 %. Figure B.6 has the two meshes plotted over each other with the red mesh found through the Crocker-Grier (CG) and the blue mesh found through the CHT algorithms, respectively. What becomes clear from both figure B.6 **A** and **B** is that in the case of the CG algorithm the outliers are filtered out much less often. Secondly, the points for the CG mesh tend to lie much more outward than those of the CHT mesh. This is due to the working principle of the CG method, where the brightest points of the particles are assumed to be the centre. However, especially in the case of figure B.6 **B** there is a huge difference in the locations of the centers, because the particles are exceptionally bright at the edges.

In order to correct for this, all samples evaluated through the CG method should be of effectively the same brightness over the entire crystals. However, as can be seen in sem samples, there are only a few of these kinds of these samples and they have all been evaluated with the CHT algorithm. Alternatively, the error can be combated by increasing the number of samples such that the outliers lose their statistical influence.

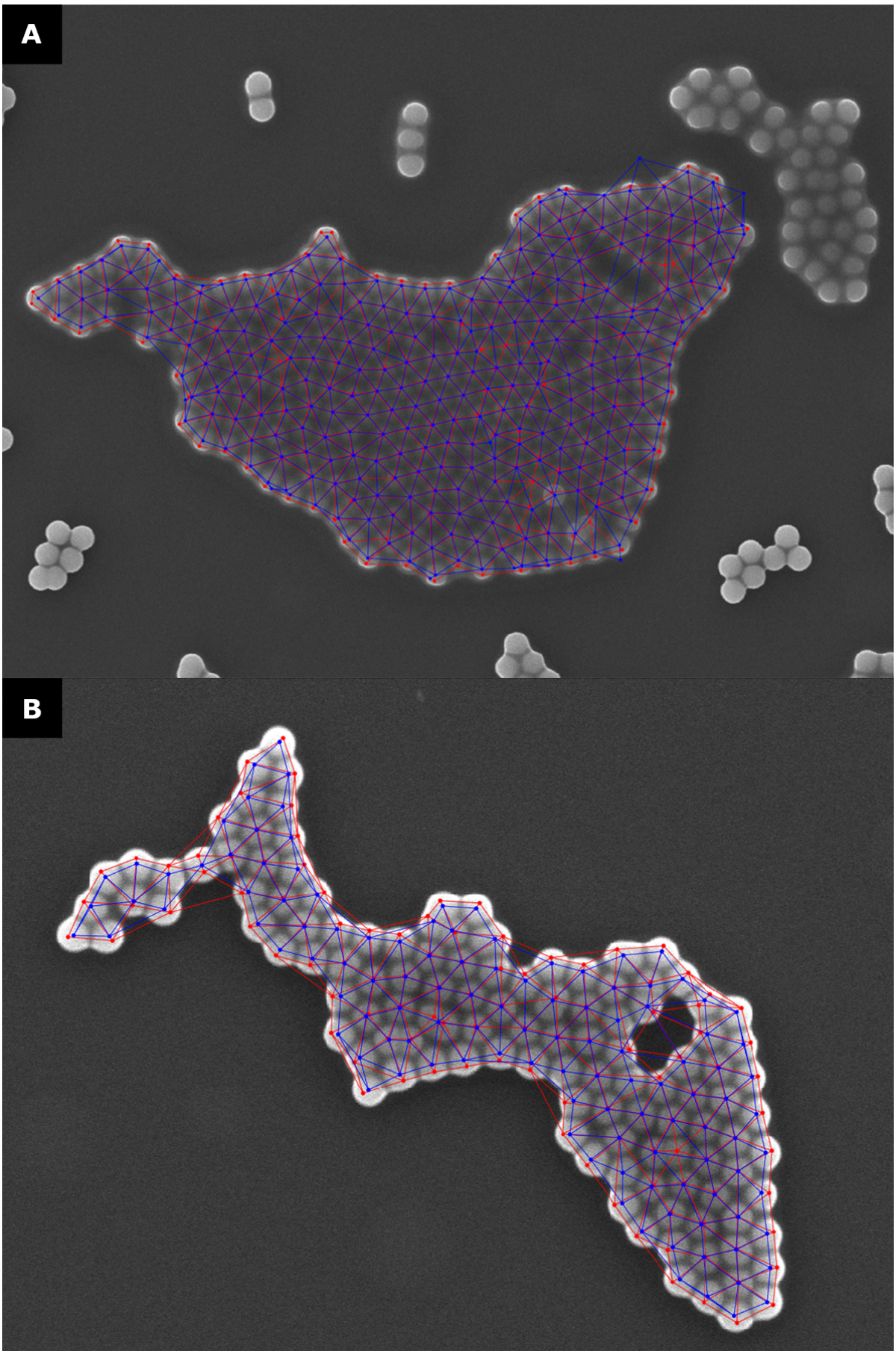

Figure B.6: Images of the two grids which have a variation in the parameter larger than 20%, with blue being the HCT mesh and red the CG mesh. **A**) Overlay on Sample 11-3. **B**) Overlay on sample 7-1.

C

Tables

C.1. Comparison Table of Self-Assembly Techniques

Method			**Particle**		**Self Assembly Parameters**					**Substrate**	**Functionalization**		**Crystaline Properties**			
Domain	Category	Subcategory	Material	Size [nm]	Solvent(s)	Particle Fraction	Time	Temp. [°C]	Stability†	Material	Substrate	Particle	Structure	Ordering	Crystallinity	Ref
Fluidic	Langmuir-Blodgett	Interface Transfer	PS	460 - 680	DI Water / Ethanol	-	-	-	Stb	Glass	Allyltrimethoxysilane (HL)	None	Mono / Multi	CP / HCP	Poly	[14]
	Dip Coating	Draining	PS	200 - 1000	Water + SDS	10 wt %	-	-	Stb	Si / Glass	None	None	Mono / Binary	CP	Mono	[36]
		Meniscus Evaporation	PMMA	250 - 400	DI Water + TEOS	~ 0.125 vol %	1 - 2 [d]	65	Stb	Si	None	None	Multi	HCP	Mono	[37]
	Droplet Dispensing	Pipet Dispension	TiO2	25	Water + HCl / NaOH	2 vol %	8.1 / 16 [s]	25.5 / 10.9	Stb	Glass	None	None	Ringlike	-	-	[38]
		Inkjet Nozzle Dispension	SiO2	330	Water + DEG + ethylhydroxypropanediol + 2-Pyrrolidone	5 wt %	50 - 2000 [s]	25	Stb	Si / Cu / PMDS	Si: OTS (HH)	None	Multi	HCP	Poly	[15]
Physical / Fluidic	Liquid Crystal Confinement	Trapping	SiO2 / Melamine	3000 / 3140	5CB	-	-	34.05	Stb	Glass	None	DMOAP	Single	-	-	[48]
Physical	Spincoating	Shear	SiO2	100 - 2000	ETPTA	19.8 vol %	30 - 960 [s]	-	Stb	Si	APTCS	None	Mono / Multi	CP/ HCP	Poly	[41, 42]
			PS	5000	Water / Ethanol	25/35/45 wt %	<30 [s]	-	Stb	Glass	None	None	Mono	CP	Incomplete	[19]
		Shear + Humidity Adjustment	SiO2	1500	Ultrapure Water	25 wt %	10 -30 [s]	-	Stb	Glass	None	None	Mono	CP	Poly	[43]
	Confinement	Surface Patterning	PS	300 - 800	Water	-	-	55	Stb	Glass + Azoaromatic Polymer	None	None	Mono	Stripes / CR / CP	Poly	[44]
	Shear and Gravity Assisted	Doctor Blade	SiO2	290 - 560	ETPTA	20 -50 % vol	-	25	Stb	Glass	None	None	Multi	CP	Poly	[51]
Physical / External Fields	Field Directed Spincoating	Shear + AC Field	SiO2	458	2-Petanon	20 vol %	-	-	Stb	Glass / ITO	None	None	Mono	CP	Poly	[53]
External Fields	Alternating Electric Field	Sheet Formation	PS	267	NIPMAm + BIS + SDS + MRB + KPS	1 wt %	103 [s]	20	Unst	Glass / ITO	None	None	Mono	Tubular / Sheet	-	[52]
		Ordering	PS	560 - 5000	DI Water + NaCl	-	<25 [s]	-	Unst	Glass / ITO	None		Mono	Oligomer	-	[34]
	Static Magnetic Field	Force Balancing	SiO2 / Fe3O4-Polymer	1050 - 5800	Ho(NO3)3 + DMSO/H2O	-	-	-	Cond	PDMS / Ni	TPI	SiO2: NH2 / Fe3O4-Polymer: COOH / RITC	Mono / 3D	Structured	-	[54]
Chemical	Patchy Particles	Kagome Lattice	Sulfonated PS	1000	DI Water + NaCl	-	~ 15 [h]	-	Unst	SiO2	-	Ti + Au	Mono	Kagome	-	[55]
		Selective Functionalization	SiO2	2000	Water	-	-	-	Unst	Glass	None	Ti + Au	Mono	K/ "Y" / "X"	-	[56]
	Template Functionalization	Surface Treatment	SiO2	67	Ethanol / Water	2.04 wt %	1.5 [h]	-	Stb	Si	APTES	None	Mono	Aggregate	-	[23]
	DNA Functionalization	Gellation	PS	500	TE Buffer	5 - 10 vol %	3000 - 4000 [s]	30 / 43	Cond	-	-	Streptavidin + DNA	3D	Aggregate	-	[57]
		Crystallization	PS / PMMA Silica / TPM	540 / 1000 / 1500	PBS	1 wt %	45 [m]	27 - 28.3	Cond	Glass	HMDS (HH)	Azide + DNA	3D / Binary	FCC / CsCl / AlB2 / Cs6C60	Poly	[58]

† Stb, Unst and Cond are abbreviations for Stable, Unstable and Conditionally Stable, respectively

C.2. Overview of Commercially Available Colloidal Particles

In table C.1 the commercially available spherical colloidal particles which were considered for use during the experiments. Including their physical properties, functionalizations, solutions and size distribution.

Supplier	Material	Size [nm]	Size Distr. (CV)	Surface Functionalization	Solution	Shell (Thickness)
NanoComposix	Gold Particles (powder)	2 ± 1	<20%	Dodecanethiol (Stabilized)	NA	NA
		4 ± 1				
		5 ± 1				
		7 ± 2	<18%	PVP		
		10 ± 2	<15%			
		12 ± 3				
		15 ± 5				
		20 ± 3				
		30 ± 3				
		40 ± 4				
		50 ± 4				
		50 ± 5				
		60 ± 4				
		70 ± 5				
		75 ± 5	<25%			
		80 ± 5	<15%			
		100 ± 5				
	Gold Particles (solution)	5 ± 2	<18%	Citrate, Tannic Acid, PVPPEG, Lipoic Acid, BPEI	Sodium Citrate / Water	NA
		7 ± 2	<15%			
		10 ± 2				
		12 ± 3				
		15 ± 3				
		15 ± 5	<25%			
		20 ± 3	<15%			
		30 ± 3				
		40 ± 4				
		50 ± 4				
		50 ± 5				
		60 ± 4				
		70 ± 5				
		75 ± 5	<25%	PVP	Water	
		80 ± 5	<15%	Citrate, Tannic Acid, PVPPEG, Lipoic Acid, BPEI	Sodium Citrate / Water	
		100 ± 5				
	Gold Particle with Shell	20 ± 3	NA	None / Aminated Shell	Ethanol	Silica (20 ± 5)
		70 ± 5				
		100 ± 5				
		20 ± 3		Citrate	2mM sodium citrate	Silver (Size?)
		60 ± 4				Silica (20 ± 5)
		80 ± 4				Silver (Size?)
	Silver Particles (powder)	4 ± 1	<25%	Dodecanethiol	NA	NA
		5 ± 2	<25 / 30%	Dodecanethiol, PVP		
		10 ± 2	<25%	PVP		
		20 ± 3	<15 / 20%			
		25 ± 5	<40%			
		30 ± 3	<15 %			
		40 ± 4				
		50 ± 4/5	<15 / 25%			
		60 ± 4	<15 %			
		70 ± 4				
		75 ± 4/5	<25%			
		80 ± 4	<15 %			
		100 ± 8				
		200 ± 10				
	Silver Particles (solution)	5 ± 2	<25%	Citrate, PVP, Lipoic Acid, BPEI	Sodium Citrate / Water	NA
		5 ± 2	<30%	PVP		
		10 ± 2	<25%	Citrate, PVP, Lipoic Acid, BPEI		
		20 ± 3	<15 / 20%			
		25 ± 5	<40%	PVP		
		30 ± 3	<15 %			
		40 ± 4		Citrate, PVP, PEG, Lipoic Acid, BPEI		
		50 ± 4	<15 / 25%			
		50 ± 5	<25%	PVP		
		60 ± 4	<15 %	Citrate, PVP, PEG, Lipoic Acid, BPEI		
		70 ± 4				
		75 ± 4/5	<25%	Citrate, PVP		
		80 ± 4	<15 %	Citrate, PVP, PEG, Lipoic Acid, BPEI		
		100 ± 8				
		200 ± 10				
	Silver Particle with Shell	50 ± 4	NA	None / Aminated Shell	Ethanol	Silica (20 ± 5)
		70 ± 10				
		100 ± 10				

Supplier	Material	Size [nm]	Size Distr. (CV)	Surface Functionalization	Solution	Shell (Thickness)
	Silica Particle with Shell	80	NA	PVP, Lipoic Acid, PEG	Water	Gold (20 ± 7)
		120				
		200				
		80?		Aminated, Streptavidin, Goat anti-mouse	PBS or Ethanol	Silica, Fluorescent
	Silicia Particles	20 ± 4	<12 %	Standard, Aminated	Water / Ethanol	NA
		50 ± 4				
		60 ± 4				
		80 ± 4				
		100 ± 4				
		120 ± 4				
		140 ± 7				
		160 ± 7				
		200 ± 7				
		300 ± 30				
		400 ± 40				
	Platinum Particles	5 ± 2	<20 %	Citrate	Aqueous Citrate	NA
		30 ± 3	<15 %			
		50 ± 4				
		70 ± 4				
	Magnetite Fe3O4 (solution)	20 ± 5	<30 %	PVP	Citrate	NA
	Magnetite Fe3O4 (powder)				Dried	
PolySciences	Silica Microspheres	150	10 - 15 %	Standard (SiOH), Amide, Carboxyl, Streptavidin	Powder	NA
		300				
		400				
		500				
		700				
		900				
		1000				
		1500				
		2500				
		3000				
		4000				
		5000				
	Silica Microspheres(Colloidal Suspension)	10	NA	Standard (SiOH), NH2, COOH, Streptavidin	Water - NaOH Stabilizer	NA
		50				
		100				
	Black Iron Oxide	200 - 300	NA	NA	Powder, wettable in water	NA
	Red Iron Oxide	300 - 800				
	Polystyrene	50	<15 %	Carboxylate	Water	NA
		100		Amino, Carboxylate		
		200	<8 %	Amino, Carboxylate, Sulfate, Hydroxylate		
		300	<5 %	Carboxylate		
		350	<3 %			
		400				
		500		Amino, Carboxylate, Sulfate, Hydroxylate		
		750		Amino, Carboxylate		
		1000		Amino, Carboxylate, Sulfate, Hydroxylate		
Sigma Aldrich	Silver	10 ± 4	NA	NA	Sodium Citrate	NA
		20 ± 4				
		40 ± 4				
		60 ± 8				
		100 ± 8				
Thermo Fisher	Silica	490 ± 20	4.1 %	?	Water	NA
		730 ± 20				
		990 ± 20	2 %			
		1570 ± 20	2.5 %			

Table C.1: Commercially available spherical colloidal particles, including their sizes and material properties.

Bibliography

[1] H. Schift, *Nanoimprint lithography: An old story in modern times? A review,* Journal of Vacuum Science & Technology B: Microelectronics and Nanometer Structures **26**, 458 (2008).

[2] A. Biswas, I. S. Bayer, A. S. Biris, T. Wang, E. Dervishi, and F. Faupel, *Advances in top-down and bottom-up surface nanofabrication: Techniques, applications & future prospects,* Advances in Colloid and Interface Science **170**, 2 (2012).

[3] D. Fan and Y. Ekinci, *Photolithography reaches 6 nm half-pitch using extreme ultraviolet light,* Journal of Micro/Nanolithography, MEMS, and MOEMS **15**, 33505 (2016).

[4] A. del Campo and E. Arzt, *Fabrication approaches for generating complex micro- and nanopatterns on polymeric surfaces,* Chemical Reviews **108**, 911 (2008).

[5] H. N. Hansen, R. J. Hocken, and G. Tosello, *Replication of micro and nano surface geometries,* CIRP Annals - Manufacturing Technology **60**, 695 (2011).

[6] S.-Y. Zhang, M. D. Regulacio, and M.-Y. Han, *Self-assembly of colloidal one-dimensional nanocrystals,* Chemical Society Reviews **43**, 2301 (2014).

[7] G. M. Whitesides and B. Grzybowski, *Self-assembly at all scales.* Science (New York, N.Y.) **295**, 2418 (2002).

[8] N. Vogel, M. Retsch, C. A. Fustin, A. Del Campo, and U. Jonas, *Advances in Colloidal Assembly: The Design of Structure and Hierarchy in Two and Three Dimensions,* Chemical Reviews **115**, 6265 (2015).

[9] M. Schwartz, *New Materials, Processes, and Methods Technology* (CRC Press, 2005).

[10] S. Sacanna, D. J. Pine, and G.-R. Yi, *Engineering shape: the novel geometries of colloidal self-assembly,* Soft Matter **9**, 8096 (2013).

[11] G. Timp, *Nanotechnology*, AIP-Press S (Springer New York, 1999).

[12] M. Grzelczak, J. Vermant, E. M. Furst, and L. M. Liz-Marzán, *Directed self-assembly of nanoparticles,* ACS Nano **4**, 3591 (2010).

[13] J. S. Sander, A. R. Studart, and R. Studart, *Multiwalled functional colloidosomes made small and in large quantities via bulk emulsification,* Soft Matter **10**, 60 (2014).

[14] S. Reculusa and S. Ravaine, *Synthesis of colloidal crystals of controllable thickness through the Langmuir-Blodgett technique,* Chemistry of Materials **15**, 598 (2003).

[15] H.-y. Ko, J. Park, H. Shin, and J. Moon, *Rapid Self-Assembly of Monodisperse Colloidal Spheres in an Ink-Jet Printed Droplet The ability of monodisperse colloidal spheres to self- assemble into crystalline arrays makes them interesting and versatile building blocks for advanced materials . Highl,* Chemistry of Materials **189**, 4212 (2004).

[16] J. W. Kim and K. D. Suh, *Monodisperse polymer particles synthesized by seeded polymerization techniques,* Journal of Industrial and Engineering Chemistry **14**, 1 (2008).

[17] U. Jeong, Y. Wang, M. Ibisate, and Y. Xia, *Some new developments in the synthesis, functionalization, and utilization of monodisperse colloidal spheres,* Advanced Functional Materials **15**, 1907 (2005).

[18] J. Castillo, L. Sasso, and W. Svendsen, *Self-Assembled Peptide Nanostructures: Advances and Applications in Nanobiotechnology* (Pan Stanford, 2012).

[19] D. T. W. Toolan, S. Fujii, S. J. Ebbens, Y. Nakamura, and J. R. Howse, *On the mechanisms of colloidal self-assembly during spin-coating,* Soft Matter **10**, 8804 (2014).

[20] P. Y. Wang, C. W. Shields, T. Zhao, H. Jami, G. P. Lõpez, and P. Kingshott, *Rapid Self-Assembly of Shaped Microtiles into Large, Close-Packed Crystalline Monolayers on Solid Surfaces,* Small **12**, 1309 (2016).

[21] L. V. Woodcock, *Entropy difference between the face-centred cubic and hexagonal close-packed crystal structures,* (1997).

[22] B. Ninham and P. Nostro, *Molecular Forces and Self Assembly: In Colloid, Nano Sciences and Biology*, Cambridge Molecular Science (Cambridge University Press, 2010).

[23] X. Li, O. Niitsoo, and A. Couzis, *Electrostatically driven adsorption of silica nanoparticles on functionalized surfaces,* Journal of Colloid and Interface Science **394**, 26 (2013).

[24] K. J. M. Bishop, C. E. Wilmer, S. Soh, and B. A. Grzybowski, *Nanoscale forces and their uses in self-assembly,* Small **5**, 1600 (2009).

[25] P. Tipler and G. Mosca, *Physics for Scientists and Engineers*, Physics for Scientists and Engineers No. pts. 1-33 (W. H. Freeman, 2007).

[26] H. Y. Kim, J. O. Sofo, D. Velegol, M. W. Cole, and A. A. Lucas, *Van der waals dispersion forces between dielectric nanoclusters,* Langmuir **23**, 1735 (2007).

[27] J. L. Li, J. Chun, N. S. Wingreen, R. Car, I. A. Aksay, and D. A. Saville, *Use of dielectric functions in the theory of dispersion forces,* Physical Review B - Condensed Matter and Materials Physics **71**, 1 (2005).

[28] M. Bendersky and J. M. Davis, *DLVO interaction of colloidal particles with topographically and chemically heterogeneous surfaces,* Journal of Colloid and Interface Science **353**, 87 (2011).

[29] E. M. V. Hoek and G. K. Agarwal, *Extended DLVO interactions between spherical particles and rough surfaces,* Journal of Colloid and Interface Science **298**, 50 (2006).

[30] J. I. Y. Min, M. Akbulut, K. Kristiansen, Y. Golan, *The Role of Interparticle and External Forces in Nanoparticle Assembly,* Nature Materials **7**, 527 (2008).

[31] R. McGorty, J. Fung, D. Kaz, and V. N. Manoharan, *Colloidal self-assembly at an interface,* Materials Today **13**, 34 (2010).

[32] J. Zhang, Z. Sun, and B. Yang, *Self-assembly of photonic crystals from polymer colloids,* Current Opinion in Colloid and Interface Science **14**, 103 (2009).

[33] M. Heckele, W. Bacher, and K. D. Müller, *Hot embossing - The molding technique for plastic microstructures,* Microsystem Technologies **4**, 122 (1998).

[34] D. T. Wu, N. Wu, F. Ma, D. T. Wu, and N. Wu, *Formation of Colloidal Molecules Induced by Alternating-Current Electric Fields,* Journal of the American Chemical Society **135**, 6 (2013).

[35] M. Petty, *Langmuir-Blodgett Films: An Introduction* (Cambridge University Press, 1996).

[36] V. Lotito and T. Zambelli, *Self-assembly of single sized and binary colloidal particles at air/water interface by surface confinement and water discharge,* Langmuir , acs.langmuir.6b02157 (2016).

[37] B. Hatton, L. Mishchenko, S. Davis, K. H. Sandhage, and J. Aizenberg, *Assembly of large-area, highly ordered, crack-free inverse opal films.* Proceedings of the National Academy of Sciences of the United States of America **107**, 10354 (2010).

[38] R. Bhardwaj, X. Fang, P. Somasundaran, and D. Attinger, *Self-assembly of colloidal particles from evaporating droplets: Role of DLVO interactions and proposition of a phase diagram,* Langmuir **26**, 7833 (2010).

[39] M. Majumder, C. S. Rendall, J. A. Eukel, J. Y. L. Wang, N. Behabtu, C. L. Pint, T. Y. Liu, A. W. Orbaek, F. Mirri, J. Nam, A. R. Barron, R. H. Hauge, H. K. Schmidt, and M. Pasquali, *Overcoming the "coffee-stain" effect by compositional marangoni-flow-assisted drop-drying,* Journal of Physical Chemistry B **116**, 6536 (2012).

[40] D. B. Hall, P. Underhill, and J. M. Torkelson, *Spin Coating of Thin and Ultrathin Polymer Films,* Polymer Engineering and Science **38**, 2039 (1998).

[41] P. Jiang and M. J. McFarland, *Large-scale fabrication of wafer-size colloidal crystals, macroporous polymers and nanocomposites by spin-coating,* Journal of the American Chemical Society **126**, 13778 (2004).

[42] P. Jiang, T. Prasad, M. J. McFarland, and V. L. Colvin, *Two-dimensional nonclose-packed colloidal crystals formed by spincoating,* Applied Physics Letters **89**, 2004 (2006).

[43] Y. Cheng, P. G. Jönsson, and Z. Zhao, *Controllable fabrication of large-area 2D colloidal crystal masks with large size defect-free domains based on statistical experimental design,* Applied Surface Science **313**, 144 (2014).

[44] Y. H. Ye, S. Badilescu, V. V. Truong, P. Rochon, and A. Natansohn, *Self-assembly of colloidal spheres on patterned substrates,* Applied Physics Letters **79**, 872 (2001).

[45] D. Xia, A. Biswas, D. Li, and S. R. J. Brueck, *Directed self-assembly of silica nanoparticles into nanometer-scale patterned surfaces using spin-coating,* Advanced Materials **16**, 1427 (2004).

[46] M. Asbahi, F. Wang, Z. Dong, J. K. W. Yang, and K. S. L. Chong, *Directed self-assembly of sub-10 nm particle clusters using topographical templates,* Nanotechnology **27**, 424001 (2016).

[47] J. J. Zhao, Y. Y. Duan, X. D. Wang, and B. X. Wang, *Effect of nanofluids on thin film evaporation in microchannels,* Journal of Nanoparticle Research **13**, 5033 (2011).

[48] N. M. Silvestre, Q. Liu, B. Senyuk, I. I. Smalyukh, and M. Tasinkevych, *Towards template-assisted assembly of nematic colloids,* Physical Review Letters **112**, 1 (2014).

[49] M. Tasinkevych, N. M. Silvestre, and M. M. Telo Da Gama, *Liquid crystal boojum-colloids,* New Journal of Physics **14** (2012), 10.1088/1367-2630/14/7/073030.

[50] T. C. Lubensky, D. Pettey, N. Currier, and H. Stark, *Topological Defects and Interactions in Nematic Emulsions,* Physical Review E **57**, 610 (1997).

[51] H. Yang and P. Jiang, *Large-scale colloidal self-assembly by doctor blade coating,* Langmuir **26**, 13173 (2010).

[52] J. J. Crassous, A. M. Mihut, E. Wernersson, P. Pfleiderer, J. Vermant, P. Linse, and P. Schurtenberger, *Field-induced assembly of colloidal ellipsoids into well-defined microtubules.* Nature communications **5**, 5516 (2014).

[53] A. P. Bartlett, M. Pichumani, M. Giuliani, W. González-Viñas, and A. Yethiraj, *Modified spin-coating technique to achieve directional colloidal crystallization,* Langmuir **28**, 3067 (2012).

[54] A. F. Demirörs, P. P. Pillai, B. Kowalczyk, and B. a. Grzybowski, *Colloidal assembly directed by virtual magnetic moulds.* Nature **2**, 3 (2013).

[55] Q. Chen, S. C. Bae, and S. Granick, *Directed self-assembly of a colloidal kagome lattice,* Nature **469**, 381 (2011).

[56] Q. Chen, E. Diesel, J. K. Whitmer, S. C. Bae, E. Luijten, and S. Granick, *Triblock colloids for directed self-assembly,* Journal of the American Chemical Society **133**, 7725 (2011).

[57] L. Di Michele, F. Varrato, J. Kotar, S. H. Nathan, G. Foffi, and E. Eiser, *Multistep kinetic self-assembly of DNA-coated colloids,* Nat. Comm. **4**, 1 (2013).

[58] Y. Wang, Y. Wang, X. Zheng, É. Ducrot, J. S. Yodh, M. Weck, D. J. Pine, E. Ducrot, J. S. Yodh, M. Weck, and D. J. Pine, *Crystallization of DNA-coated colloids,* Nat. Commun. **6**, 7253 (2015).

[59] X. Yan, J. Yao, G. Lu, X. Li, J. Zhang, K. Han, and B. Yang, *Fabrication of non-close-packed arrays of colloidal spheres by soft lithography,* Journal of the American Chemical Society **127**, 7688 (2005).

[60] N. J. Trujillo, S. H. Baxamusa, and K. K. Gleason, *Grafted functional polymer nanostructures patterned bottom-up by colloidal lithography and initiated chemical vapor deposition (iCVD),* Chemistry of Materials **21**, 742 (2009).

[61] W. E. Tenhaeff and K. K. Gleason, *Initiated and oxidative chemical vapor deposition of polymeric thin films: ICVD and oCVD,* Advanced Functional Materials **18**, 979 (2008).

[62] Y. Diao, T. Harada, A. S. Myerson, T. A. Hatton, and B. L. Trout, *The role of nanopore shape in surface-induced crystallization,* Nature Materials **10**, 867 (2011).

[63] H. K. Choi, M. H. Kim, S. H. Im, and O. O. Park, *Fabrication of ordered nanostructured arrays using poly(dimethylsiloxane) replica molds based on three-dimensional colloidal crystals,* Advanced Functional Materials **19**, 1594 (2009).

[64] J. C. Yang and J. Y. Park, *Polymeric Colloidal Nanostructures Fabricated via Highly Controlled Convective Assembly and Their Use for Molecular Imprinting,* ACS Applied Materials and Interfaces **8**, 7381 (2016).

[65] M. Palacios-Cuesta, I. Vasiev, N. Gadegaard, J. Rodríguez-Hernández, and O. García, *Direct micrometer patterning and functionalization of polymer blend surfaces by using hot embossing,* European Polymer Journal **59**, 333 (2014).

[66] T. Ding, D. O. Sigle, L. O. Herrmann, D. Wolverson, and J. J. Baumberg, *Nanoimprint lithography of Al nanovoids for deep-UV SERS,* ACS Applied Materials and Interfaces **6**, 17358 (2014).

[67] V. N. Goral, Y.-C. Hsieh, O. N. Petzold, R. A. Faris, and P. K. Yuen, *Hot embossing of plastic microfluidic devices using poly(dimethylsiloxane) molds,* Journal of Micromechanics and Microengineering **21**, 017002 (2011).

[68] Shin-Etsu Silicone, *Silane Coupling Agents,* Last accessed 29-08-2017.

[69] Ciba, *Ciba Darocur 1173 Product Data Sheet,* Last accessed 29-08-2017.

[70] V. Jančovičová, M. Mikula, B. Havlínová, and Z. Jakubíková, *Influence of UV-curing conditions on polymerization kinetics and gloss of urethane acrylate coatings,* Progress in Organic Coatings **76**, 432 (2013).

[71] K. Studer, C. Decker, E. Beck, and R. Schwalm, *Overcoming oxygen inhibition in UV-curing of acrylate coatings by carbon dioxide inerting, Part I,* Progress in Organic Coatings **48**, 92 (2003).

[72] E. V. Shevchenko, D. V. Talapin, N. A. Kotov, S. O'Brien, and C. B. Murray, *Structural diversity in binary nanoparticle superlattices,* Nature **439**, 55 (2006).

[73] M. Schaffner, G. England, M. Kolle, J. Aizenberg, and N. Vogel, *Combining Bottom-Up Self-Assembly with Top-Down Microfabrication to Create Hierarchical Inverse Opals with High Structural Order,* Small **11**, 4334 (2015).

[74] X. Sun, Y. Li, T. H. Zhang, Y. Q. Ma, and Z. Zhang, *Fabrication of large two-dimensional colloidal crystals via self-assembly in an attractive force gradient,* Langmuir **29**, 7216 (2013).

[75] J. Stewart, *Calculus* (Cengage Learning, 2011).

[76] Roald Hoffmann, *Box Plot: Display of Distribution,* Last accessed 31-08-2017.

[77] M. Pichumani, P. Bagheri, K. M. Poduska, W. González-Viñas, and A. Yethiraj, *Dynamics, crystallization and structures in colloid spin coating,* Soft Matter **9**, 3220 (2013).

[78] T. J. Rehg and G. Higgins, *Spin coating of colloidal suspensions,* AIChE Journal **38**, 489 (1992).

[79] P. Fanzio, A. Cagliani, K. G. Peterffy, and L. Sasso, *High throughput soft embossing process for micro-patterning of PEDOT thin films,* Microelectronic Engineering **176**, 15 (2017).

[80] H. D. Rowland and W. P. King, *Polymer deformation and filling modes during microembossing,* Journal of Micromechanics and Microengineering **14**, 1625 (2004).

[81] H. Yang and P. Jiang, *Scalable fabrication of superhydrophobic hierarchical colloidal arrays,* Journal of Colloid and Interface Science **352**, 558 (2010).

[82] S.-H. Hong, J. Hwang, and H. Lee, *Replication of cicada wing's nano-patterns by hot embossing and UV nanoimprinting,* Nanotechnology **20**, 385303 (2009).

[83] N. Patrito, C. Mccague, S. Chiang, P. R. Norton, and N. O. Petersen, *Photolithographically patterned surface modification of poly(dimethylsiloxane) via UV-initiated graft polymerization of acrylates,* Langmuir **22**, 3453 (2006).

[84] Dentafarm SRL, *Photopol Light: User and Maintenance Manual,* Last accessed 21-08-2017.

[85] F. Oytun, M. U. Kahveci, and Y. Yagci, *Sugar overcomes oxygen inhibition in photoinitiated free radical polymerization,* Journal of Polymer Science, Part A: Polymer Chemistry **51**, 1685 (2013).

[86] A. Sydney Gladman, E. A. Matsumoto, R. G. Nuzzo, L. Mahadevan, and J. A. Lewis, *Biomimetic 4D printing.* Nature materials **15**, 413 (2016).

[87] PubChem - Open Chemistry Database, *Compound summary for sucrose,* Last accessed 22-08-2017.

[88] AZO Materials, *Using Photo-Differential Scanning Calorimetry (DSC) for Investigating UV-Curing Systems,* Last accessed 24-08-2017.

[89] Dow Corning, *Sylgard®184 Silicone Elastomer Datasheet,* Last accessed 08-09-2017.

[90] Engineers Edge, *Water - Material Properties,* Last accessed 08-09-2017.

[91] B. Bhushan, *Modern Tribology Handbook, Two Volume Set*, Mechanics & Materials Science (CRC Press, 2000).

[92] S. J. K. Pedersen, *Circular hough transform,* Aalborg University, Vision, Graphics, and Interactive Systems **123** (2007).

[93] Brett Shoelson, *Circle Finder - File Exchange - Matlab Central,* Last accessed 08-09-2017.

[94] J. Crocker and D. Grier, *Methods of Digital Video Microscopy for Colloidal Studies,* Journal of Colloid and Interface Science **179**, 298 (1996).

[95] Maria Kilfoil, *2D Feature Finder and Tracking Algorithm,* Last accessed 08-09-2017.

[96] Utrecht University - Department of Information and Computing Sciences, *Computational Geometry - Lecture 12: Delaunay Triangulations,* Last accessed 08-09-2017.

[97] Lester Hedges, *Structural order parameters (the easy way),* Last accessed 09-09-2017.